# AN INVESTIGATION INTO THE PHOTOCATALYTIC ACTIVITY OF TITANIUM DIOXIDE

**Raymond Michael Calder**

**A Thesis Submitted for the Degree of PhD**
**at the**
**University of St. Andrews**

**1990**

# AN INVESTIGATION INTO THE PHOTOCATALYTIC ACTIVITY OF TITANIUM DIOXIDE

A Thesis

presented for the degree of

DOCTOR OF PHILOSOPHY

in the Faculty of Science of the

University of St. Andrews

by

Raymond Michael Calder , B.Sc.

United College of

St. Salvator and St. Leonard,

St. Andrews

November 1989

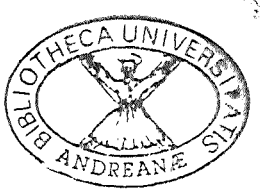

## DECLARATION

I , Raymond Michael Calder , hereby declare that this thesis is my own composition , that the work of which it is a record has been carried out by me , and that it has not been submitted in any previous application for a higher degree.

This thesis describes the results of research work carried out at the Department of Chemistry , United College of St. Salvator and St. Leonard , University of St. Andrews, under the supervision of Professor J.R. MacCallum since 1st. October 1985.

Signed  November 1989

I was admitted to the Faculty of Science of the University of St. Andrews under Ordinance General No. 12 on 1/10/85 and as a candidate for the degree of Ph.D. on 1/10/87.

Signed 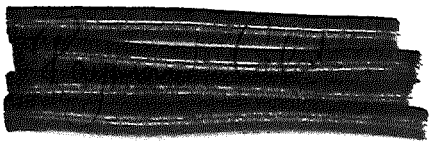 November 1989

## CERTIFICATE

I hereby certify that Raymond Michael Calder has fulfilled the conditions of the Resolution and Regulations appropriate to the degree of Ph.D.

Signed November 1989

## COPYRIGHT

## ACKNOWLEDGEMENTS

First of all , I would like to thank Professor MacCallum for his tremendous enthusiasm , encouragement and advice throughout my research work at St. Andrews.

I would also like to thank the Science and Engineering Research Council and Tioxide U.K. Ltd. for the award of a Studentship over the period 1985 - 1988. Special thanks are due to Mr. R.D. Murley of Tioxide for some interesting discussions and for making sure I was well looked after during my industrial visit.

Several members of the technical staff deserve a mention for ther much appreciated assistance at various stages in my work. In particular Mrs. M. Smith (NMR Technician) , Mr J. Bews (Computing Officer) , Mr. C. Smith (Glassblowing) and Mr.J. Smith (Technician/pigeon fancier). I am also indebted to Dr. C. Thomson and Dr. D. Higgins who helped a great deal with the work involving theoretical chemistry.

Finally , and most importantly , I must thank my family for their understanding and support throughout my 7 years at St. Andrews University , both as an undergraduate and postgraduate ; and Julie for making the final year the happiest.

# CONTENTS

## CONTENTS

CHAPTER 2

To Mum and Dad

## SUMMARY

The photocatalytic activity of titanium dioxide has been studied using an oxygen-uptake monitoring technique. The purpose of the work was to model pigment/polymer interactions when such systems are exposed to ultra-violet light under different conditions. The method used involved stirring the rutile form of the pigment with a variety of substrates, or model compounds , and monitoring the rate at which oxygen was taken up , on irradiation of the resulting slurry with a U.V. light source.

Substrates of different functionality were used in an attempt to mimic a number of possible polymeric environments in which the pigment may be found in real situations (e.g. paints and plastics). Kinetic data were obtained by varying conditions of temperature and oxygen partial pressure in the uptake experiments. As a result , a general mechanism for the $TiO_2$ mediated oxidation of hydroxyl containing compounds has been proposed.

Due to certain interesting anomalies in the oxygen-uptake work , self-association studies of the compounds 1,3-butanediol and 2,3-butanediol were carried out using $^1H$ n.m.r. spectroscopy. Variable concentration data in $CDCl_3$ revealed that both diols existed primarily as dimers ; variable temperature work yielded heat of association data for these molecules.

Theoretical studies using a semi-empirical quantum mechanical computer package (MOPAC) have been carried out on these diols. Optimum monomer structures have shown that intra-molecular hydrogen-bonding may play an important role. Calculations carried out on dimers have demonstrated the feasibility of the formation of cyclic dimer structures.

# CHAPTER 1

## INTRODUCTION

## INTRODUCTION

Titanium dioxide in its pure state is represented by the formula $TiO_2$ and is a bright, white solid. It is used primarily in the powder form as an inorganic pigment in the paints and plastics industries, though as can be seen from fig. 1.1 it also has a wide variety of other minor uses [1].

Pigments may be organic or inorganic in nature and are best described as being small, discrete, solid particles which are dispersed within paint or plastic media while remaining insoluble therein. A pigment is meant to serve two main purposes. Firstly it is introduced to impart colour to the system by, for example, acting as a support for dyes. Secondly, and perhaps more importantly, it is dispersed in paints and plastics and other polymeric media in order to render them opaque. This ability of a pigment to render a material opaque is sometimes termed 'hiding power'.

This chapter briefly outlines the history of early pigments and two of the basic processes used for the manufacture of titanium dioxide pigments. The structure and resultant properties are then discussed with particular reference to the photocatalytic activity of $TiO_2$.

# USES OF TITANIUM DIOXIDE
## 1987 FIGURES

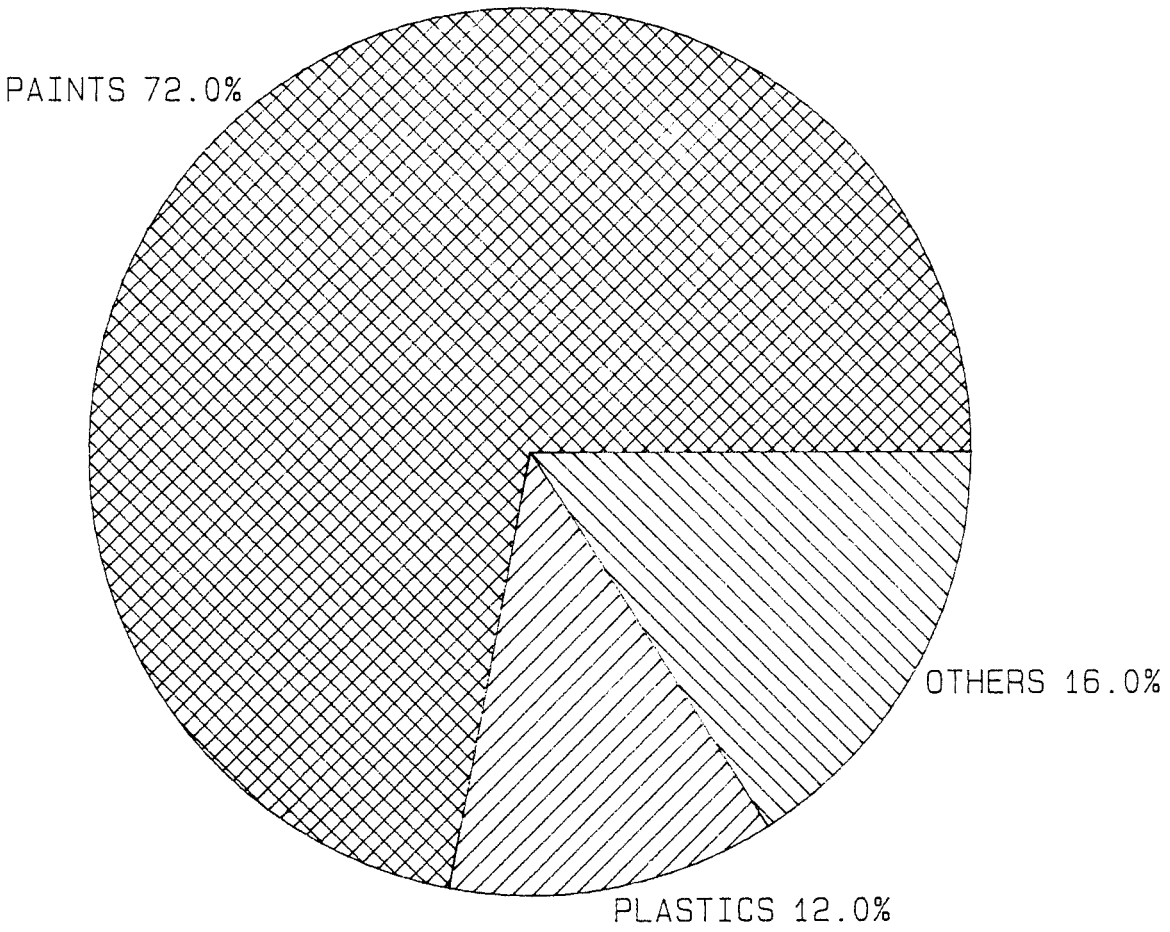


OTHERS include paper, inks
pharmaceuticals and food

**Figure 1.1**

## 1.1 HISTORICAL BACKGROUND

All titanium dioxide pigments are of synthetic origin , unlike the early pigments such as calcium carbonate and white lead. The first commercial titanium dioxide pigments were manufactured in 1916 and consisted of titanium dioxide - calcium/barium sulphate composites. Composite pigments were preferred because the optical performance of the 'neat' $TiO_2$ was poor , mainly due to the incomplete removal of ionic impurities such as $Fe^{3+}$. The need for improved hiding power and low bulk value for use in the paints industry, however , spurred research into the production of pure titanium dioxide pigments and the 1940's saw the introduction of the first commercial pigments.

These pigments were optically superior to the other white pigments then in use , namely zinc oxide , zinc sulphide and white lead , but suffered from practical defects , in particular the accelerated erosion of organic binders in which the $TiO_2$ was dispersed. This erosion results from $TiO_2$ photocatalysed degradation reactions which can occur when pigmented materials are exposed to sources of near ultra-violet light e.g. the high energy part of sunlight. The photocatalytic activity of $TiO_2$ will be discussed in detail in a later section.

Since then , tremendous progress has been made in improving and refining the properties of $TiO_2$ - for example better dispersion , enhanced hiding power , greater uniformity of particle size and increased resistance to degradation - in order to meet the many and varied demands placed on the pigment in today's society.

## 1.2 PRODUCTION OF PIGMENTARY TITANIUM DIOXIDE

Titanium derivatives occur in nature as minor components in many rocks. The main sources of $TiO_2$ are from rutile ore , principally obtained from heavy sands, and from ilmenite , an iron titanate with the idealised composition $FeO.TiO_2$. Ilmenite is the more widely distributed of the two sources and is the major source for pigment production. There are two basic processes for the commercial production of pigments , namely the sulphate process and the chloride process both of which are described briefly below.

### 1.2.1 THE SULPHATE PROCESS

The sulphate process (1918) involves the dissolution of ilmenite ore in hot concentrated sulphuric acid. The iron is removed as a precipitate of ferrous sulphate and hydrolysis of the mother liquors

yields a precipitate of $TiO_2$. This is then calcined at high temperatures to allow the crystallisation and growth of the $TiO_2$ particles to a uniform size of 200 to 250nm cross-section. Particles of this size provide the greatest hiding power and the most uniform reflection of white light [2,3]. The sulphate process is technically the simpler of the two methods and conditions for production of optimum crystalline form and particle sizes have been well established.

## 1.2.2 THE CHLORIDE PROCESS

The chloride process is a relatively recent development. The raw material for this method is $TiCl_4$ which is prepared by heating rutile ore or ilmenite with carbon in a stream of chlorine at 1173K. After purification the $TiCl_4$ is mixed with a catalyst and burned in a stream of oxygen at 1270 to 1770K to yield pigmentary $TiO_2$. The particles produced are then milled and sieved to remove those having sizes outside the optimum range. Although the chloride process is superficially simple , proper control of reaction conditions is critical for the production of pigments having an optimum particle size and free from aggregates and oversized particles.

## 1.3 STRUCTURE OF TITANIUM DIOXIDE

Titanium dioxide can occur in three crystalline modifications ; two different tetragonal forms , namely anatase and rutile as shown in figure 1.2 , and a less common orthorhombic form , brookite. Only anatase and rutile are of commercial importance as pigments since there is no abundant supply of brookite in nature.

Rutile has a structure of 6:3 coordination. That is to say that every titanium atom is surrounded by 6 oxygen atoms approximately at the corners of a regular octahedron and every oxygen by 3 titanium atoms approximately at the corners of an equilateral triangle.

The main structural difference between anatase and rutile lies in the fact that one of the Ti - O bonds in anatase is slightly shorter than in rutile ( 196 and 198pm respectively ) [4,5]. Also the packing in anatase is cubic and in rutile is hexagonal [6].

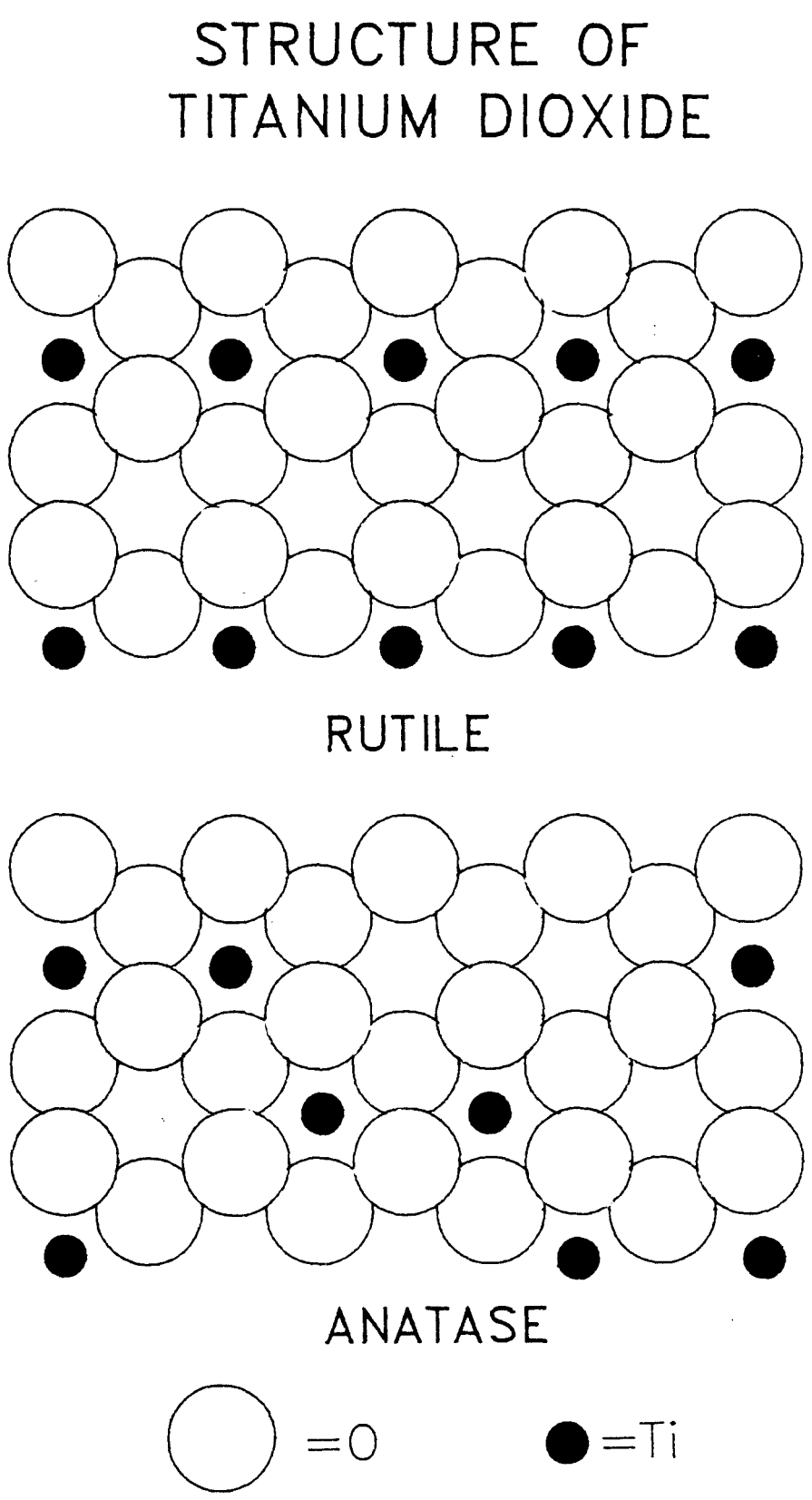


Figure 1.2

## 1.4 PHYSICAL PROPERTIES OF TITANIUM DIOXIDE

Rutile has a greater density , hardness and a higher refractive index than anatase. Both forms absorb radiation in the near ultra-violet of the spectrum (up to 400nm) and the consequences of this will be discussed later.

Pigmentary anatase and rutile consist of irregular but roughly spherical particles having diameters in the range 200 to 300nm. Pigments give the maximum scattering of light of a particular wavelength when the particle diameters are equal to half that wavelength , and are evenly dispersed in the medium [3,7].

The scattering of light , hiding power and brightness of the pigment are also functions of the difference in the refractive indices of the pigment and the medium in which it is dispersed. The refractive indices of some common white pigments and media are given in table 1.1.

| Pigment | R.I. | Medium | R.I. |
|---|---|---|---|
| Rutile | 2.76 | Polystyrene | 1.59 |
| Anatase | 2.52 | PVC | 1.53 |
| PbO | 2.00 | PMMA | 1.50 |
| ZnO | 1.99 | Water | 1.33 |
| $CaCO_3$ | 1.57 | Air | 1.00 |

Table 1.1

Since the opacity of a particular pigment / medium system is a function of the difference in the refractive indices of the two , it is clear from the above table that $TiO_2$ is by far and away the best pigment in this respect.

One other advantage of titanium dioxide lies in the fact that it is such a chemically inert material and is thus relatively non-toxic. The health problems associated with competing pigments such as lead oxide have resulted in major public concern in recent years. Consequently , such pigments have largely been replaced by $TiO_2$ in paint and plastic media. $TiO_2$ is also finding increasing use in the food packaging industry and indeed , is present in certain foodstuffs such as tartare sauce and 'Polo' mints.

## 1.5 THE PHOTOCATALYTIC ACTIVITY OF $TiO_2$

Despite all the advantages of using $TiO_2$ as a white pigment , it does possess one major detrimental feature. It is a well established fact that over a period of time, $TiO_2$ pigmented polymeric materials exposed to the atmosphere undergo chemical breakdown. A good example of this is the flaking of paint on an outside wall or fence. It is generally accepted that the presence of $TiO_2$ enhances the degradation process in which the polymer is gradually eroded to expose the pigment particles. This phenomenon is known as 'chalking' , and is defined in ASTM D 695-74 as "...that phenomenon manifested in paint films by the presence of loose removable powder , evolved from the film itself , at or just beneath the surface. Chalking may be detected by rubbing the film with the fingertip or by other means , e.g. a black cloth ....." [8].

Although it sounds simple , the process of chalking is extremely complicated. Because of the widespread use of $TiO_2$ pigments it is obviously desirable to study this process in some detail in order to understand why it occurs and , ultimately , to be able to minimise it. Indeed , much effort has been expended to elucidate the mechanism and it has become

clear that several factors are responsible for the chalking process. These factors are detailed below.

## 1.5.1 INFLUENCE OF ULTRA - VIOLET RADIATION

Both rutile and anatase absorb strongly in the near ultra-violet region of the electromagnetic spectrum , rutile having an absorption maximum at about 360nm and anatase at 350nm. It has been shown that in order for photocatalysed degradation to take place , the wavelength of the impinging light must be below a certain threshold value [9]. In the case of rutile , this value is ca. 415nm and for anatase ca. 385nm. Figures 1.3 and 1.4 show the u.v. absorption spectra of rutile and anatase respectively. In both cases there is a sharp cut-off point in their absorption corresponding to the threshold values mentioned above. This arises as a direct consequence of the semi-conducting nature of $TiO_2$.

Figure 1.5 shows a simplified way of describing the electronic properties of three different types of solid i.e. an insulator , a metal and a semi-conductor. The complex nature of overlap which exists in the atomic and molecular orbitals of solids leads to the formation of a band structure for the electronic energy levels.

In simple terms there exist two electronic bands in solids , namely the valence band and the conduction

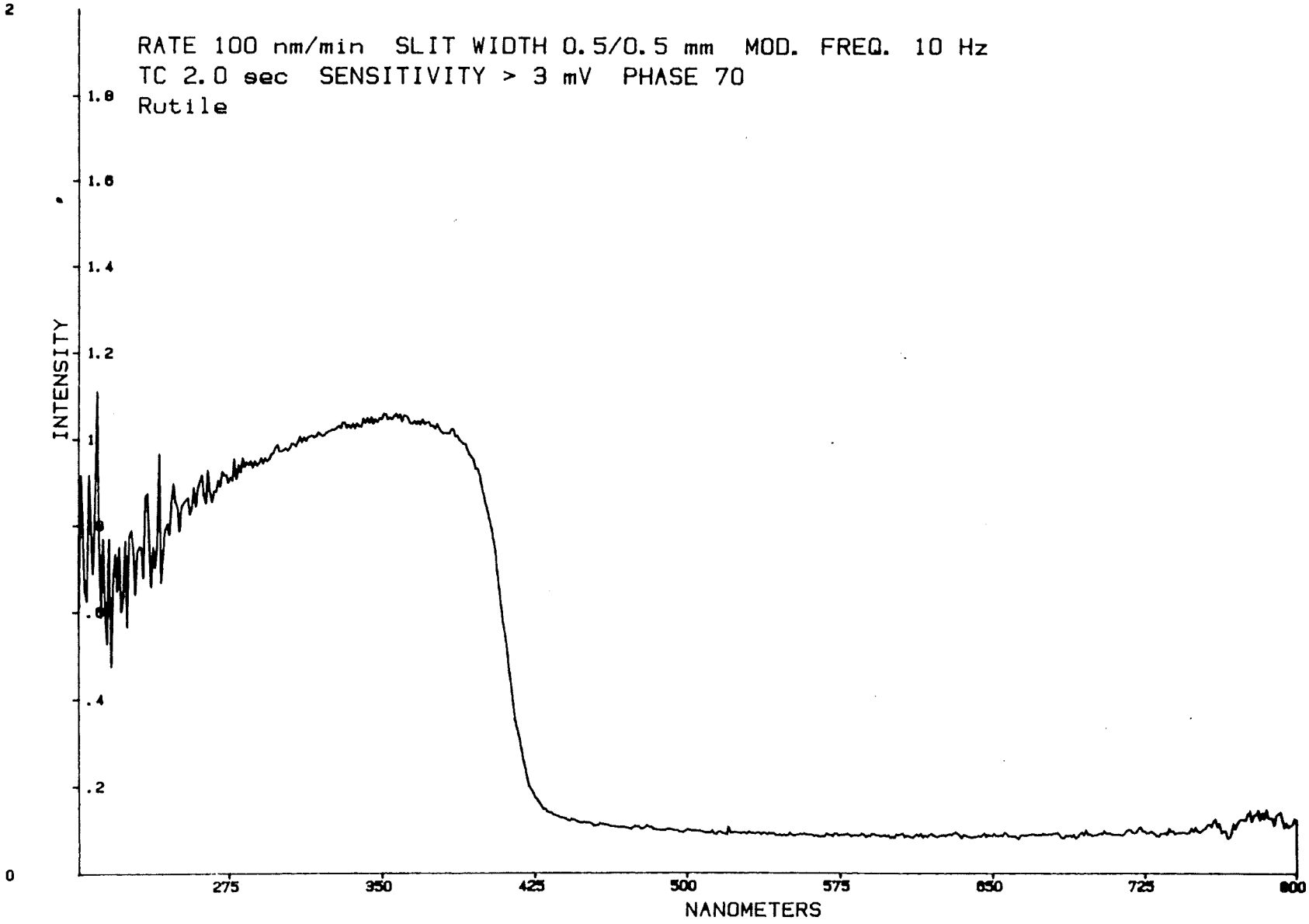
RATE 100 nm/min SLIT WIDTH 0.5/0.5 mm MOD. FREQ. 10 Hz
TC 2.0 sec SENSITIVITY > 3 mV PHASE 70
Rutile
INTENSITY
2
1.8
1.6
1.4
1.2
1
.8
.6
.4
.2
0
275
350
425
500
575
650
725
800
NANOMETERS

Figure 1.3

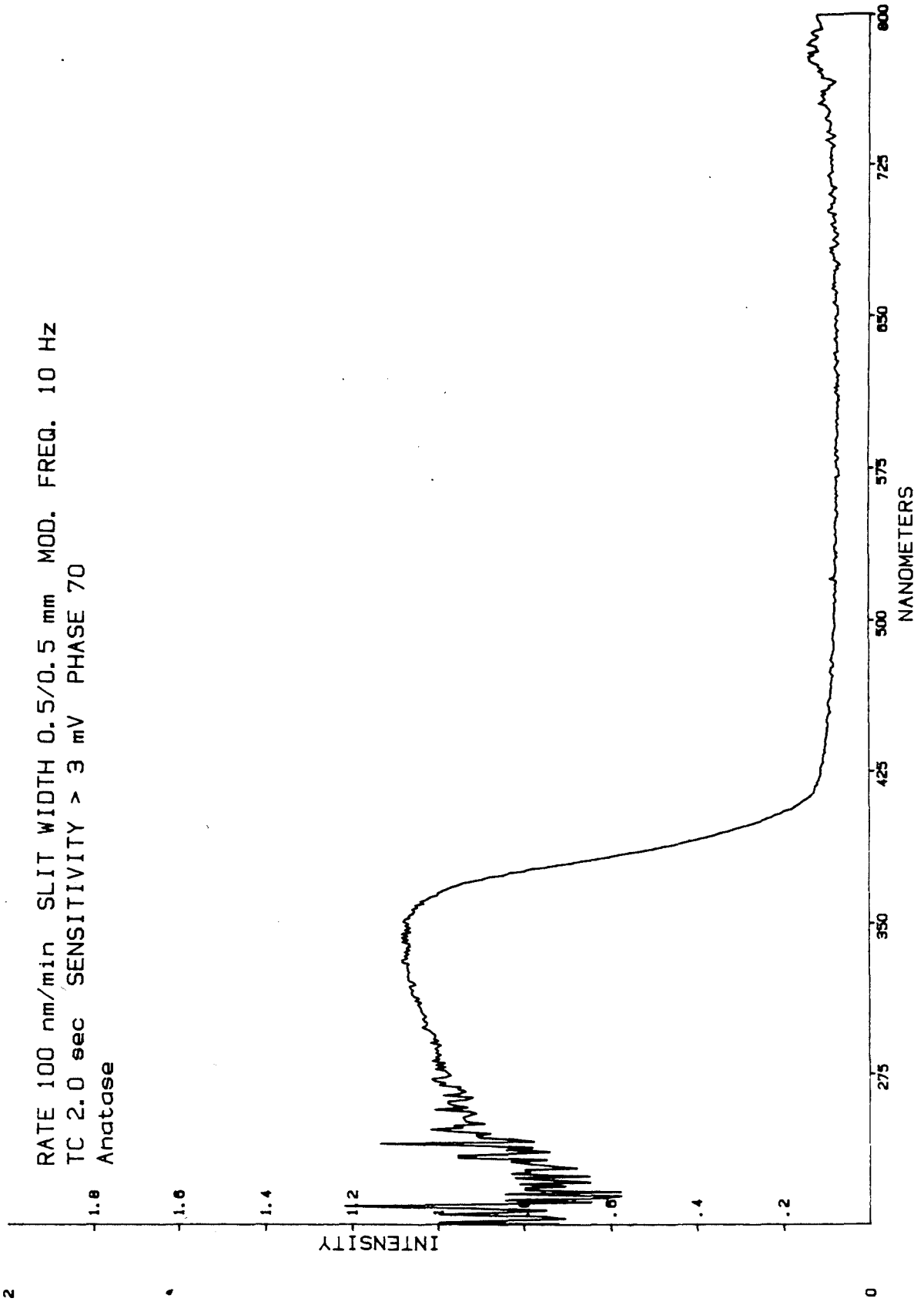
RATE 100 nm/min SLIT WIDTH 0.5/0.5 mm MOD. FREQ. 10 Hz
TC 2.0 sec SENSITIVITY > 3 mV PHASE 70
Anatase
INTENSITY
NANOMETERS
1.8
1.6
1.4
1.2
.6
.4
.2
275
350
425
500
575
650
725
800
2
0

Figure 1.4

band.If the conduction band is separated from the valence band by a sufficiently large energy gap then no electrons can be excited to the conduction band and the material is an insulator. If the uppermost energy band is only partially filled ( as for the alkali metals ) , or the filled band overlaps an empty band ( as for the divalent metals ) then these electrons are free to move in an electric field and high conductivities result.

For semi-conductors the empty conduction band is separated from the filled valence band by a relatively small energy gap. In rutile the band-gap corresponds to an energy of ca. 3.0eV and in anatase , ca. 3.2eV. If sufficient energy is provided , either thermally or by radiation of energy greater than the band-gap , electrons may be excited to the conduction band , leaving positive holes in the valence band. These electron / hole pairs are called excitons ( see fig. 1.6 ).

In $TiO_2$ the formation of an exciton corresponds to the transfer of an electron from an oxygen 2p orbital to a titanium 3d orbital [10,11]. It is generally accepted that exciton formation in $TiO_2$ via photon capture is a necessary prerequisite for photocatalytic degradation to occur.

# BAND LEVELS IN SOLIDS

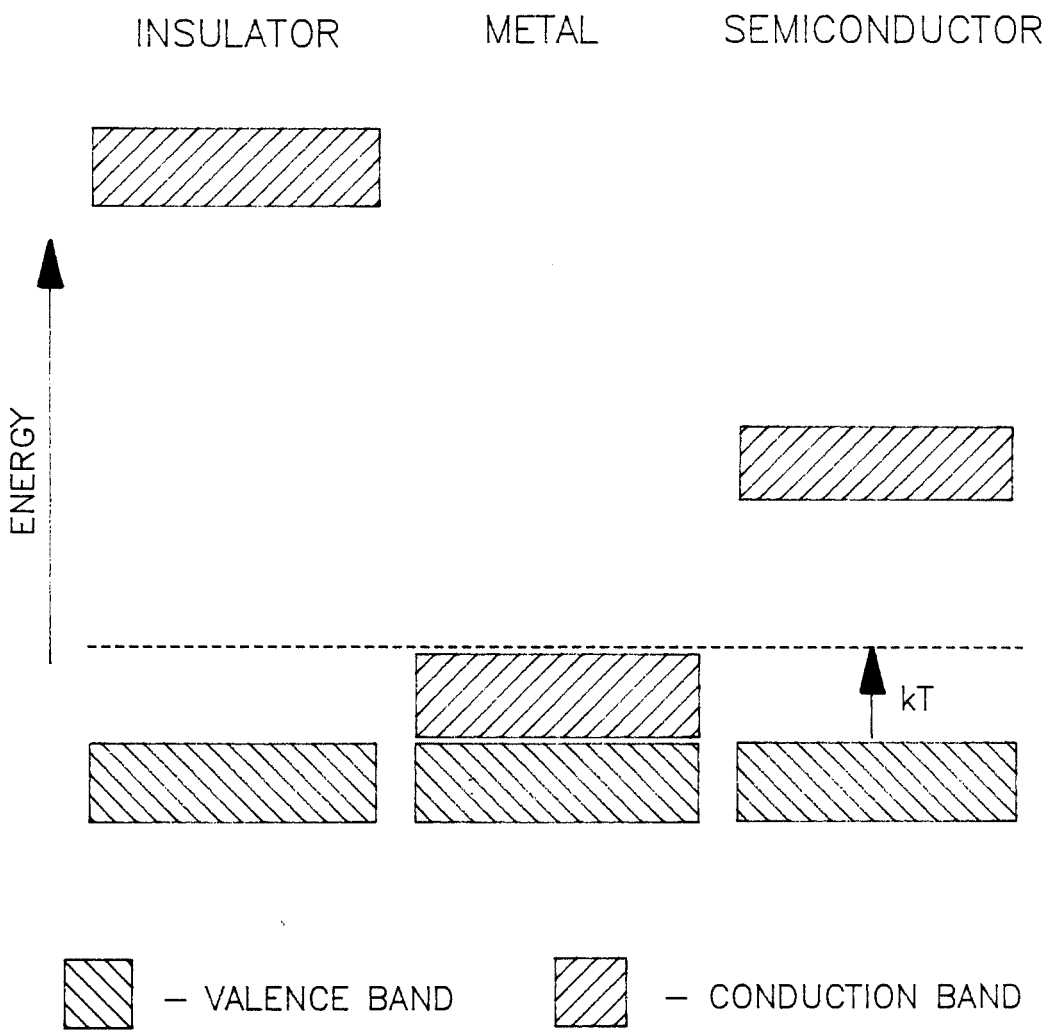


Figure 1.5

# EXCITON FORMATION IN SEMICONDUCTORS

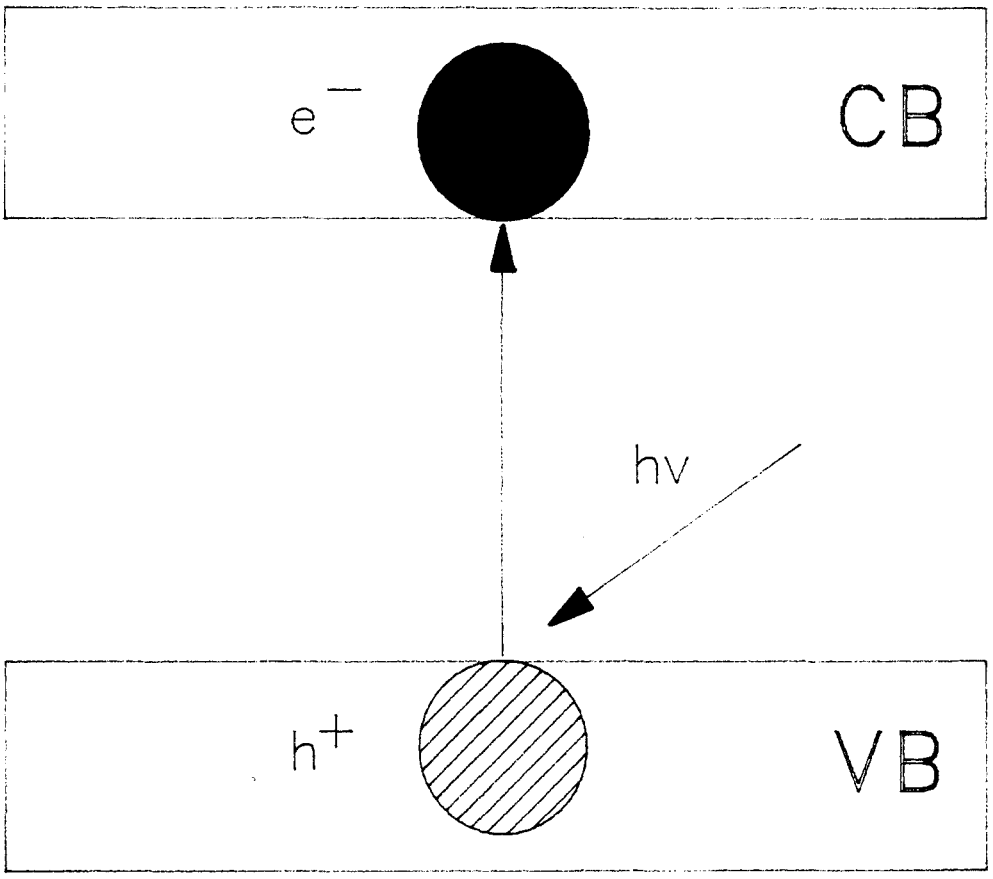


Figure 1.6

## 1.5.2 THE INFLUENCE OF WATER

Several workers have studied the influence of water on the photodegradative process [12,13]. It was observed that in the absence of water , polymer samples containing $TiO_2$ showed no tendency to undergo photocatalysed degradation. Volz et al. [12] carried out experiments whereby the permeability of water through pigmented films was measured and was found to be extremely high. A number of workers [14-16] have dealt with the adsorption of water on anatase and rutile and all agree that the surface contains weakly and strongly bound molecular water , and hydroxyl groups formed by the dissociative chemisorption of water. Bickley and Stone [13] have suggested that the presence of these surface hydroxyls plays a key role in the photoactivity of $TiO_2$ since they can act as traps for the photo-holes generated by u.v. irradiation of the pigment ( equation 1.1 )

$$OH^- + h^+ \text{ -----> } OH^\cdot \qquad (1.1)$$

## 1.5.3 THE INFLUENCE OF OXYGEN

It has also been established that oxygen must be present for chalking to occur. Volz et al. [12] irradiated paint specimens in the absence of $O_2$ by carrying out the experiment in an atmosphere of $N_2$.

Under these conditions , no degradation occurred. On re-admission of oxygen to the system the paint samples showed marked signs of chalking.

## 1.6 COMPARISON OF THE PHOTOACTIVITY OF ANATASE AND RUTILE

Pigmentary anatase has been found to be more active than rutile in the degradation of pigmented plastics and polymers. The reason for this difference is not clear and several explanations have been proposed. Boonstra and Mutsaers [17] found that there was an apparent linear relationship between the amount and rate of oxygen photoadsorption and the hydroxyl group concentration on the surface of anatase or rutile powders ; and that anatase was capable of adsorbing up to twice as much oxygen as rutile containing the same number of surface hydroxyl groups. Murley [10] also noted a twofold difference in the amount of oxygen adsorbed per unit area of surface of anatase and rutile when these were irradiated for similar periods. Allen and co-workers attributed the difference in activities to the difference in energies of their photo-excited states [18-20].

The situation is further complicated by the fact that polymeric media also undergo direct ultra-violet degradation if exposed to radiation of less than ca. 400nm. This radiative degradation leads to two types of

reactions , namely chain-scission - leading to the formation of low molecular weight moeities - and crosslinking which results in the formation of insoluble and infusible network structures.

The mechanisms for these processes are not clear but the presence of carbonyl impurities [21] and catalyst residues [22] are thought to play a role in the initiation of the degradation , whilst free radicals [23] and oxygen [24] are known to be involved in the propagation steps.

It is clear , therefore , that in pigmented polymer samples , two processes can occur i.e. direct u.v. degradation of the polymer and $TiO_2$ catalysed photodegradation.

It has been found that in polymers containing anatase as the pigment , the rate of catalysed degradation in the vicinity of the pigment particles proceeds faster than direct u.v. degradation [24,25]. This results in a 'pitting' effect on the surface of the material and is illustrated in figure 1.7.

The rate of photodegradation when catalysed by rutile , on the other hand , is less rapid than direct u.v. degradation and this results in a markedly different surface morphology. ( see figure 1.8 ). In this case the pigment particles serve to protect the polymer beneath them , leading to a 'pedestal' effect.

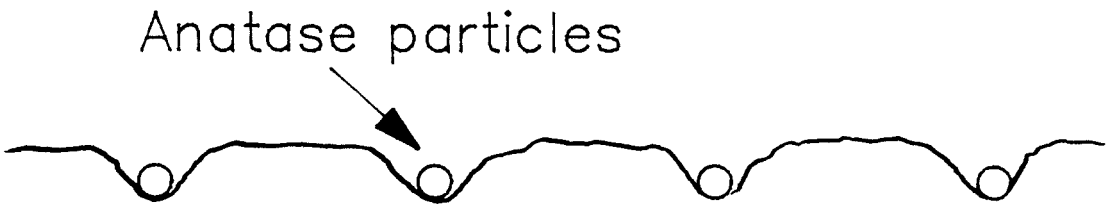


PITTING EFFECT OF ANATASE

Figure 1.7

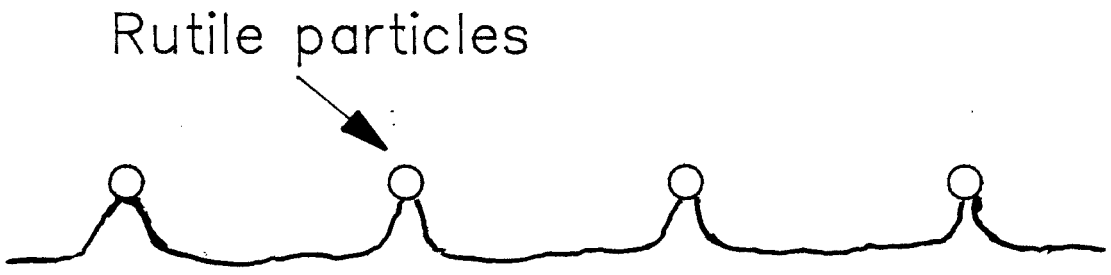


PEDESTAL EFFECT OF RUTILE

Figure 1.8

It is clear that anatase pigments are unsuitable for use in plastics or paints where they may be exposed to bright sunlight and in practice rutile pigments are used almost exclusively in exterior applications. Anatase is however still widely used in fibres , paper and printing inks since it is less abrasive than rutile. This is a very general and simplified view. For a more complete picture , other factors such as the polymer durability [26,27] should be taken into account.

## 1.7 MEASUREMENT OF PHOTOCATALYTIC DEGRADATION

Many chemical and physical techniques have been employed in the paints and plastics industries in order to determine the extent of degradation or 'weatherability' of their products on being exposed to the elements for long periods of time. This is necessary since the result of degradation has an economic impact on the application of materials in differing environments. It is thus desirable to be able to predict the probable lifetimes of these materials under a variety of conditions.

The simplest method of monitoring the degradation of paints and plastics is through visual observation , for example blistering of paint , loss of colour and cracking [28,29]. Mechanical properties can also be measured , for example tensile strength and stiffness [30].

The experimental techniques used for such tests fall into two categories and these are described briefly below.

### 1.7.1 OUTDOOR WEATHERING TECHNIQUES

There are many problems associated with carrying out meaningful tests outdoors. Obviously the extent of weathering of a particular sample will vary with

geographical location , height above sea level etc. Other external factors such as exposure to sunlight , temperature variations and humidity are extremely difficult to control. Another major problem is the length of time involved in these experiments. In order to obtain consistent and therefore , reliable results , long periods of exposure ( 3-5 years ) are required in order that seasonal variations and general changes in climate are averaged out.

In recent years attempts have been made to standardise experimental conditions and one way in which this has been done is to mount the samples at the focal point of a concave , mirrored dish. The dish is equatorially mounted and follows the path of the sun across the sky [31]. As a result , the intensity of radiation impinging on the sample is considerably higher than normal and the weathering process is accelerated. One of the consequences of this , however, is that the temperature of the sample at the focal point is high ( ca 150 $^{o}$C ) and despite attempts to keep it cool by circulating air , a certain amount of thermal degradation is bound to occur.

## 1.7.2 LABORATORY WEATHERING TECHNIQUES

Several devices have been developed for use in laboratories which mimic the natural environment but lead to accelerated degradation. These devices or

'Weather-ometers' consist of a vertical , cylindrical drum which revolves around a source of high intensity u.v. radiation ( e.g. a carbon arc or xenon lamp ). The polymer samples are sprayed with water or exposed to the required humidity at a constant temperature [32].

However , despite being subjected to more controlled conditions than in outdoor testing methods , it is still extremely difficult to ensure that the weathering conditions remain constant throughout the experiment. An exposure time of the order of 200 - 300 hours is required for appreciable weathering to occur and in that time , important parameters such as humidity , temperature and lamp intensity can fluctuate. Because of this , it is also meaningless to compare results obtained from two different 'Weather-ometers'.

## 1.8 MODEL SYSTEMS

The major problem with the above accelerated testing methods is the length of time involved in accumulating useful results. As has been mentioned previously , it is extremely difficult to control conditions and maintain a constant environment over the timescales required.

The basic aim of research into the degradation of these pigmented polymer systems is to discover the mechanism by which it occurs. Obviously this is not

possible if reproducible results cannot be achieved. Consequently the use of the aforementioned artificial weathering techniques is limited to predicting the probable lifetime of a particular pigment / polymer sample.

It was discovered by Irick [33] that a good correlation existed between the rate of photodegradation of propan-2-ol mediated by $TiO_2$ to form propanone , and the degradation rates of various pigmented systems. More specifically , it was found that the activity series of several different $TiO_2$ grades was the same for both alcohol conversions and polymer photodegradation. Another important factor is that sustained propan-2-ol conversion, like paint film weathering , requires the presence of u.v. light , oxygen in the gas phase and water or surface hydroxyl ions. Because of this parallel with polymeric systems , the $TiO_2$ / propan-2-ol system has subsequently become the subject of a great deal of interest.

Early work concentrated on the gas phase photoconversion of propan-2-ol to acetone on the surface of $TiO_2$ [34]. The kinetics of the process were studied by monitoring the concentration of acetone present by sampling the gas during the reaction and analyzing the mixture with a gas chromatograph. Munuera and Stone [35] used the technique of temperature programmed desorption to show that the alcohol molecule was more tightly bound to the $TiO_2$ surface than the

ketone and that the propan-2-ol displaces the acetone from the surface in a 1:1 molar ratio.

Much work has also been done in the liquid phase. Obviously propan-2-ol liquid is a much better model for real polymer systems than the gas , since it resembles the solid state more closely. Other advantages of using the liquid phase are that variables such as concentration and temperature are much more easily controlled and determined. In this way , a considerable amount of kinetic and mechanistic information can be obtained.

A typical experimental set-up would involve irradiating a stirred suspension of $TiO_2$ in propan-2-ol with a high intensity light source such as a medium pressure mercury arc lamp. By employing filters , or using a pyrex vessel , it can be ensured that light of wavelength greater than 300nm impinges on the suspension. The only absorbing species then is the $TiO_2$ since propan-2-ol absorbs at much shorter wavelengths.

The rate of the reaction can be measured by analyzing aliquots of the irradiated suspension for the presence of acetone at measured time intervals. These aliquots are first of all centrifuged and spectroscopic or chromatographic techniques are then used to determine the amount of ketone present [36-39] , the more common technique being gas-liquid chromatography.

Thus the reaction rate is taken to be the rate at which acetone is formed.

More recently , Fraser and MacCallum [40,41] used the fact that , during the photocatalysed conversion of propan-2-ol to acetone , oxygen is consumed from the atmosphere. Their experimental technique involved measuring the amount of oxygen consumed as a function of time by monitoring pressure changes in a closed $TiO_2$ / propan-2-ol / air system. The apparatus used will be described in more detail in the next chapter. In this way , the reaction rate is obtained by monitoring a reaction participant which is involved at an early stage in the photoconversion.

This technique has major advantages over the ones which involve following propanone formation. In the latter case , samples have to be extracted from the irradiated suspension and this involves disturbing the system. Also , removal of a large number of samples , while yielding more data , involves a large change in volume which could alter the kinetics of the process. Another problem is that removal of a sample takes a finite time. It is therefore impossible to get information about the initial stages of the reaction.

Pressure changes , on the other hand , can be monitored continuously and in a non-intrusive manner so that the system need not be disturbed. Many readings of

oxygen consumption can be made over a short period of time .

Using this technique , Fraser and MacCallum were able to propose a detailed mechanism for the photocatalysed conversion of propan-2-ol to acetone. It was also concluded that the oxygen-uptake method could be used in a quantitative manner to compare the relative photoactivities of different pigment grades over a very short period of time.

# CHAPTER 2

## OXYGEN–UPTAKE STUDIES

## 2 OXYGEN-UPTAKE STUDIES

The oxygen-uptake work which has been done on propan-2-ol proved to be of great value in elucidating a mechanism for it's photocatalysed oxidation. However the mode of action for propan-2-ol oxidation is not necessarily the same as that for polymers. These substances , in general , contain many functional groups , vary in chain length , molecular weight , viscosity and so on. Since it is polymer degradation that we are ultimately interested in , a different course of study was undertaken. In order to model polymer / pigment systems in a more realistic manner , it was decided to look at the photocatalysed oxidation of a variety of molecules using the oxygen-uptake technique.

The choice of model compounds was based on several factors:

1) The compounds used were all liquids at the temperatures at which the experiments were carried out. There were several reasons for this. The oxygen-uptake method relies on the ability to stir the $TiO_2$ / model compound slurry efficiently and at a constant rate. In this way the $TiO_2$ particles are well dispersed ensuring optimum contact between the particles and substrate. Equilibration of $O_2$ in the slurry was facilitated and it was also hoped that by working in the liquid phase ,

the rate of reaction would be sufficiently high that appreciable pressure changes would be observed over reasonably short periods of time.

2) All of the model compounds used contained at least one polar functional group. It is generally agreed that the oxidation of substrates takes place on the $TiO_2$ surface. If this is the case , then the compound under investigation must have some means of interacting with the surface , and it was anticipated that this would occur via the polar group.

3) It was also ensured that none of the compounds used absorbed light above a wavelength of ca. 300nm. This guaranteed that the only species capable of absorbing the impinging radiation was the $TiO_2$ thus eliminating the possibility of direct u.v. degradation of the compound.

## 2.1 EXPERIMENTAL SECTION

A schematic diagram of the oxygen-uptake apparatus is shown in figure 2.1. The various components of the apparatus are described below.

### 2.1.1 OXYGEN-UPTAKE VESSEL

The vessel in which the oxidations were carried out had a capacity of ca. 200ml and was made of pyrex. Consequently , only radiation of wavelength greater than ca. 300nm could penetrate the slurry. Because pressure changes were being measured , it was critical to ensure that the temperature was maintained constant throughout the experiment. This was facilitated by a water jacket which surrounded the bottom half of the vessel. Water from a thermostatic bath ( Grant Instruments Ltd. ) was circulated round the jacket at the required temperature which could be set at anywhere between room temperature and 345K.

In order to ensure efficient heat transfer between the slurry and the surrounding jacket , stirring was provided by a magnetic stirrer ( Gallenkamp ). This also ensured good equilibrium mixing of $TiO_{2}$ particles, $O_{2}$ , and the substrate. It was critical that the rate of stirring was kept constant since the pressure in the vessel was extremely sensitive to changes in this variable.

# OXYGEN-UPTAKE APPARATUS

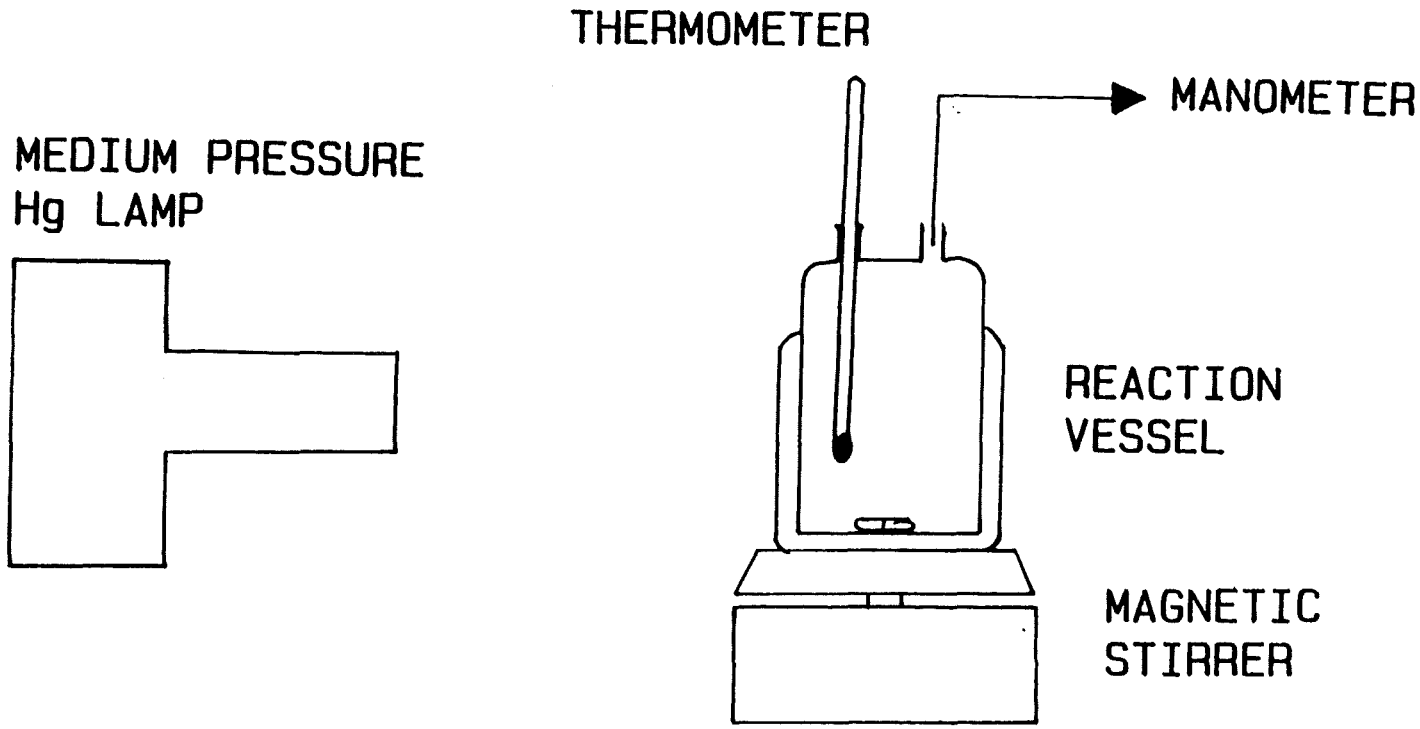


Figure 2.1

Once thermal equilibrium had been achieved ( after ca. 1 hr. ) the temperature of the slurry remained constant to within +/- 0.1 °C. Temperature measurements were made with a mercury thermometer which was inserted into the vessel via a B14 quickfit socket.

Pressure measurements were made with a differential manometer. This consisted of a U-shaped glass tube , each arm of the 'U' being approximately 80cm long. The diameter of the capillary inside the tube was 2mm and propan-2-ol ( Fisons ) was used as the manometer fluid. These factors combined to make the sensitivity of the manometer system extremely high. One arm of the manometer was connected to the uptake vessel via rubber tubing and a B14 quickfit right-angled adapter. The other arm was fitted with a tap which was kept closed during an uptake run. A ruler with millimeter divisions was attached to the U-tube so that the fluid level in the manometer could be measured.

## 2.1.2 SOURCE OF RADIATION

Ultra-violet radiation was supplied by a 500W medium pressure mercury arc lamp ( Englehard Hanovia). The output from this is shown in figure 2.2 and the main emission lines and relative energies are given in table 2.1 [42].

| Wavelength (nm) | Rel.Energy |
|---|---|
| 366 | 1.00 |
| 405 | 0.42 |
| 436 | 0.78 |
| 546 | 0.93 |
| 578 | 0.77 |

Table 2.1

It can be seen that the most intense line in the spectrum of the lamp is at 366nm. The energy of this wavelength is sufficiently high for exciton formation [8,12] to occur and can thus "trigger" photocatalytic oxidation.

It is important that the lamp intensity remains constant during an experiment. For this reason , the lamp was connected to a stabilised power supply (Englehard Hanovia ) which compensated for a gradual fall off in lamp output by supplying a gradually increasing current. It was also possible to monitor the

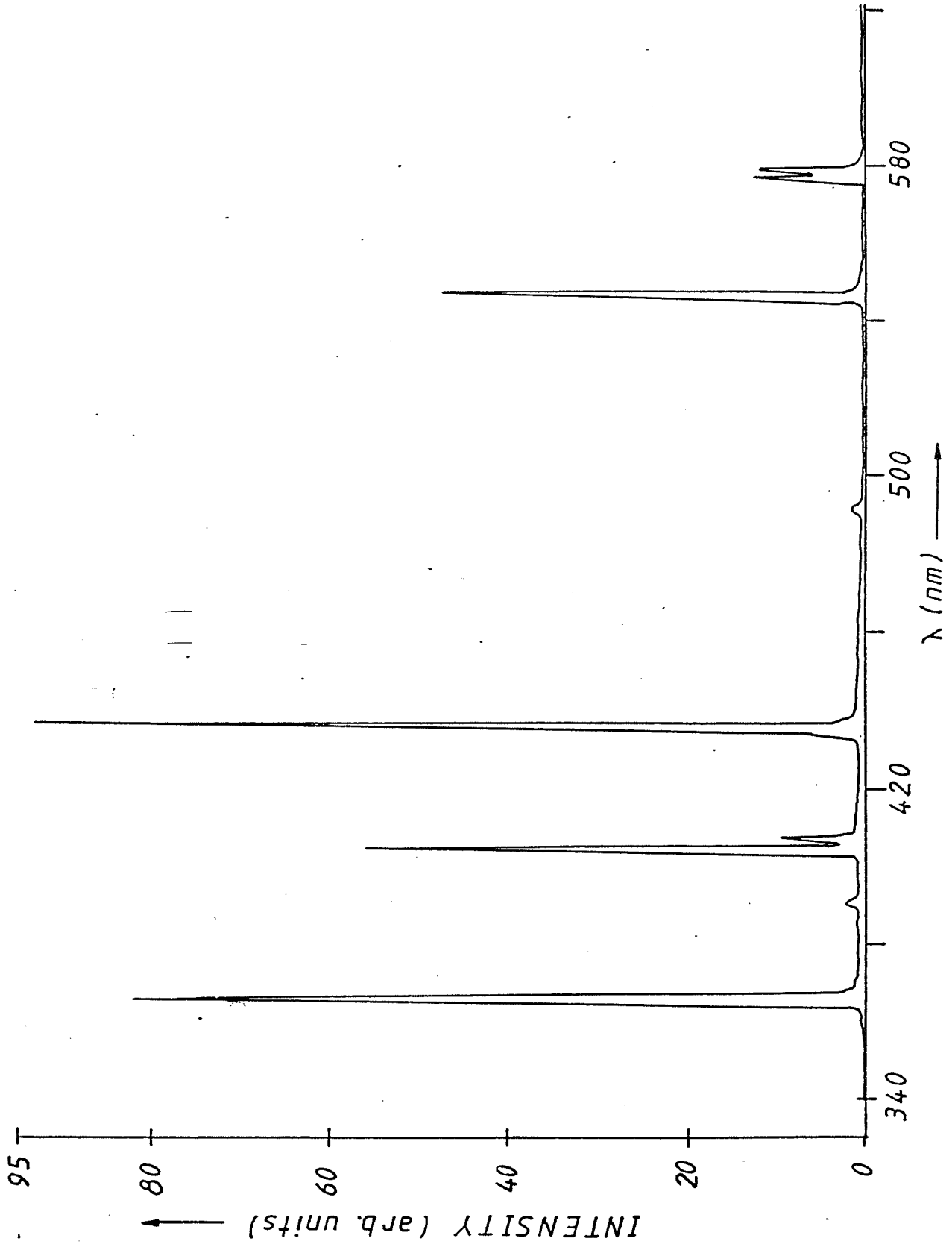


Figure 2.2

lamp intensity directly via a photodiode ( RCA ) which was connected to a chart recorder ( Beckman ). Any fluctuations in intensity during an uptake run would thus show up on the chart paper. In practice it was found that virtually no fluctuations occurred.

One of the consequences of using high intensity ultra-violet light sources , emitting at a wavelength less than 250nm , is that atmospheric oxygen is converted to ozone around the lamp housing. Exposure to ozone in concentrations greater than ca. 10 ppm constitutes a health hazard [43] and for this reason , the oxygen-uptake apparatus was set up in a fume cupboard to ensure adequate ventilation.

## 2.1.3 MATERIALS USED

In the experiments that follow , the pigment which was used was an uncoated rutile grade supplied by Tioxide U.K. Ltd. (CLD 1729/A). Uncoated $TiO_2$ was used to ensure that any reaction which took place was due only to the pigment and not to any coating material. The surface area of this pigment was approximately 100 $m^2g^{-1}$.

Various substrates were used in the course of these oxygen-uptake studies and these are listed below.

1,2-ethanediol ( Fisons ) , 1,3 propanediol , 1,4-butanediol , 1,3-butanediol , 2,3-butanediol , 2-

methylpropan-2-ol , 1,3-dichlorobutane ( all Aldrich ) and triethanolamine (International Paints Ltd.). Prior to use , all substrates were purified in the recommended manner.

The detection of hydrogen peroxide was effected by an acidic solution of $Ti^{4+}$ ions which was made up by dissolving 5 mls. $TiCl_4$ ( Aldrich ) in 45 mls. 0.1M HCl [44]. The addition of this solution to $H_2O_2$ produces a titanium (IV) peroxo complex the colour of which varies from yellow through to deep red depending on its concentration [45,46]. This proved to be an extremely sensitive qualitative test for the detection of $H_2O_2$.

In some experiments , $H_2O_2$ ( 100 vols. , Fisons ) was added to the slurry.

In order to aid characterisation of some of the reaction products , 2,4-dinitrophenylhydrazine ( 2,4-DNPH ) derivatives were prepared. The 2,4-DNPH was added in the form of Brady's reagent. This was made up using the method recommended by Kamm [47].

## 2.1.4 EXPERIMENTAL PROCEDURE

So that the results obtained were meaningful , it was important to adopt a standard experimental procedure. Before each experiment the vessel was thoroughly washed and dried. The rubber tubing

connecting the manometer to the vessel was checked and changed regularly since it tended to perish on prolonged exposure to the u.v. radiation. It was also important to use a fixed pigment mass : substrate volume ratio throughout these experiments [37]. Thus , in all cases , 1g of $TiO_2$ was mixed with $100cm^3$ of the compound under study. Also , by using this volume of liquid , the volume of air above it was kept reasonably small facilitating the measurement of pressure differences.

Prior to irradiation of the slurry , the mercury lamp was allowed to warm up for ca. 2 hrs. The slurry itself was thermally equilibrated in the 'dark' at the required temperature. This was done by placing a cover round the cell in order to shield it from the lamp , and connecting the water jacket to the thermostatic bath. During this time the lamp intensity was monitored as described previously.

At the start of the experiment , the manometer was connected to the vessel , and once the fluid had settled at a constant level , the cover was removed. At the same time a stopwatch was started and readings were taken at 4 minute intervals over a period of 1 - 2 hours. On completion of an experiment , plots of volume of $O_2$ consumed v. time were constructed from which reaction rate data were obtained.

## 2.2 THE OXYGEN-UPTAKE PROFILE

Oxygen-uptake experiments were carried out with the various substrates which have been mentioned previously. The results of these experiments varied from substrate to substrate and these will be detailed individually in subsequent sections. However , in the cases where oxygen-uptake did occur , it was apparent that there were general similarities in the nature of the $O_2$-uptake v. time plots. A typical plot , in this case for 1,4-butanediol , is shown in figure 2.3 and it is clear that it can be considered in two sections.

### 2.2.1 NEGATIVE REGION - HEATING EFFECT

Between ca. 0 and 12 minutes the oxygen-uptake became negative , indicating an apparent increase in temperature inside the reaction vessel. This appeared to be due to a slight heating effect since it was noted that on exposure to the lamp , there was an associated increase in temperature of the slurry , amounting to roughly 0.5K. An obvious source of heat was from the lamp itself. As well as supplying the ultra-violet light necessary for $TiO_2$ activation , the lamp gave off a certain amount of heat , attributable to an infra-red component in it s emission spectrum.

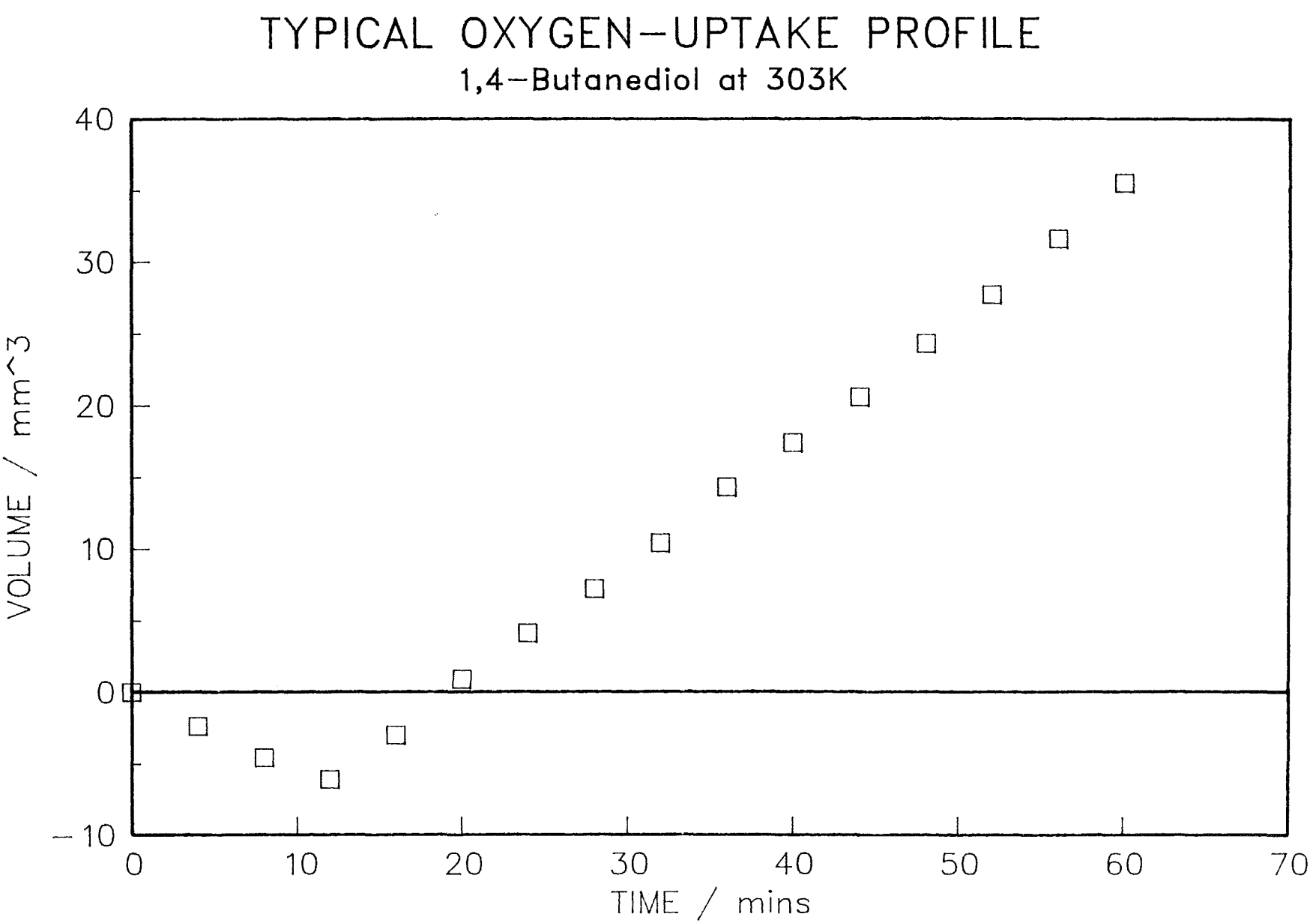
TYPICAL OXYGEN–UPTAKE PROFILE
1,4–Butanediol at 303K
VOLUME / mm^3
TIME / mins
40
30
20
10
0
−10
0
10
20
30
40
50
60
70

Figure 2.3

Another source of heat , however , may have been the $TiO_2$ itself. On irradiation of the pigment , electron/hole pairs ( excitons ) are generated

$$TiO_2 + hv \longrightarrow e^- + h^+ \qquad (2.1)$$

and these can suffer one of two fates. They can either be trapped by species on the $TiO_2$ surface ( equations 2.2 and 2.3 )

$$e^- + O_{2(ads)} \longrightarrow O_2^{-}{}_{(ads)} \qquad (2.2)$$

$$h^+ + OH^-{}_{(ads)} \longrightarrow OH^{\cdot}{}_{(ads)} \qquad (2.3)$$

or they can recombine ( eq. 2.4)

$$h^+ + e^- \longrightarrow HEAT \qquad (2.4)$$

It has been shown that at high light intensities , such as those provided by a medium pressure mercury arc

lamp , the dominant process in $TiO_2$ crystals is electron / hole recombination [9,48]. The energy released when the excited electron returns to the valence band is dissipated as heat throughout the crystal [49]. If sufficient heat were generated , it is conceivable that this process may be at least partly responsible for the initial temperature increase of the slurry.

In order to investigate this , two very simple experiments were carried out.

i) 100 mls. cyclohexane ( Fisons analytical grade) were measured out into the reaction vessel and stirred at the standard stirring rate while shielded from the U.V. lamp. The temperature of the cyclohexane was monitored and once it had been established to be constant the lamp cover was removed. The temperature was then measured at intervals of 30 seconds. Over a period of 10 minutes a rise of 0.5K was observed before it settled out at a new constant value. The data obtained is represented in figure 2.4.

ii) The above experiment was repeated , this time irradiating a slurry of 1g $TiO_2$ / 100 mls. cyclohexane. On exposure to the lamp , a rise in temperature of 0.5K over 10 mins. was again observed ( see also fig. 2.4 ). Both of these experiments were repeated several times with good reproducibility.

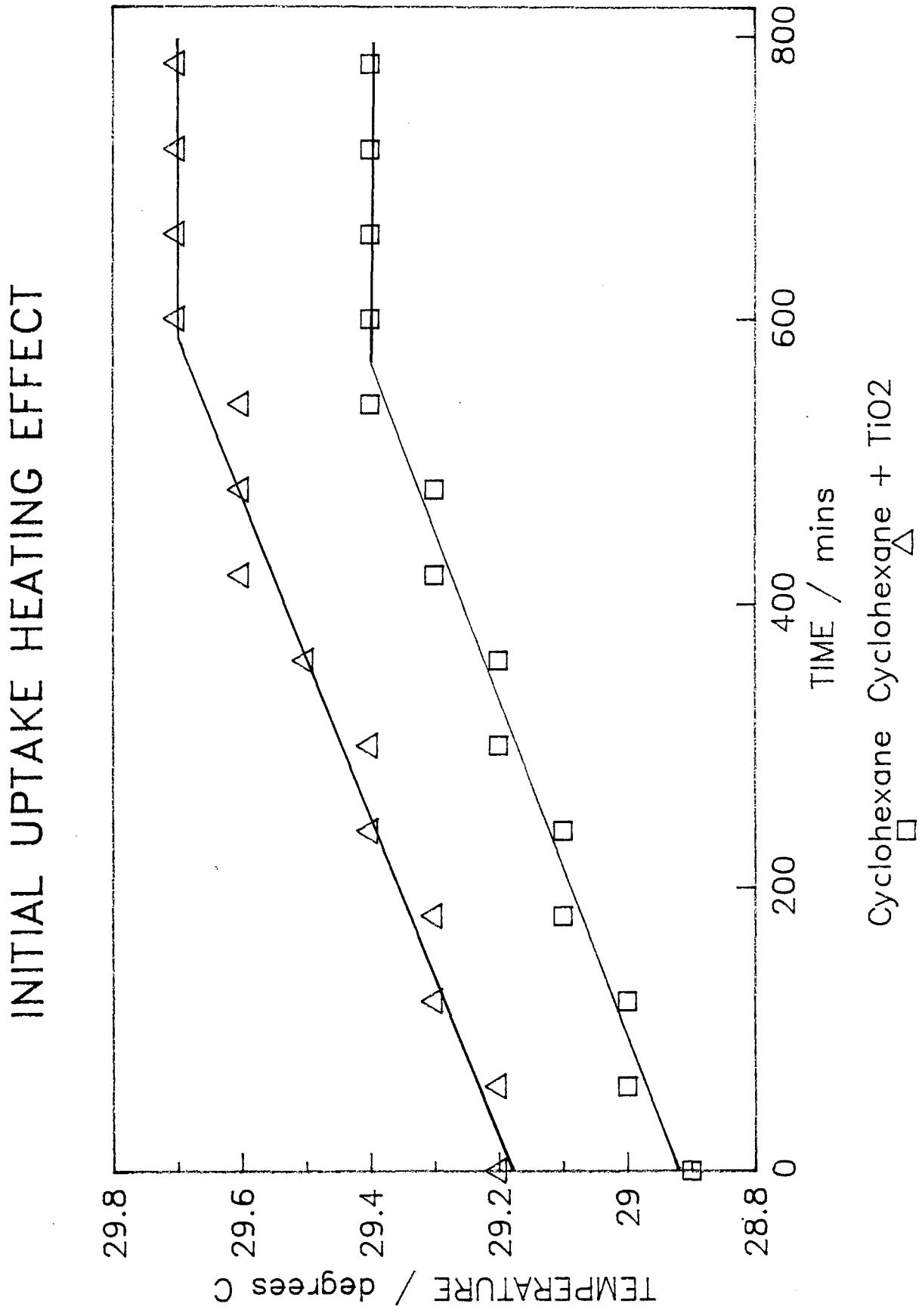
INITIAL UPTAKE HEATING EFFECT
TEMPERATURE / degrees C
29.8
29.6
29.4
29.2
29
28.8
0
200
400
600
800
TIME / mins
Cyclohexane
Cyclohexane + TiO2

Figure 2.4

The reason for using cyclohexane as the substrate was that it is inert as far as photocatalytic degradation by $TiO_2$ is concerned. In this way it was ensured that any heat evolved was not due to any reaction taking place.

The conclusion drawn from this work is that the observed initial temperature increase is due to theinfra-red component of the lamp. Any heat provided by electron / hole recombination must be negligible.

## 2.2.2 LINEAR REGION : PSEUDO-ZERO ORDER KINETICS

Once the temperature of the reaction cell had stabilised , after ca. 12 minutes , the oxygen-uptake rate became highly linear. The kinetics of the reaction were zero-order [50] with respect to the reactant concentration , thus

$$-d[R]/dt = k \qquad (2.5)$$

In fact , this is really an apparent zero-order situation , since the volume changes involved during a reaction are so small relative to the volume of air in the system that the oxygen partial pressure can be

considered to be constant. A parallel can be drawn with the reaction of iodine and acetone.

$$CH_3COCH_3 + I_2 \longrightarrow CH_3COCH_2I + HI \qquad (2.6)$$

This reaction is acid catalysed , and if the acid is in great excess , the reaction becomes zero-order in both iodine and acetone concentrations.

It is clear from equation 2.5 that the slope of the linear region will give the rate of oxygen-uptake , k , directly. This holds true for the particular conditions under which the experiment is carried out (e.g. lamp intensity , temperature , stirrer speed etc.). To standardise the analysis of the data , the reaction rate for any particular experiment was taken to be the slope over the period 20 - 60 minutes. This allowed time for thermal equilibration of the vessel and ensured that all observed pressure changes were due to photocatalytic oxidation of the substrate.

## 2.3 THE EFFECT OF TEMPERATURE

The main purpose of this work was to compare the photo-oxidation results for a number of compounds , under standard conditions , and to attempt to correlate these results with the functionality of the compounds in question. One parameter which could readily be varied to give useful information , however , was the temperature of the slurry. By varying the temperature of the water circulating in the jacket of the reaction vessel , oxygen-uptake rate determinations could be carried out at any temperature between ca. 293K and 345K.

In the cases where oxygen-uptake occurred , it was established that the slope of the plot increased as the temperature increased. Harvey et. al. [37] and Fraser et. al. [40] studied the effect of temperature variation on the rate of propanone formation in the propan-2-ol / $TiO_2$ system using the techniques described previously. From the rate data they collected, they were able to calculate activation energies for rutile-catalysed propanone formation as being 54 $kJmol^{-1}$ and 59 $kJmol^{-1}$ respectively.

With a view to obtaining activation energies of oxidation of the various substrates , variable temperature studies were carried out. The results of these studies are detailed in subsequent sections which deal with the compounds individually.

## 2.4 THE EFFECT OF OXYGEN PARTIAL PRESSURE

Another parameter which could readily be varied , if only to a limited extent , was the partial pressure of oxygen in the atmosphere above the slurry. However , due to the structure of the reaction cell , only qualitative experiments could be carried out. Two 'atmospheres' were looked at.

1) An atmosphere of air which would therefore be comprised of approximately 20% oxygen by volume.

2) An atmosphere comprised mainly of oxygen. This was achieved by thoroughly purging the slurry with $O_2$. Because of the way the manometer system had been constructed , it was impossible to ensure complete displacement of air. Since there was no way of knowing the actual partial pressure of $O_2$ in the system , only qualitative work could be carried out.

Details for individual substrates are given in the relevant sections but in all cases , the higher oxygen concentration led to an increase in oxygen-uptake rate. This can easily be rationalised in terms of zero-order kinetics.

There exists an equilibrium between the oxygen in the atmosphere in the vessel and that in solution,

$$O_{2(g)} \rightleftharpoons O_{2(soln)} \qquad (2.7)$$

with an associated equilibrium constant

$$K = [O_2]/p(O_2) \qquad (2.8)$$

If the oxygen-uptake rate is proportional to the partial pressure then , from equation 2.7 , we can say

$$\text{Rate} = k[O_2] \qquad (2.9)$$

where k is the rate constant for the reaction.

Combining equations 2.8 and 2.9 we have ,

$$\text{Rate} = k'Kp(O_2) \qquad (2.10)$$

where ,

k′= apparent rate constant for reaction

K = equilibrium constant

$p(O_2)$ = oxygen partial pressure

Since , over the period of a typical experiment , $p(O_2)$ does not undergo any significant change , the rate of reaction will remain constant. However , this constant includes the oxygen partial pressure and , in theory , if this parameter is increased , then the rate should increase proportionately.

## 2.5 OXIDATION OF 1,3-PROPANEDIOL AND 1,4-BUTANEDIOL

In this section , the results of using the oxygen-uptake technique to study the two substrates , 1,3-propanediol (I) and 1,4-butanediol (II) are presented.Both of these molecules contain two primary hydroxyl functions , the difference being that in (I) they are separated by 3 methylene units whilst in (II) they are separated by 4.

$HOCH_2CH_2CH_2OH$ (I)

$HOCH_2CH_2CH_2CH_2OH$ (II)

1,3-propanediol is a liquid at room temperature and thus presented no problems as far as it's use in the experimental system was cocerned. However , 1,4-butanediol is a low melting point solid (MPt. 25°C) and as a consequence , all oxygen uptake work had to be carried out at a temperature higher than this. In practice , all of the experiments carried out on these compounds were conducted at temperatures of greater than 30°C to help overcome their inherent viscosity.

It was anticipated that by obtaining information about the kinetics of photocatalysed oxidation and by identification of the resultant products , that some conclusions about the effect of chain length on the mechanism of the reaction could be drawn.

## 2.5.1 BLANK RUNS

Previous work had shown that in order for photocatalytic degradation of pigmented polymers to occur , $O_2$ and $H_2O$ had also to be present [12]. To check that the substrates under study conformed to these requirements , several blank runs were carried out using the oxygen-uptake equipment. The experimental details are outlined in brief below.

i) Absence of $TiO_2$

Each of the substrates , (I) and (II) , were stirred and irradiated at a range of temperatures (300K - 340K) in the absence of pigment. No oxygen-uptake was observed.

ii) Absence of $O_2$

Slurries of the substrates were made up in the usual manner. These were stirred and thoroughly purged with $N_2$. After closing the reaction vessel the oxygen-free systems were irradiated. No gas uptake was observed.

iii) Absence of $H_2O$

Exclusion of water from the system was not at all easy since both the pigment and the substrates used were hydrophilic in nature. In order to minimise the amount of water present , each of the diols were

distilled onto molecular seive (4A) and the $TiO_2$ was dried by pumping it down on a vacuum line using a diffusion pump and stored in a vacuum desiccator over $CaCO_3$. Prior to the experiment , the reaction vessel was dried in an oven. All materials were used as soon after drying as was possible. Oxygen-uptake rates under these conditions were negligible.

iv) Absence of U-V radiation

Pigment and substrate were stirred in the presence of water and oxygen but with the lamp switched off. No uptake was observed.

It was establihed that when the slurries were exposed to all of these parameters i.e $O_2$ , $H_2O$ and U-V light , oxygen-uptake proceeded readily. In this respect , 1,3-propanediol and 1,4-butanediol were seen to be satisfactory models for pigmented polymer degradation.

## 2.5.2 VARIATION OF TEMPERATURE

Once it had been established that both of the chosen substrates were oxidisable , runs were carried out for both at a variety of temperatures. The results of these experiments are summarised in tables 2.2 and 2.3. Plots of oxygen-uptake v. time at each of the temperatures are shown in figures 2.5 and 2.6 for 1,3-propanediol and 1,4-butanediol respectively.

It is apparent that the linearity of these plots in the time region studied is excellent and the slope was calculated by applying linear regression analysis to the data ( See appendix I ). The correlation coefficient , r , for the linear region was always greater than 0.99. In addition it was found that the same slurry could be used repeatedly giving results which were reproducible to within +/- 10%.

For the purpose of this work , only the slope of the oxygen-uptake isotherms is of any interest and for clarity , the plots have been 'normalised'. In other words , they have been modified in such a way that they retain their original slope but , on extrapolation , pass through the origin.

As was explained earlier , the rate data were calculated using results taken from 20 minutes into each run to allow time for equilibration of the slurry.

The rate of reaction , k , is given by the Arrhenius equation ,

$$k = A \exp(-E/RT) \qquad (2.11)$$

in which A is a constant dependent on a number of parameters , R and T are the gas constant and the absolute temperature respectively and E is the activation energy of the reaction expressed in $kJmol^{-1}$. Thus , provided that rate measurements at different temperatures are carried out under the same

concentration conditions , the energy of activation may be calculated from the slope of a plot of ln(k) vs. 1/T.

From the rate data obtained , Arrhenius plots for each of the substrates were constructed (figures 2.7 and 2.8). It is clear from these graphs that a linear relationship exists for both substrates. This suggests that in both cases there exists a single rate determining process , giving a single valued activation energy.

**1,3-PROPANEDIOL**

| T (K) | k ($mols^{-1}$) | 1/T ($10^{-3}$/K) | ln (k) |
|---|---|---|---|
| 301.5 | $5.63x10^{-10}$ | 3.32 | -21.30 |
| 307.5 | $6.76x10^{-10}$ | 3.25 | -21.11 |
| 313.0 | $6.81x10^{-10}$ | 3.19 | -21.10 |
| 328.0 | $10.90x10^{-10}$ | 3.05 | -20.64 |
| 335.5 | $14.11x10^{-10}$ | 2.98 | -20.38 |

r = -1.00 A.E. = 22.2 $kJmol^{-1}$

Table 2.2

**1,4-BUTANEDIOL**

| T (K) | k ($mols^{-1}$) | 1/T ($10^{-3}$/K) | ln (k) |
|---|---|---|---|
| 303.5 | $5.76x10^{-10}$ | 3.29 | -21.27 |
| 309.0 | $7.15x10^{-10}$ | 3.24 | -21.06 |
| 313.5 | $7.44x10^{-10}$ | 3.19 | -21.02 |
| 330.0 | $11.47x10^{-10}$ | 3.03 | -20.59 |
| 338.5 | $14.40x10^{-10}$ | 2.95 | -20.36 |

r = -0.98 A.E. = 21.4$kJmol^{-1}$

Table 2.3

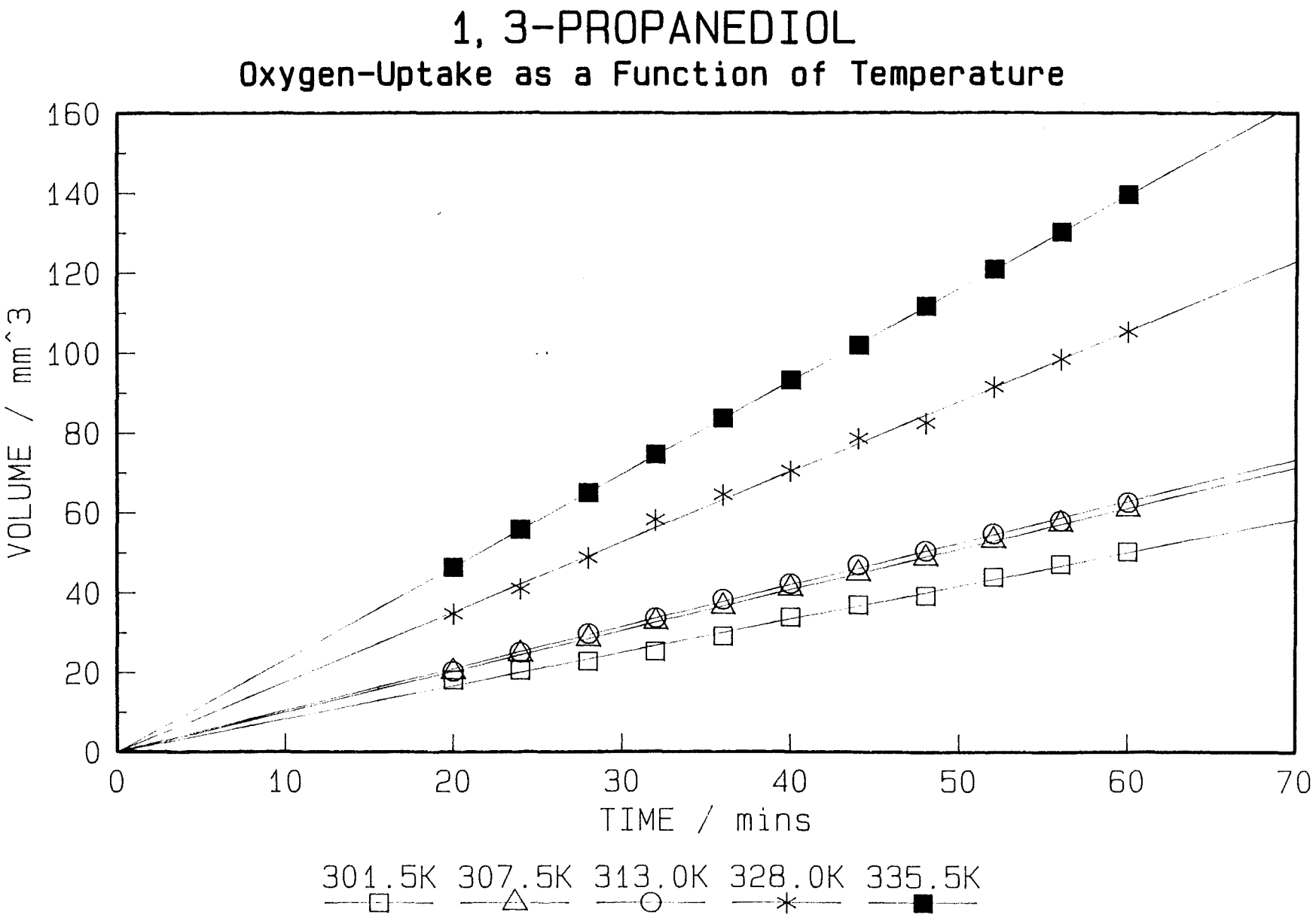
1, 3-PROPANEDIOL
Oxygen-Uptake as a Function of Temperature
VOLUME / mm^3
TIME / mins
0
20
40
60
80
100
120
140
160
0
10
20
30
40
50
60
70
301.5K
307.5K
313.0K
328.0K
335.5K

Figure 2.5

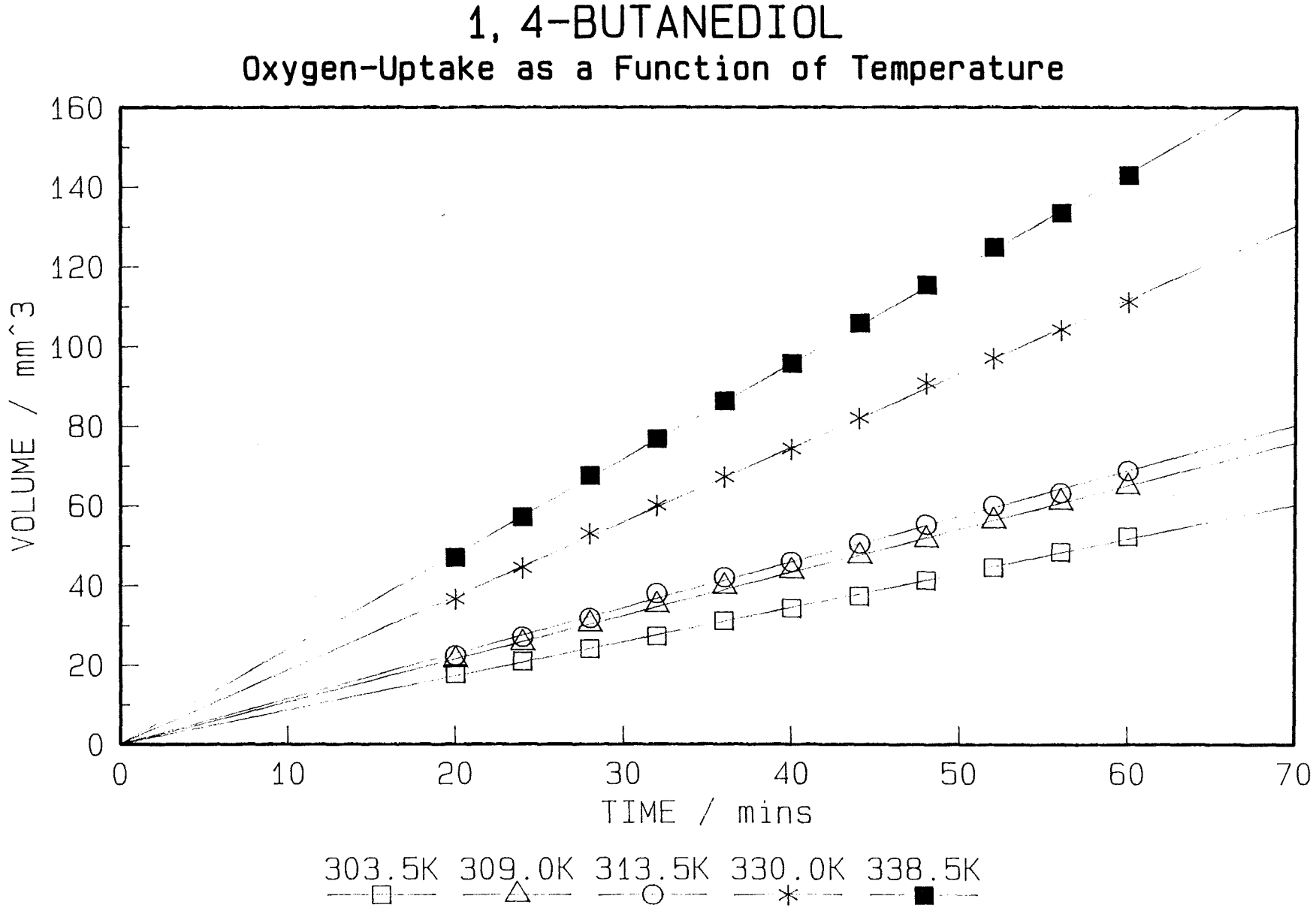
1, 4-BUTANEDIOL
Oxygen-Uptake as a Function of Temperature
VOLUME / mm^3
TIME / mins
0
20
40
60
80
100
120
140
160
0
10
20
30
40
50
60
70
303.5K
309.0K
313.5K
330.0K
338.5K

Figure 2.6

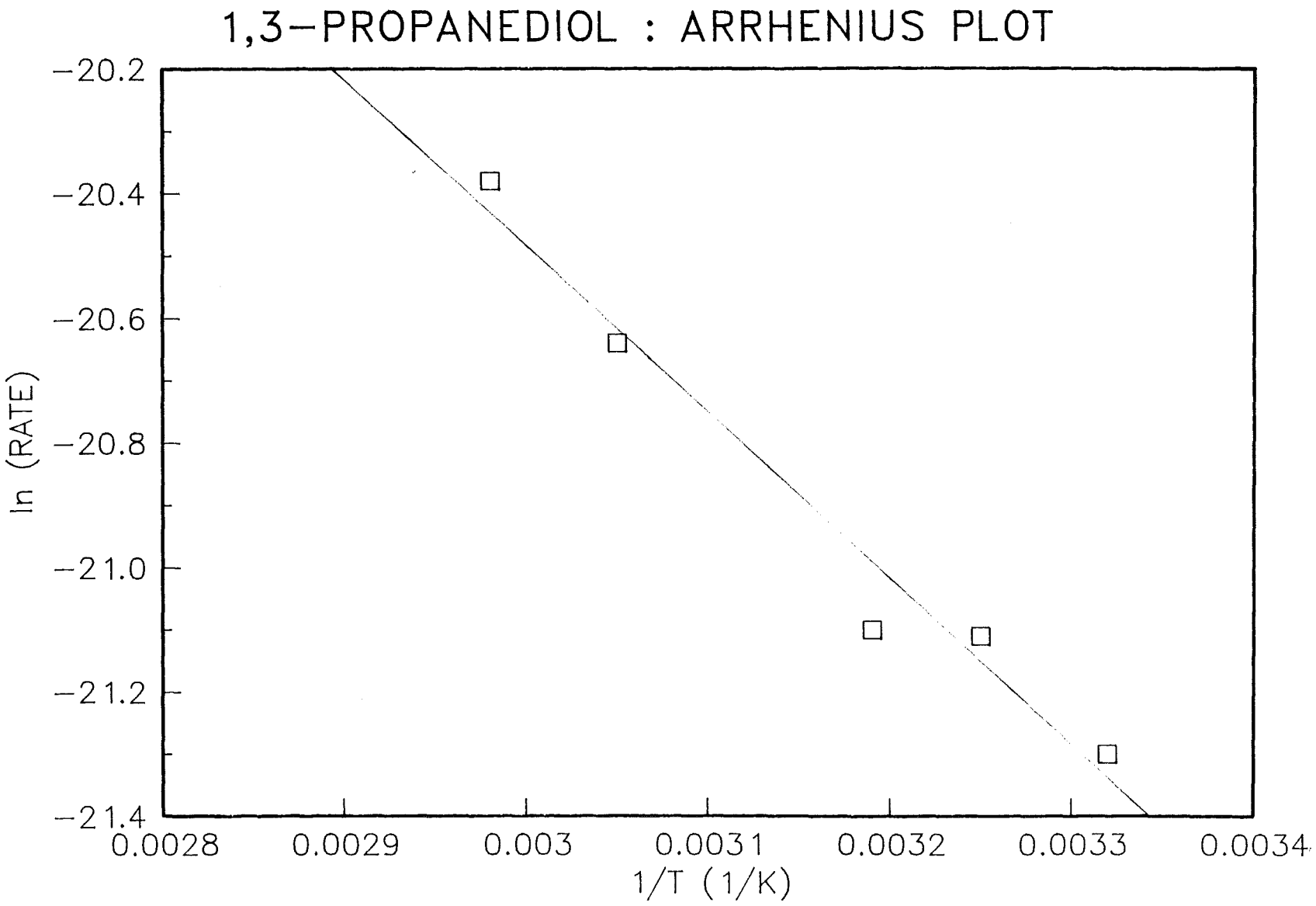
1,3–PROPANEDIOL : ARRHENIUS PLOT
ln (RATE)
−20.2
−20.4
−20.6
−20.8
−21.0
−21.2
−21.4
0.0028
0.0029
0.003
0.0031
0.0032
0.0033
0.0034
1/T (1/K)

Figure 2.7

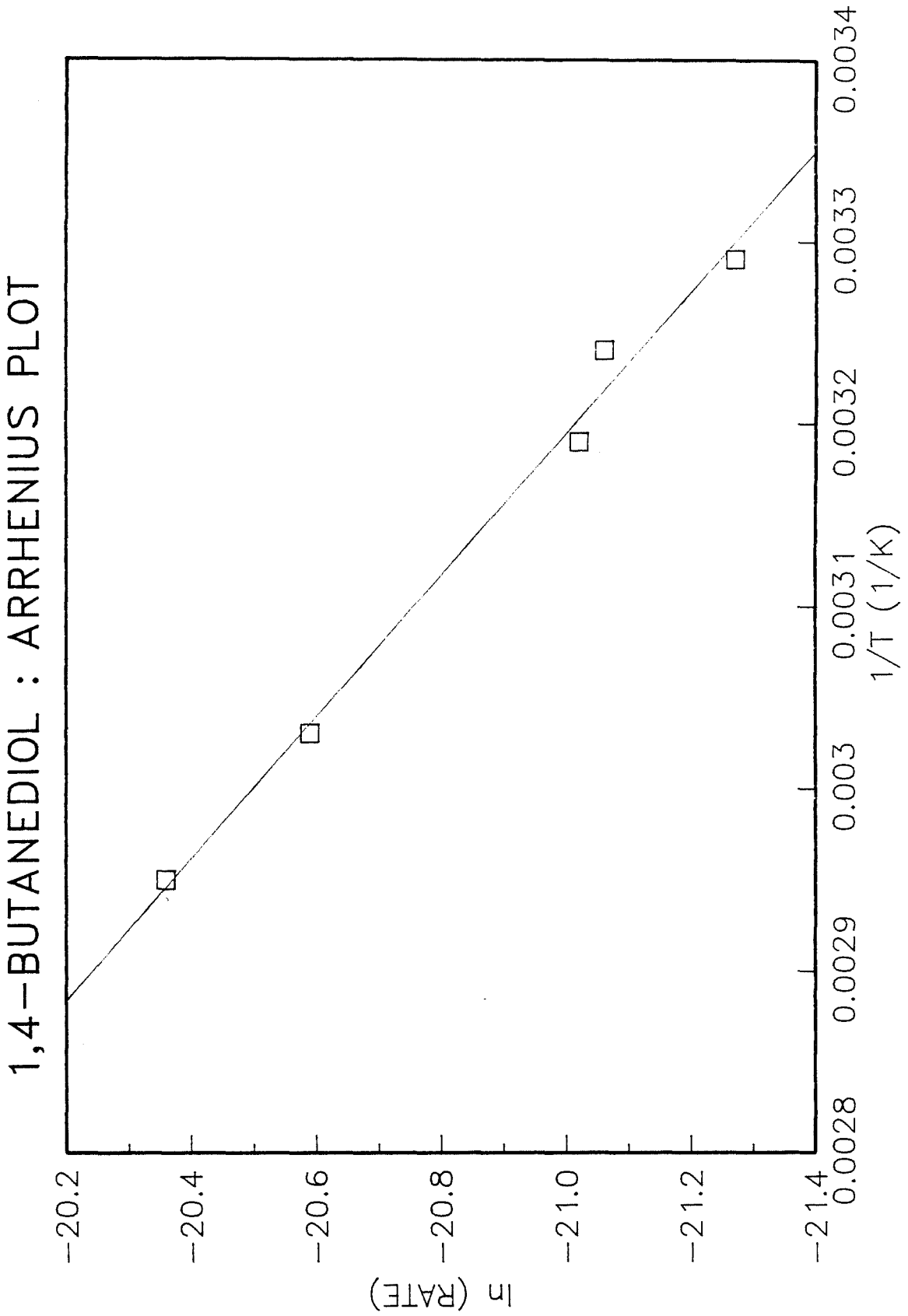
1,4-BUTANEDIOL : ARRHENIUS PLOT
ln (RATE)
-20.2
-20.4
-20.6
-20.8
-21.0
-21.2
-21.4
0.0028
0.0029
0.003
0.0031
0.0032
0.0033
0.0034
1/T (1/K)

Figure 2.8

It is interesting to note the close similarity between the two activation energies and it is probable that the rate determining step for the oxidation of both diols is the same in each case. These activation energies are compared with that obtained for the rutile catalysed photo-oxidation of propan-2-ol , as measured by Fraser et. al. [40] using the oxygen-uptake technique , in table 2.4.

| Substrate | A.E. ($kJmol^{-1}$) |
|---|---|
| 1,3-propanediol | 22.2 |
| 1,4-butanediol | 21.4 |
| propan-2-ol | 59.2 |

Table 2.4

It is immediately obvious that there is a large difference between these values , the activation energy for propan-2-ol oxidation being approximately a factor of 2 greater than those for the two diols. One major difference between the diols and the mono-alcohol is that the former contain primary hydroxyl functions while the latter contains a secondary hydroxyl.

Work has been carried out by Harvey et. al. [38] on the rutile photocatalysed oxidation of ethanol and propan-1-ol , both primary alcohols. In this case the rate of ketone formation was monitored by gas-liquid chromatography. A.E.s are given in table 2.5.

| Substrate | A.E (kJmol$^{-1}$) | REF |
|---|---|---|
| ethanol | 28 | [38] |
| propan-1-ol | 28 | [38] |

Table 2.5

These values are much closer to those obtained for diol photo-oxidation. It would therefore seem that the activation energy is dependent on the type of functional group being oxidised.

## 2.5.3 VARIATION OF $O_2$ PARTIAL PRESSURE

As described in section 2.4 , the rates of photo-oxidation of 1,4-butanediol and 1,3 propanediol were measured in an atmosphere of $O_2$ and compared to the rates when run in air. The results are summarised in table 2.6 and shown graphically in figures 2.9 and 2.10.

| | SUBSTRATE | |
|---|---|---|
| | 1,3-propanediol | 1,4-butanediol |
| $RATE_{AIR}$ (mols$^{-1}$) | $6.6 \times 10^{-10}$ | $6.8 \times 10^{-10}$ |
| $RATE_{O2}$ (mols$^{-1}$) | $27.0 \times 10^{-10}$ | $25.8 \times 10^{-10}$ |
| FACTOR INCREASE | 4.1 | 3.8 |

Table 2.6

These results were obtained at a temperature of 315 K . Obviously it was important to compare rates at the same temperature since this parameter also had a significant influence on the rate.

The kinetics explaining the rate increase are also detailed in section 2.4. An increase by a factor of 5 would be expected since the oxygen concentration had been increased from 20% in air to approximately 100% after the system had been thoroughly purged by $O_2$. The figures obtained are lower than this and can probably be explained by the fact that it was impossible to ensure a 100% $O_2$ atmosphere by virtue of the nature of the experimental set-up used.

It is interesting to note that similar work carried out by Fraser [40] on the propan-2-ol / rutile system showed no increase in uptake rate with increasing oxygen partial pressure.

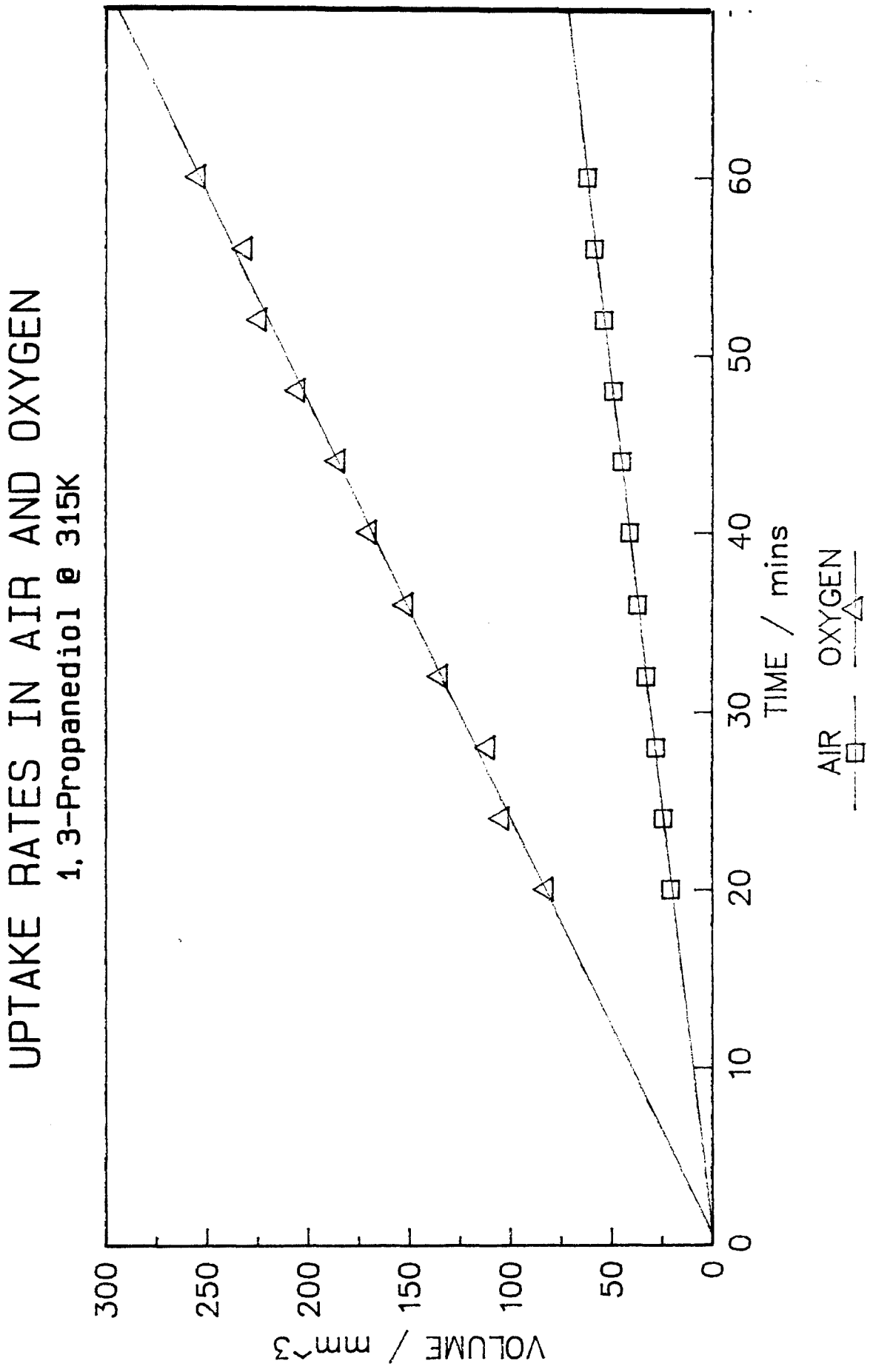
UPTAKE RATES IN AIR AND OXYGEN
1,3-Propanediol @ 315K
VOLUME / mm^3
300
250
200
150
100
50
0
0
10
20
30
40
50
60
TIME / mins
AIR
OXYGEN

Figure 2.9

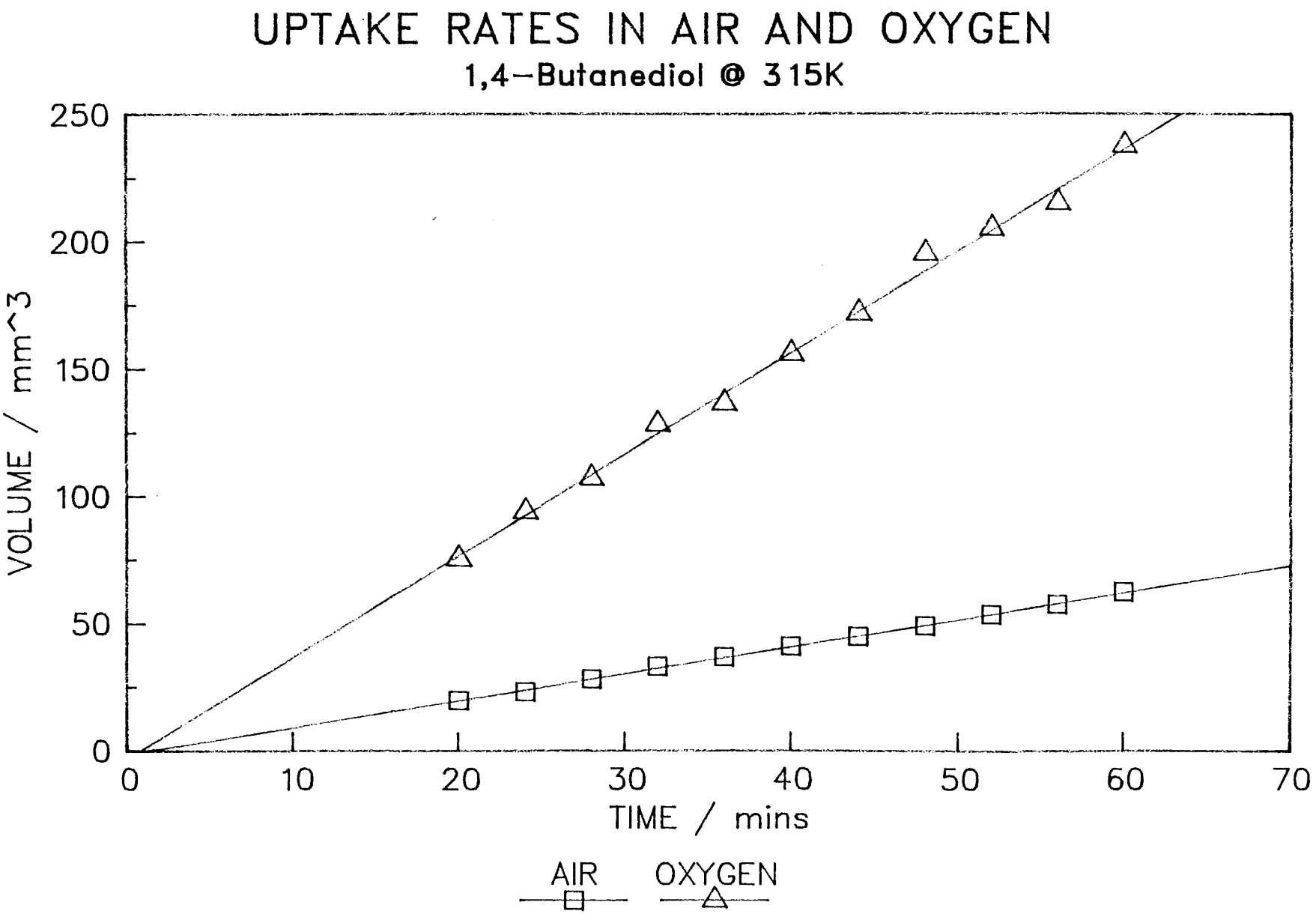
UPTAKE RATES IN AIR AND OXYGEN
1,4-Butanediol @ 315K
VOLUME / mm^3
250
200
150
100
50
0
0
10
20
30
40
50
60
70
TIME / mins
AIR
OXYGEN

Figure 2.10

## 2.5.4 IDENTIFICATION OF PRODUCTS

2 methods were used to characterise the oxidation products of the diols , namely ,

i) Infra-red spectroscopy

ii) Melting point of 2,4-dinitrophenylhydrazine derivative.

The major problem with product identification was the fact that , relatively speaking , the amount of product generated over the period of an oxygen-uptake run was very small. Typical uptake rates of $10^{-10}$ to $10^{-9}$ $mols^{-1}$ were observed , depending on reaction conditions. Thus , assuming a 1:1 oxygen to substrate reaction stoichiometry , it is easy to calculate that only ca. $10^{-6}$ moles of product will be formed in a 1-2 hour period. In order to increase product yield , 1,3-propanediol and 1,4-butanediol were photocatalytically oxidised for periods of ca. 100 hours , the reaction vessel having first been purged with $O_2$ beforehand.

### 2.5.4.1 INFRA-RED SPECTRA

Infra-red spectra of each of the diols were run before and after oxidation on a Perkin-Elmer 1420 Ratio Recording Infra-red Spectrophotometer. In order to sparate the pigment from the substrate , samples were taken from the slurry and cetrifuged. A drop of the

supernatant liquid was then placed between the NaCl disks and the spectrum run. Figures 2.11 and 2.12 show the spectra obtained for 1,4-butanediol ; 1,3-propanediol gave very similar results. The important feature to notice is the appearance of a peak at 1710$cm^{-1}$ in the spectrum of the photo-oxidised material. It would appear on this evidence that a carbonyl grouphad been formed via the oxidation of one of the diol hydroxyls. This conversion is represented below.

$$HO(CH_2)_4OH \text{ -----> } HO(CH_2)_3CHO \qquad (2.12)$$

**(III)**

III = 4-hydroxybutanal

In the case of 1,3-propanediol , a peak appeared at 1705 $cm^{-1}$ , again corresponding to the introduction of a carbonyl function to the molecule.

$$HO(CH_2)_3OH \text{ -----> } HO(CH_2)_2CHO \qquad (2.13)$$

**(IV)**

IV = 3-hydroxypropanal

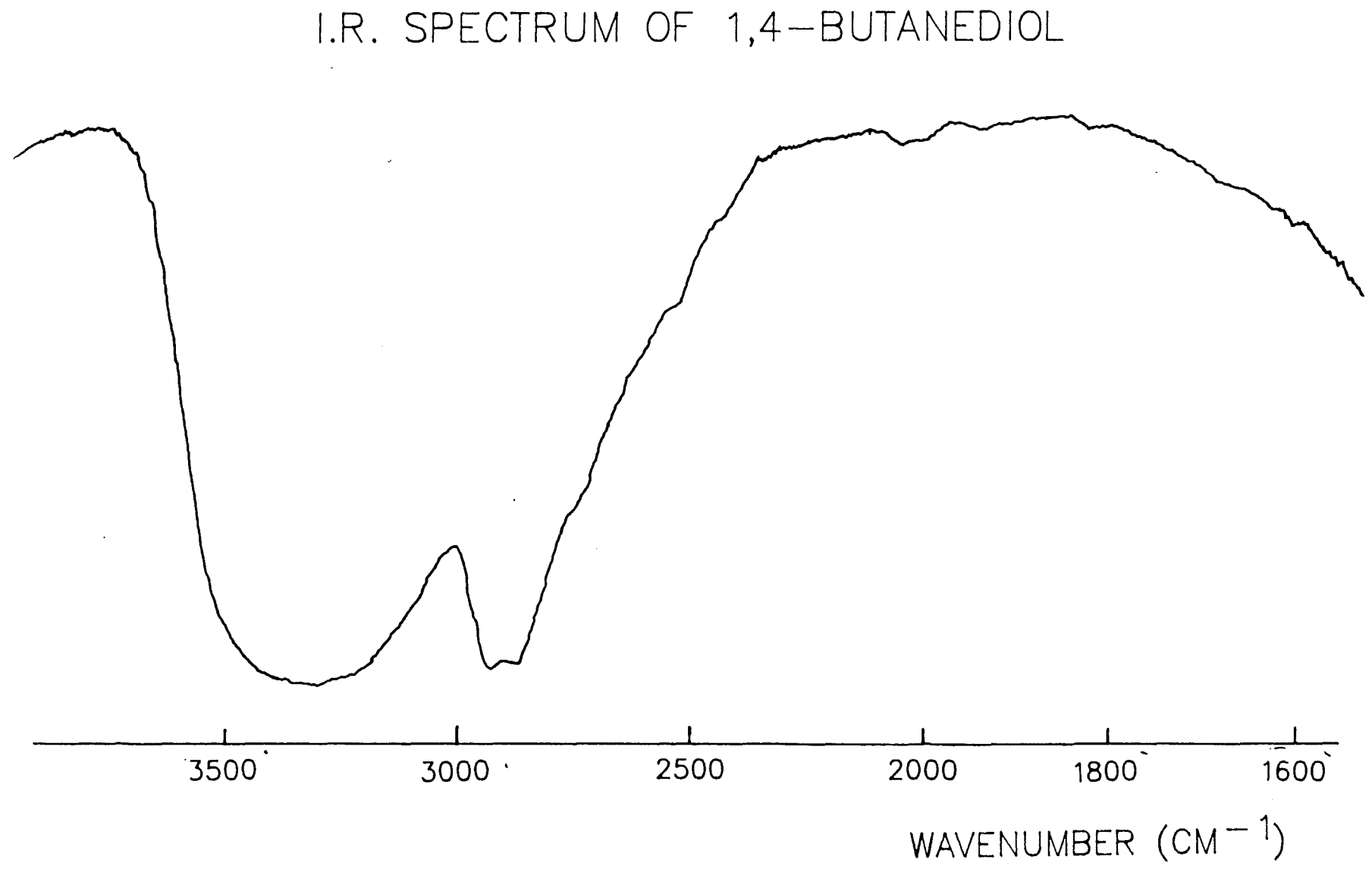
I.R. SPECTRUM OF 1,4—BUTANEDIOL
3500
3000
2500
2000
1800
1600
WAVENUMBER (CM⁻¹)

Figure 2.11

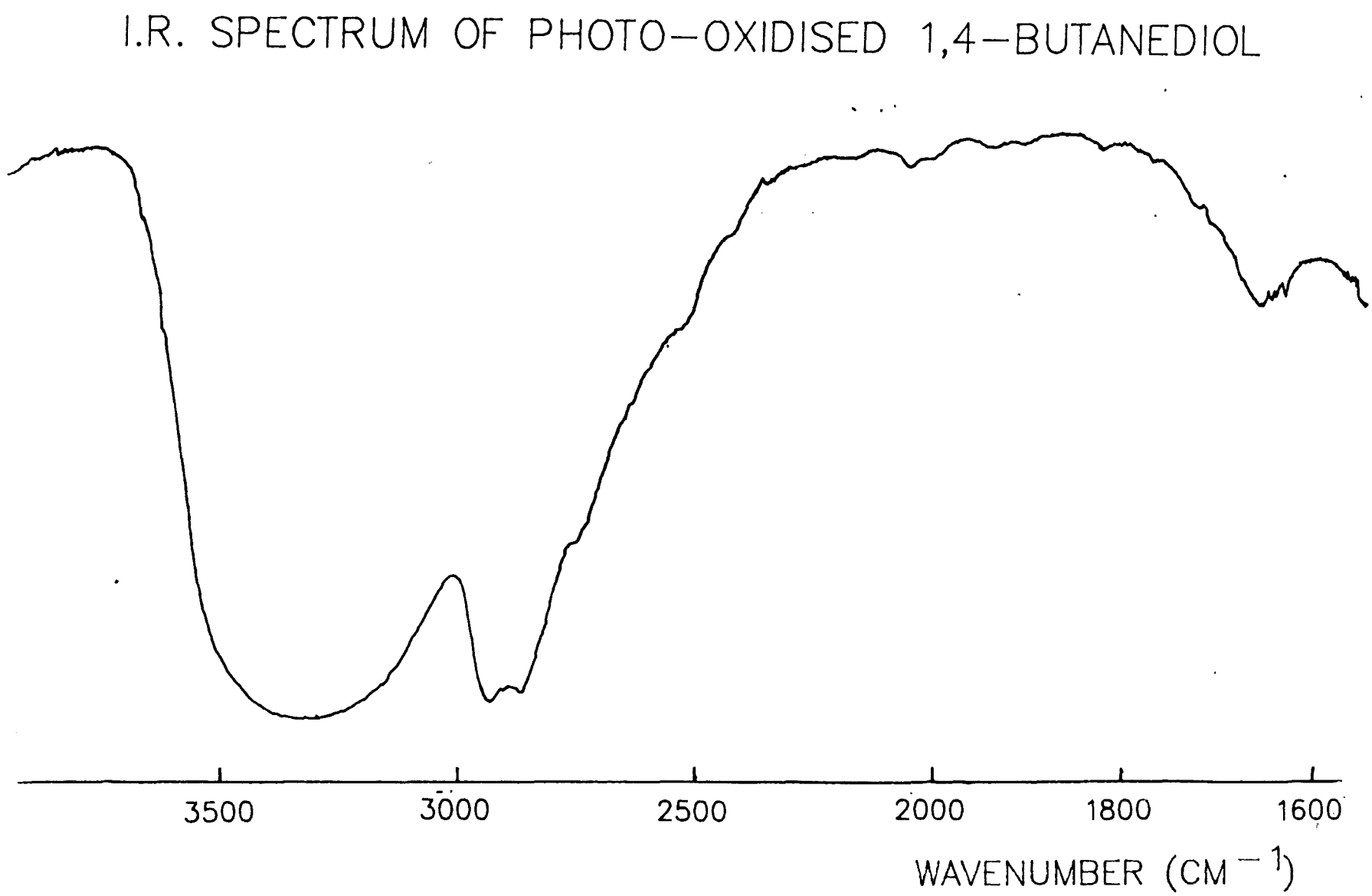
I.R. SPECTRUM OF PHOTO-OXIDISED 1,4-BUTANEDIOL
3500
3000
2500
2000
1800
1600
WAVENUMBER (CM⁻¹)

Figure 2.12

## 2.5.4.2 2,4-DINITROPHENYLHYDRAZINE DERIVATIVES

In order to verify that the products were as stated above it was decided to prepare their 2,4-dinitrophenylhydrazine derivatives ( V , 2,4-DNPH).

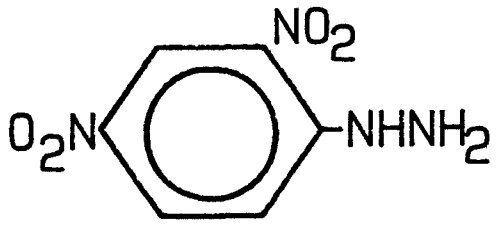


(V)

A solution of 2,4-DNPH in acid/ethanol ( Brady's reagent ) was prepared as described in the experimental section. As before , samples of the photo-oxidised slurry were taken and centrifuged. The clear substrate was transferrsd to a boiling tube and to it was added an excess of Brady's reagent. At this point it was assumed that any reaction which took place would be between any carbonyl species present and the reagent.

In the case of both oxidised 1,3-propanediol and 1,4-butanediol an orange precipitate formed. This precipitate was subsequently filtered off , dried and recrystallised from ice cold methanol. The melting points of the resulting crystals were measured using Gallenkamp melting point apparatus. The results are shown in table 2.7

| PRODUCT | M.PT OF DERIVATIVE | LIT. VALUE |
|---|---|---|
| III | 128-131°C | 133.0°C [51] |
| IV | 115-117°C | 118.0°C [52] |

Table 2.7

Since the melting points obtained were in good agreement with the quoted literature values , it was concluded that the oxidation products were in fact III and IV.

## 2.5.5 DETECTION OF HYDROGEN PEROXIDE

Previous work on $TiO_2$ / propan-2-ol systems had shown that during photo-oxidation , a quantity of hydrogen peroxide formed [37,40]. The peroxide appeared to build up to a steady state concentration during the first few minutes of the reaction and was believed to play an important role in the oxidative mechanism.

It was decided to investigate whether or not any $H_2O_2$ was formed as a result of photo-oxidation of either or both of the diols. This was done by sampling photo-oxidised slurries of the two compounds , centrifuging and testing the supernatant liquids with an acidic $Ti^{4+}$ solution. The preparation of this solution is described in the experimental section (2.1.3). The presence of $H_2O_2$ was shown by the formation of a characteristic yellow-red $Ti^{4+}$ / $H_2O_2$ complex as described by Schwarzenbach et. al. [45,46].

This constitutes an extremely sensitive test for hydrogen peroxide.

Both 1,3-propanediol and 1,4-butanediol gave positive results to this test after photocatalytic oxidation. On testing prior to reaction , no complex was detected in either case. No attempt was made to quantify the amount of hydrogen peroxide formed.

## 2.6 OXIDATION OF 1,3-BUTANEDIOL

The previous section looked at the oxidation of two compounds containing two primary hydroxyl groups. In this section , a molecule with both a primary and a secondary hydroxyl function was studied using the oxygen-uptake technique , namely 1,3-butanediol (VI).

$$HOCH_2CH_2CH(OH)CH_3$$

**(VI)**

1,3-butanediol is a liquid at room temperature and was thus appropriate for use in the experimental system. As with 1,4-butanediol and 1,3-propanediol , blank runs were carried out. These established that the presence of $O_2$ , $H_2O$ , pigment and ultra-violet light were all necessary for oxygen-uptake to occur. 1,3-butanediol was therefore deemed to be a suitable model for pigmented polymer photo-oxidation.

The kinetics of photo-oxidation of this compound were studied by varying the temperature and $O_2$ partial pressure. The results obtained were compared with those for I and II to establish the effect of having two different hydroxyl functions in the same molecule.

## 2.6.1 VARIATION OF TEMPERATURE

Oxygen-uptake runs were carried out , using 1,3-butanediol as the substrate , at various temperatures in the range 303K - 345K. The experimental results are summarised in table 2.8 and figures 2.13 and 2.14 show the oxygen-uptake isotherms and the Arrhenius plot which was constructed from the rate data obtained. Again , the oxygen-uptake v. time plots have been normalised for the sake of clarity and againthey all displayed a high degree of linearity. All correlation coefficients were greater than 0.99 and experimental runs could be repeated at each temperature to give rates which were within $^{+}/_{-}$ 10% of each other.

### 1,3-BUTANEDIOL

| T (K) | k ($mols^{-1}$) | 1/T ($10^{-3}$/K) | ln (k) |
|---|---|---|---|
| 303.0 | $1.96 \times 10^{-10}$ | 3.30 | -22.35 |
| 309.0 | $6.30 \times 10^{-10}$ | 3.24 | -21.19 |
| 315.0 | $9.80 \times 10^{-10}$ | 3.17 | -20.74 |
| 323.0 | $14.60 \times 10^{-10}$ | 3.10 | -20.34 |
| 329.7 | $16.90 \times 10^{-10}$ | 3.03 | -20.20 |
| 336.5 | $19.77 \times 10^{-10}$ | 2.97 | -20.04 |
| 344.1 | $22.14 \times 10^{-10}$ | 2.91 | -19.93 |

Table 2.8

However , it is immediately obvious that the Arrhenius plot is distinctly non-linear. The logical conclusion to be drawn from this observation is that , in this case , there is no longer a single rate determining step in the photo-oxidation mechanism.

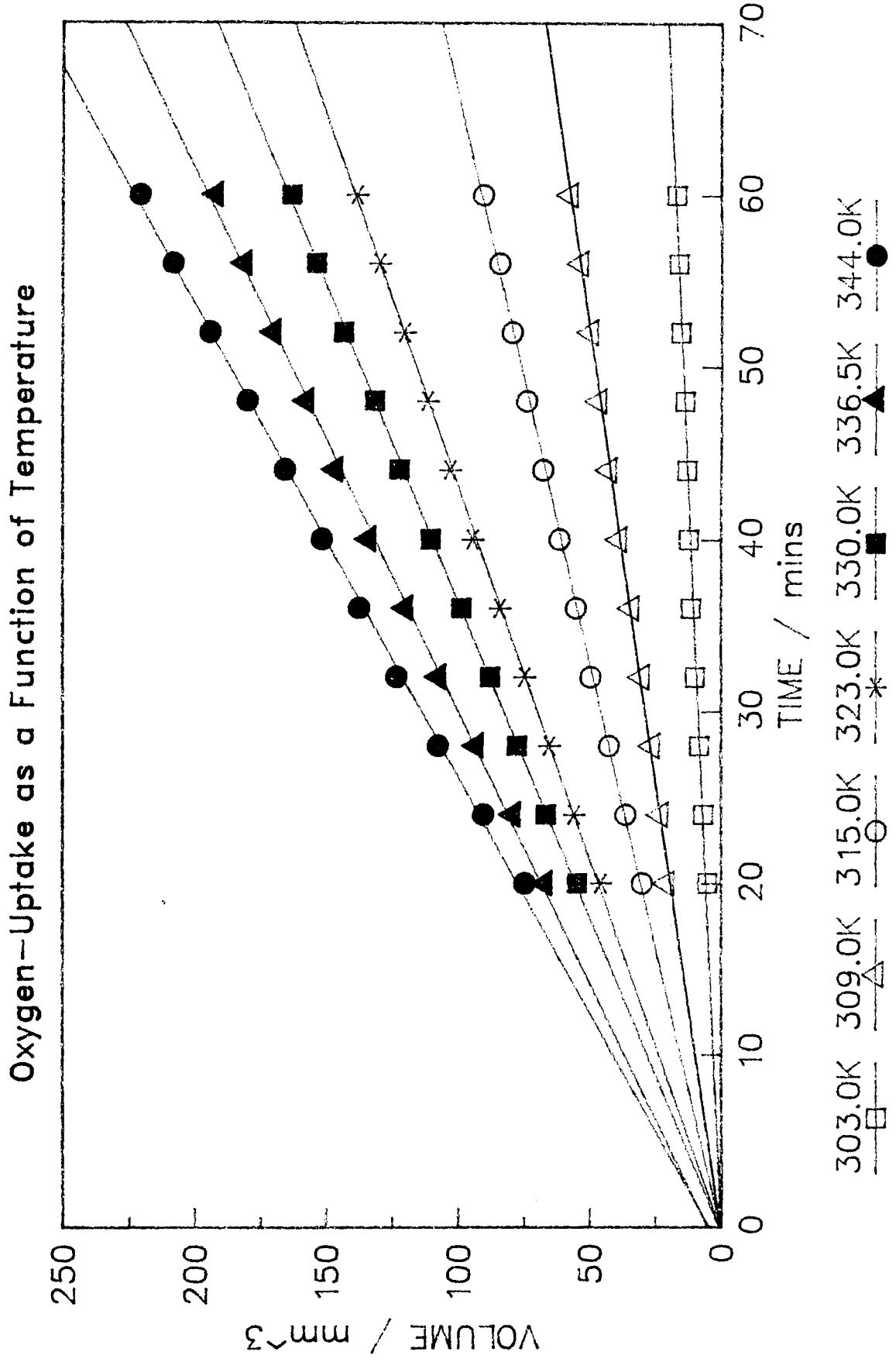
1,3-BUTANEDIOL
Oxygen-Uptake as a Function of Temperature
VOLUME / mm^3
250
200
150
100
50
0
0
10
20
30
40
50
60
70
TIME / mins
303.0K
309.0K
315.0K
323.0K
330.0K
336.5K
344.0K

Figure 2.13

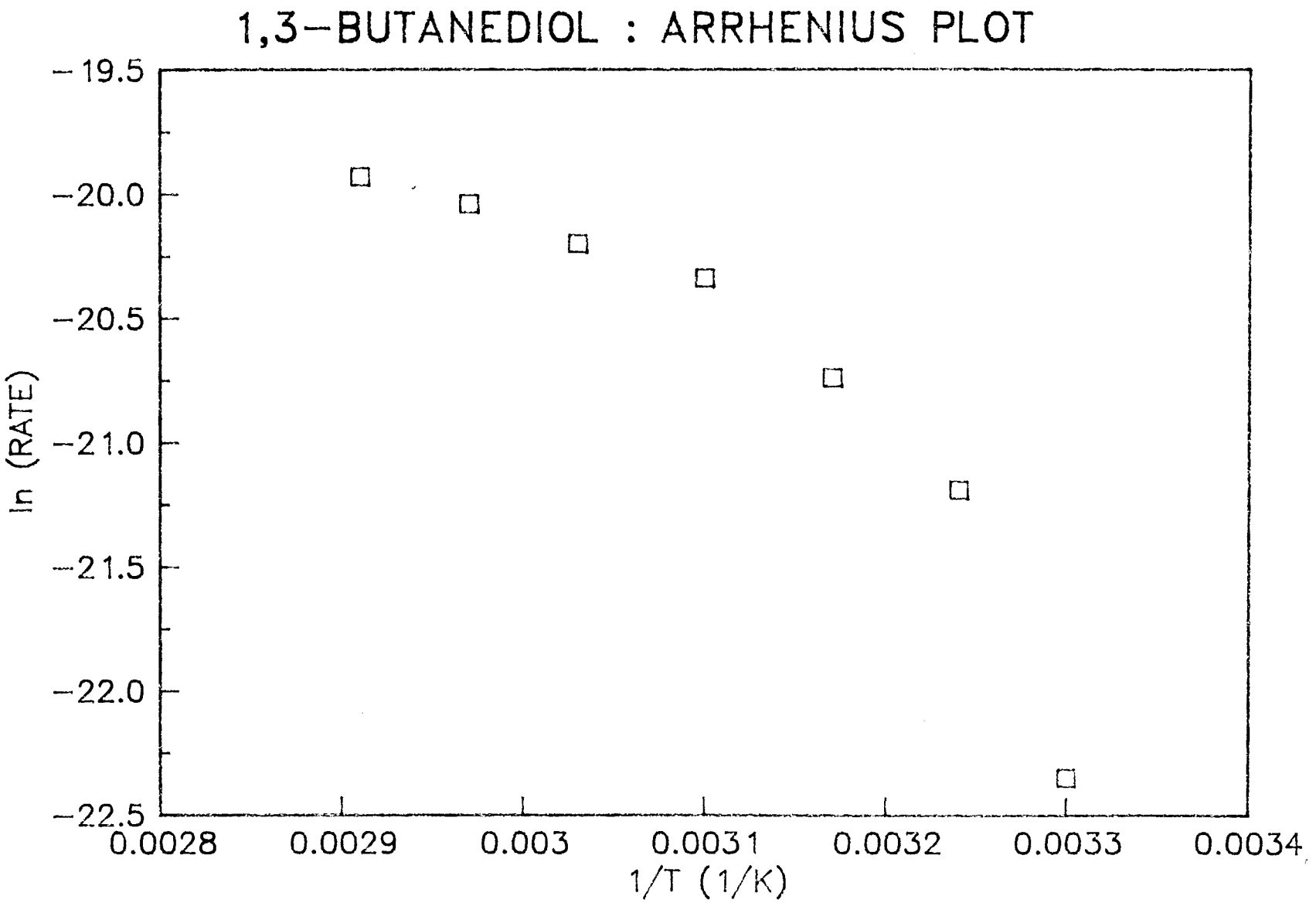
1,3-BUTANEDIOL : ARRHENIUS PLOT
-19.5
-20.0
-20.5
-21.0
-21.5
-22.0
-22.5
ln (RATE)
0.0028
0.0029
0.003
0.0031
0.0032
0.0033
0.0034
1/T (1/K)

Figure 2.14

On closer examination of the plot , it would appear that the points obtained at the 4 higher temperatures lie on a straight line. The slope of the line through these 4 points was measured and from it an activation energy of 18.3 $kJmol^{-1}$ was calculated. Obviously this activation energy is only valid over the temperature range 323K - 345K. It is interesting to note that it is of the same order of magnitude as those obtained for the primary diols in the previous section. No attempt was made to extract an activation energy from the remaining three points since it was felt that any figure obtained would be meaningless. However it is apparent that it increases over this lower temperature region.

It should be remembered that the substrate under study contained a primary and a secondary hydroxyl function. One explanation for the non-Arrhenius behaviour may be that there is intra-molecular competition for oxidation between the two hydroxyl groups. At higher temperatures , oxidation of the primary hydroxyl dominates , hence the activation energy of similar order of magnitude to those of primary diols. At lower temperatures , oxidation of the secondary hydroxyl comes into play and the resultant activation energy is then a function of the photo-oxidation of both groups. This increase in activation energy can be rationalised in light of the fact that

secondary hydroxy photo-oxidation has a higher A.E. than that for a primary hydroxyl group.

One of the pre-requisites for photocatalytic oxidation of the alcohols to take place was that they had to be bound to the surface of the pigment by some means. In the slurries used for these reactions the substrates will be in a dynamic state. Individual molecules will continually be adsorbed on the rutile surface and desorbing to the bulk liquid. As a consequence , the following equilibrium will be set up:

$$[TiO_2][S]_{ads} \underset{}{\overset{k_1}{\rightleftharpoons}} [TiO_2] + [S]_{bulk} \qquad (2.13)$$

where $[S]_{ads}$ = adsorbed substrate and $[S]_{bulk}$ = substrate in the bulk.

The rate of adsorption / desorption , $k_1$ , will be dependent upon the temperature of the slurry and the strength of the substrate bond to the $TiO_2$. It would appear , therefore , that the primary hydroxyl in 1,3-butanediol is more firmly bound than the secondary and at higher temperatures the rate of adsorption / desorption of the secondary is so great that it has little chance of being oxidised. Thus oxidation of the primary hydroxyl dominates at higher temperatures.

Neagle and Rochester [53] studied the adsorption of 1,4-butanediol , 1,3-butanediol and 2,3-butanediol on silica using Fourier Transform Infra-red

spectroscopic techniques. The conclusion from this work was that the relative binding strengths of these substrates to silica surface decreased in the order :

1,4-butanediol > 1,3-butanediol > 2,3-butanediol

Thus it would appear that the binding energy for a primary hydroxyl to silica is greater than that for a secondary. This work , albeit involving a different surface , would seem to back up the conclusions drawn form the work on 1,3-butanediol.

## 2.6.2 EFFECT OF $O_2$ PARTIAL PRESSURE

The rate of photo-oxidation of 1,3-butanediol / $TiO_2$ was measured in an atmosphere of $O_2$ and compared to the rate when run in air at an equivalent temperature. The results of this experiment are shown in table 2.9.

| $RATE_{AIR}$ ($mols^{-1}$) | $RATE_{O_2}$ ($mols^{-1}$) | FACTOR INCREASE |
|---|---|---|
| $9.8x10^{-10}$ | $38.3x10^{-10}$ | 3.9 |

Table 2.9

As in the cases of 1,4-butanediol and 1,3-propanediol , there is a marked increase in the rate of reaction as the oxygen partial pressure in the reaction vessel increases. Again the expected factor increase of

5 was not seen , probably due to incomplete purging by $O_2$.

## 2.6.3 IDENTIFICATION OF PRODUCTS

As was noted in previous experiments , the major problem with product identification was that the amount formed was extremely small over the timescale of a typical experiment. To overcome this , an extended run (ca. 100 hrs. ) was carried out using a slurry which had been thoroughly purged with $O_2$.

### 2.6.3.1 INFRA-RED SPECTRUM

After centrifuging an aliquot of the photo-oxidised slurry , an I,R. spectrum was run. Figures 2.15 and 2.16 show the spectra of 1,3-butanediol before and after reaction respectively. It is immediately apparent that two peaks have appeared in the latter spectrum , one at 1660 $cm^{-1}$ and the other at 1705 $cm^{-1}$. These peaks correspond to carbonyl vibrational frequencies.

### 2.6.3.2 2,4-DINITROPHENYLHYDRAZINE DERIVATIVES

Attempts were made to synthesise , isolate and characterise the 2,4-DNPH derivatives of the carbonyl compounds , evidenced by the I.R. spectra , in the usual manner. On adding Brady's reagent to a sample of the photo-oxidised liquid , orange crystals were

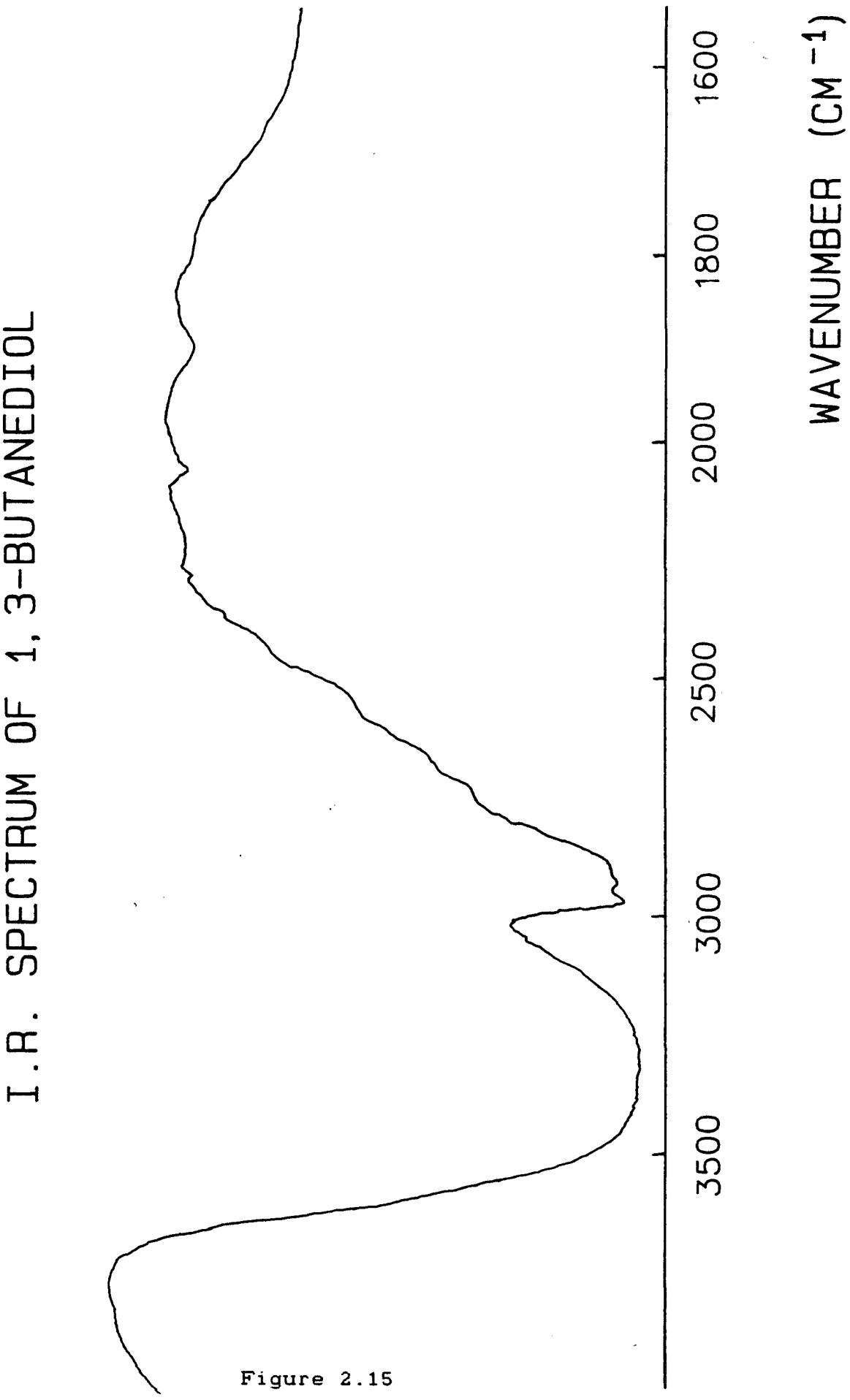
I.R. SPECTRUM OF 1,3-BUTANEDIOL
3500
3000
2500
2000
1800
1600
WAVENUMBER (CM -1)

Figure 2.15

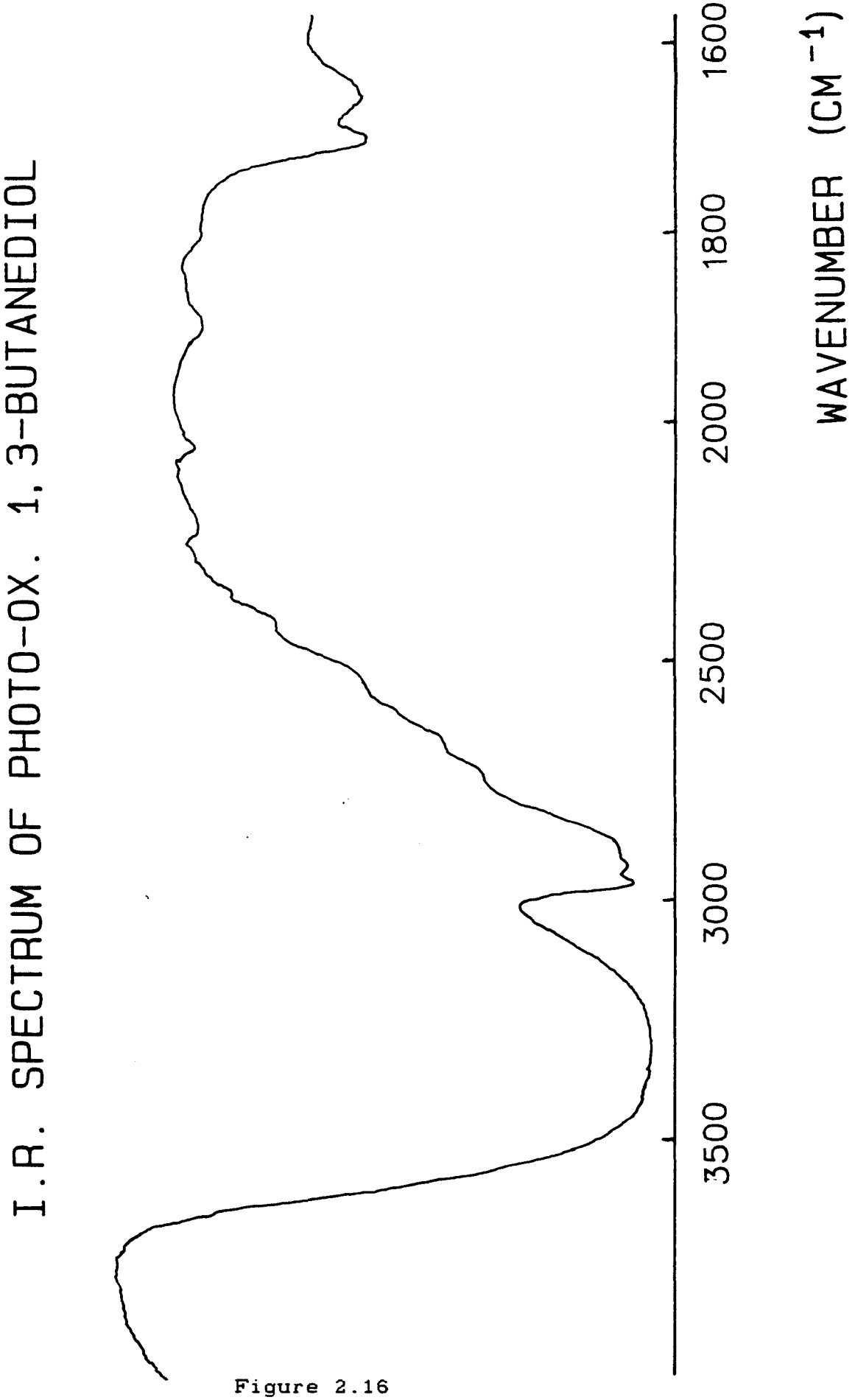
I.R. SPECTRUM OF PHOTO-OX. 1,3-BUTANEDIOL
3500
3000
2500
2000
1800
1600
WAVENUMBER (CM-1)

Figure 2.16

formed. These were subsequently filtered , washed and dried. Since it was suspected that the crystals consisted of more than one compound , a thin layer chromatogram was run. The chromatogram itself consisted of a sheet of aluminium coated with athin layer of silica. The crystals were dissolved in methylene chloride and eluted with petroleum ether. Two spots were observed indicating the presence of two distinct compounds.

The two compounds were then separated by column chromatography. The mixture was dissolved in $CH_2Cl_2$ and passed down a 10 cm alumina column , using petroleum ether as eluent. The two fractions were collected , the solvent removed on a rotary evaporater. and the resulting solids were recrystallised from ethanol. The melting point of the two crystal samples were then recorded.

There are two obvious possible products from the oxidation of 1,3-butanediol.

$$CH_3CH(OH)CH_2CH_2OH \text{ -----> } CH_3C(O)CH_2CH_2OH \quad (2.14)$$

**(VII)**

and ,

$$CH_3CH(OH)CH_2CH_2OH \text{ -----> } CH_3CH(OH)CH_2CHO \quad (2.15)$$

**(VIII)**

where VII = 4-hydroxy-2-butanone and VIII = 3-hydroxybutanal.

The literature melting points of compounds VII and VIII are given in table 2.10 and compared with measured melting points of the two crystal products.

| COMPOUND | LIT M.PT. | EXPERIMENTAL M.PT. |
|---|---|---|
| VII | 110-111°C [54] | 106-110°C |
| VIII | 93-95°C [55] | 90-93°C |

Table 2.10

Thus it was concluded with a high degree of confidence that rutile catalysed photo-oxidation of 1,3-butanediol leads to the formation of two products , namely 4-hydroxy-2-butanone and 3-hydroxybutanal.

## 2.6.4 DETECTION OF $H_2O_2$

Using the acidic $Ti^{4+}$ solution as described in section 2.5.5 , samples of 1,3-butanediol were tested before and after photo-oxidation for the presence of hydrogen peroxide. Before oxidation , the test proved negative. Subsequent to reaction , a deep red complex formed on testing , indicating the presence of peroxide. Again , no attempt was made to quantify it.

## 2.7 OXIDATION OF 2,3-BUTANEDIOL

This section describes the results of using the oxygen-uptake technique to study the compound 2,3-butanediol (IX). This molecule contains two secondary hydroxyls on adjacent carbon atoms.

$CH_3CH(OH)CH(OH)CH_3$

**(IX)**

2,3-butanediol is a viscous liquid at room temperature and was thus suitable for use in the experimental set-up.

The usual blank runs were carried out ( see section 2.5.1 ) with no oxygen-uptake taking place.

However , a major difference between the behaviour of 2,3-butanediol and the other diols studied emerged. On irradiation of a slurry of 2,3-butanediol in $TiO_2$ in the presence of $O_2$ and water no oxygen uptake took place. Experiments were carried out over a wide range of temperatures ( 293K - 343K ) and with the cell having been flushed with oxygen ; no reaction was observed.

Despite yielding an apparently negative result , it was decided to investigate this compound further since there was no apparent reason for its non-oxidative behaviour.

## 2.7.1 EFFECT OF HYDROGEN PEROXIDE

In all of the previous diol oxygen-uptake studies it was discovered that hydrogen peroxide was formed as a result of photo-oxidation. Fraser et.al. [41] also noted the formation of $H_2O_2$ and discussed its role in the mechanism of propan-2-ol photo-oxidation in some detail. It was concluded from their work that the peroxide played a major role in the reaction scheme and provided a possible pathway for propan-2-ol oxidation.

In light of this it was decided to investigate the effects of adding hydrogen peroxide to a $TiO_2$ / 2,3-butanediol slurry.

100 mls. 2,3-butanediol and 1g rutile were stirred and irradiated at a temperature of ca. 313K and no oxygen-uptake was observed. The slurry was then shielded from the lamp and 0.25 mls $H_2O_2$ ( 100 mls. ) was added to the slurry. Once the temperature had re-equilibrated the slurry was exposed to the lamp once again and the pressure monitored. Rapid oxygen-uptake ensued.

A further blank experiment was also carried out , whereby diol and $H_2O_2$ were irradiated in the absence of $TiO_2$. No uptake occurred and it was concluded that the presence of all three components , diol , pigment and peroxide , were necessary for reaction to occur.

Experiments were also carried out in which the volume of $H_2O_2$ added was varied ( 0.1 ml - 1 ml ). For a given temperature the rate of reaction was independent of the amount of peroxide added.

## 2.7.2 VARIABLE TEMPERATURE STUDIES OF 2,3-BUTANEDIOL/$H_2O_2$

In order to find out more about the kinetics of the 2,3-butanediol / $TiO_2$ / $H_2O_2$ system , variable temperature studies were carried out. The slurry used in each case comprised 100 mls. 2,3-butanediol , 1g rutile and 0.25 mls. $H_2O_2$ ( 100 vols.). Oxygen-uptake profiles are shown in figure 2.1.8 and the subsequent Arrhenius plot in figure 2.1.7. Table 2.11 contains the relevant data.

2,3-BUTANEDIOL

| T (K) | k ($mols^{-1}$) | 1/T ($10^3$/K) | ln (k) |
|---|---|---|---|
| 303.0 | $7.1 \times 10^{-10}$ | 3.30 | -21.07 |
| 309.0 | $12.1 \times 10^{-10}$ | 3.24 | -20.53 |
| 319.0 | $20.6 \times 10^{-10}$ | 3.13 | -20.00 |
| 327.0 | $31.6 \times 10^{-10}$ | 3.06 | -19.57 |

**r = -0.99** **A.E. = 49.8 $kJmol^{-1}$**

Table 2.11

The Arrhenius plot was highly linear ( r = -0.99 ) yielding an activation energy of 49.8 $kJmol^{-1}$ for the reaction. This compares with values of ca. 22 $kJmol^{-1}$ obtained for photo-oxidation of the primary diols , 1,3-propanediol and 1,4-butanediol and a value of 59.2 $kJmol^{-1}$ obtained by Fraser [40] for the rutile

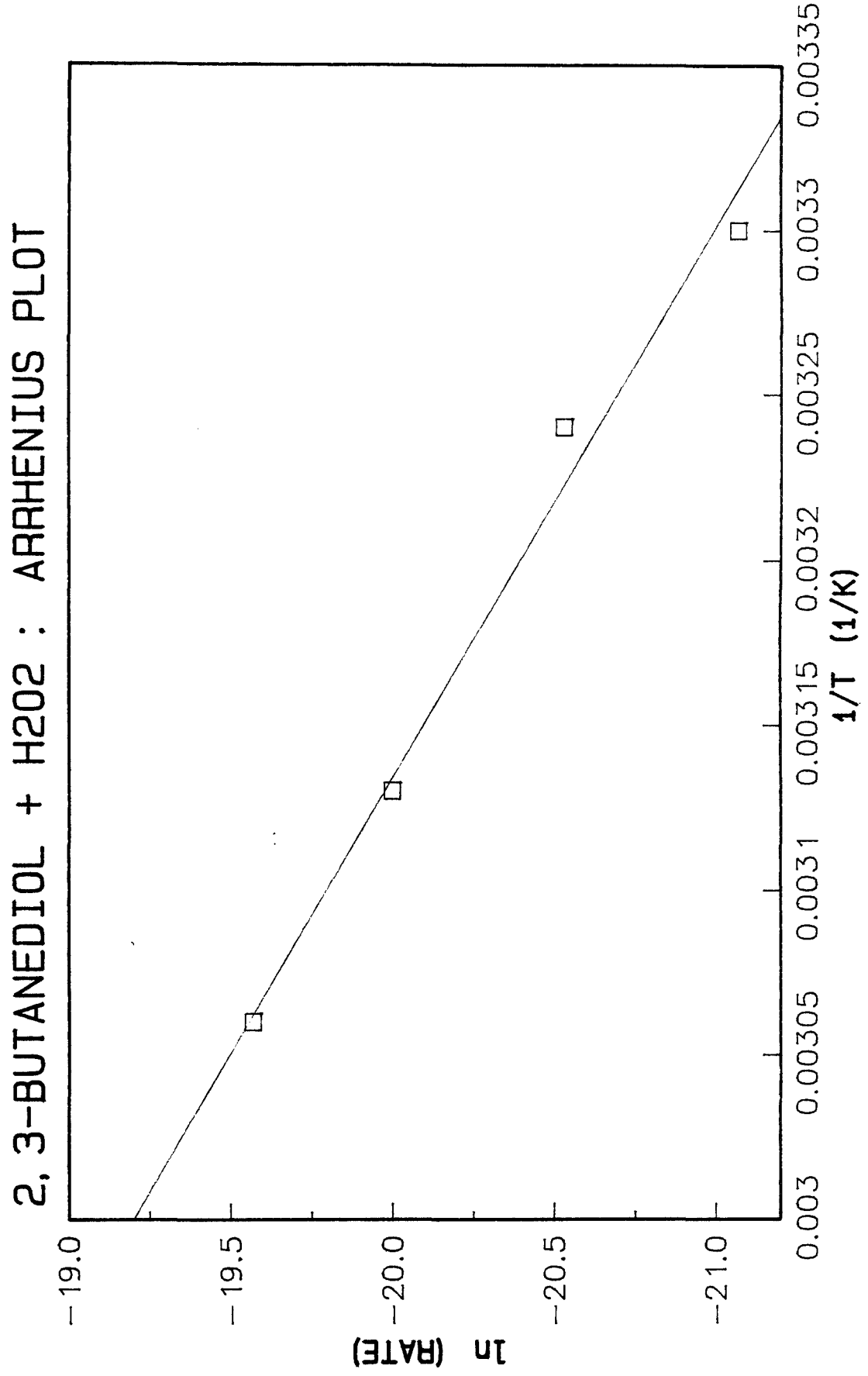
2, 3-BUTANEDIOL + H2O2 : ARRHENIUS PLOT
ln (RATE)
-19.0
-19.5
-20.0
-20.5
-21.0
0.003
0.00305
0.0031
0.00315
0.0032
0.00325
0.0033
0.00335
1/T (1/K)

Figure 2.17

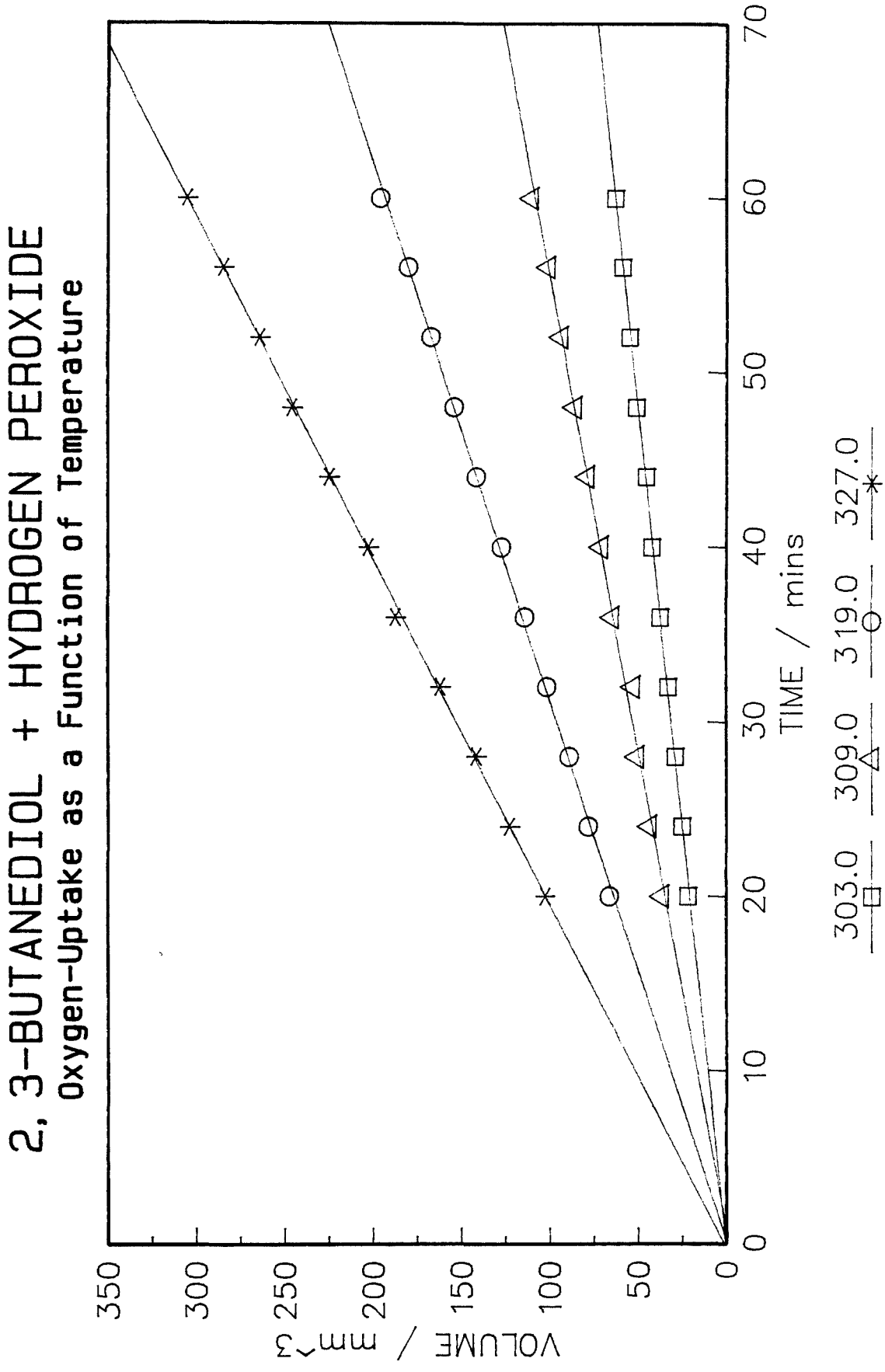
2, 3-BUTANEDIOL + HYDROGEN PEROXIDE
Oxygen-Uptake as a Function of Temperature
VOLUME / mm^3
TIME / mins
0
50
100
150
200
250
300
350
0
10
20
30
40
50
60
70
303.0
309.0
319.0
327.0

Figure 2.18

catalysed photo-oxidation of the secondary alcohol propan-2-ol.

## 2.7.3 EFFECT OF $O_2$ PARTIAL PRESSURE

As was done previously with other substrates , qualitative experiments were carried out to establish the effect of oxygen partial pressure on the oxygen-uptake rate. The same slurry as was used in the variable temperature work was employed again. Uptake runs were carried out in air and after thorough purging with oxygen at a temperature of ca. 315 K. The relevant data is displayed in table 2.12.

| $RATE_{AIR}$ ($mols^{-1}$) | $RATE_{O2}$ ($mols^{-1}$) | $RATE_{O2}:RATE_{AIR}$ |
|---|---|---|
| $14.4x10^{-10}$ | $15.3x10^{-10}$ | 1.06 |

Table 2.12

Thus there is virtually no increase in oxidation rate with increase in $O_2$ partial pressure. It is interesting to compare this result with those obtained for the other diols studied. In all previous cases there was a significant increase in rate.

## 2.7.4 IDENTIFICATION OF PRODUCTS

Once again the major problem with product identification was the low rate of formation. In order to overcome this a slurry containing 100mls 2,3-

butanediol , 1g pigment and 0.25 mls. $H_2O_2$ was stirred and irradiated for ca. 120 hrs. Infra-red spectra of the resulting photo-oxidised substrate showed the onset of a peak at around 1670 $cm^{-1}$ indicating the presence of a carbonyl group.

Various attempts were made to derivatise the product , without success. Some crystals were obtained but even after several attempts to purify them , the melting point range was too broad to permit positive identification by this method. It seems likely however that the diol is oxidised to the hydroxyketone as indicated below.

$$CH_3CH(OH)CH(OH)CH_3 \longrightarrow CH_3C(O)CH(OH)CH_3 \quad (2.16)$$

**(IX)**

IX = 3-hydroxybutan-2-one

The reasons for the non-reactivity of 2,3-butanediol are not clear. Rochester et.al. [53] have suggested that the binding affinity of 2,3-butanediol for the surface of silica is lower than that for both 1,4- and 1,3-butanediol , based on FT-IR results. It may be that the affinity of the diol for the $TiO_2$ surface is so low that it is not in contact with the surface for a long enough period of time for reaction to take place.

One feature of the diols studied so far is their tendency to undergo self-association , in common with all alcohols [71]. This process involves the formation of hydrogen bonded links between alcohol molecules , resulting in chains or cyclic structures [62]. It may be that in the case of 2,3-butanediol , most of the hydroxyl groups are tied up in inter-molecular hydrogen bonding and therefore unable to interact with the pigment surface , preventing reaction.

The phenomenon of hydrogen bonding in diols is discussed in greater detail in Chapter 3.

The reason for reaction when $H_2O_2$ is present is also not clear. It is our belief that , in this case , a bulk rather than a surface reaction is taking place. The hydrogen peroxide may react at the pigment surface yielding free hydroxyl radicals. These reactive species may then migrate from the surface to the bulk liquid where reaction with the diol takes place. This topic is discussed further at the ned of this chapter.

## 2.8 UPTAKE STUDIES ON 2-METHYLPROPAN-2-OL AND TRIETHANOLAMINE

In this section , results of oxygen-uptake work carried out on the compounds 2-methylpropan-2-ol (X) and triethanolamine (XI) are reported. These molecules are quite different from each other and from previous compounds studied. 2-methylpropan-2-ol is a tertiary alcohol and was chosen for study in order to determine the effect of using a compound with a tertiary hydroxyl function in the oxygen-uptake technique. Triethanolamine contains 3 primary hydroxyls and a tertiary amine function. The main interest in this molecule was to investigate the effect of the amine group on reactivity.

$(CH_3)_3COH$ $:N(CH_2CH_2OH)_3$

(X) (XI)

(X) is a solid at less than 20°C and uptake runs had to be carried out at slightly elevated temperatures. (XI) is a liquid at room temperature. Triethanolamine is of further interest because it is a component in the formulation of some paints.

The oxygen-uptake technique was employed in the usual manner , using 100 mls. of each of the substrates to 1g of pigment. On irradiation of the resultant slurries , no uptake was observed. Experiments were repeated over a wide range of temperatures (298K -

345K) , after thorough flushing with oxygen and after addition of hydrogen peroxide. Under no set of conditions was oxygen-uptake observed.

It is perhaps not surprising that 2-methylpropan-2-ol did not react in any way since tertiary alcohols are not easily oxidised. The reason for this is that they do not have a hydrogen attached to the carbon that bears the -OH group [56]. Tertiary alcohols can be oxidised but only under forcing conditions involving cleavage of a carbon-carbon bond.

The fact that triethanolamine did not undergo reaction does not invite any immediately obvious explaination. Mention has already been made of the fact that exciton , or electron / hole pair formation is a necessary pre-requisite for photocatalytic oxidation to take place. In particular , an exciton must be "trapped" for a sufficiently long period of time in order that it initiates activity. It is possible that there are specific types of sites on the $TiO_2$ surface at which excitons may be preferentially "trapped". An analogy may be drawn here with the field of enzymology. Enzyme inhibitors bind to specific sites in an enzyme which then causes a reduction in its ability to act as a catalyst [57,58].

The identification and characterisation of surface sites on rutile and anatase has been the subject of a great deal of attention [7,59,60] and certain defect

sites , which are potential exciton traps , have been identified as being acidic [61]. Bearing in mind that the nitrogen in triethanolamine acts as an organic base, there is a strong possibility that it is adsorbed onto the active site on the rutile surface thus inhibiting any interaction with "trapped" excitonic species.

Work carried out by Fraser et.al. [41] involved adding the di-tertiary amine , diazobicyclooctane (DABCO) , in relatively small concentrations to slurries of $TiO_2$ in propan-2-ol. The addition of DABCO resulted in dramatic reductions in oxygen-uptake rates. Conclusions drawn from this work were similar , in that it was thought that the DABCO co-ordinated strongly with acidic sites on the pigment surface , thus blocking the sites at which exciton "trapping" occurred.

Rochester et.al. [63] studied the adsorption of triethylamine on rutile using FT-IR techniques. They concluded that hydrogen bonds formed between surface hydroxyl groups and triethylamine molecules. They also claim to have observed co-ordinative interactions between triethylamine and Lewis-acidic surface sites which were resistant to desorption at ambient temperatures. Other tertiary amines have been shown to be strong chelating agents of transition metal ions [64].

It would appear then , that triethanolamine binds to the surface of the pigment at these active acidic sites via the basic nitrogen atom. This prevents oxidation of the hydroxyls in the molecule and no oxygen-uptake is observed.

## 2.9 DISCUSSION OF RESULTS

Following the observations and experimental results obtained from the preceding oxygen-uptake work, it is relevant to conclude this chapter with a section which considers a possible reaction mechanism for rutile-mediated photocatalytic oxidation based on the various substrates studied.

A summary of results from the oxygen-uptake work is presented in figure 2.19. Uptake rates under certain conditions and activation energies can readily be compared for each of the substrates ; data for the photo-oxidation of propan-2-ol [40,41] is also included for comparison purposes.

It is clear that in all cases where reaction occurs , the presence of oxygen , water , pigment and U.V.-radiation are required. Also , products of reactions are aldehydic / ketonic in nature and hydrogen peroxide is formed. It was also concluded that the activation energy for photo-oxidation is dependent on the type of hydroxyl being oxidised , i.e. whether

# SUMMARY OF RESULTS

| SUBSTRATE | Uptake rate @ 315K ($\times 10^{-10}$ mol/s) | Uptake rate 315K + $O_2$ ($\times 10^{-10}$ mol/s) | Uptake rate 315K + $H_2O_2$ ($\times 10^{-10}$ mol/s) | $\Delta H^\circ$ ( kJ/mol ) | Require presence of | | |
|---|---|---|---|---|---|---|---|
| | | | | | $H_2O$ | $O_2$ | U.V. |
| 1,3–propanediol | 6.6 | 27.0 | –– | 22.2 | Y | Y | Y |
| 1,4–butanediol | 6.8 | 25.8 | –– | 21.4 | Y | Y | Y |
| 1,3–butanediol | 9.8 | 38.3 | –– | non–linear Arrhenius | Y | Y | Y |
| 2,3–butanediol | –– | –– | 14.4 | 49.8 | Y | Y | Y |
| 2–methyl–propan–2–ol | –– | –– | –– | –– | –– | –– | –– |
| triethanolamine | –– | –– | –– | –– | –– | –– | –– |
| propan–2–ol | 22.0 | 22.0 | –– | 59.2 | Y | Y | Y |

Figure 2.19

it is a primary or a secondary. This rather fundamental observation has not been noted in previous studies. It has also been established in this work , and that of others [40] , that the presence of a base inhibits dehydrogenation , suggesting that the active sites on the pigment surface are acidic in nature.

On the basis of the observations made in this chapter the following mechanism is proposed for reactions occurring on the pigment surface.

The first step in the reaction sequence is the absorption of a photon by the pigment ( < 415nm for rutile ) , generating an exciton :

$$Ti^{4+} + h\nu \longrightarrow Ti^{4+} + h^{+} + e^{-} \qquad (2.17)$$

The hole may be trapped by a neighbouring surface hydroxide ion and the electron by a $Ti^{4+}$ , thus

$$Ti^{4+}[OH^{-}]_{S} + \text{exciton} \longrightarrow Ti^{3+}[OH\cdot]_{S} \qquad (2.18)$$

yielding a (nominally) $Ti^{3+}$ ion and a hydroxyl radical which remains adsorbed on the surface.

The next step involves the reaction of oxygen :

$$Ti^{3+}[OH\cdot]_{S} + O_2 \longrightarrow Ti^{4+}[OH\cdot, O_2^{-}]_{S} \qquad (2.19)$$

Here , the oxygen is reduced to the superoxide ion by the $Ti^{3+}$. Both the superoxide ion and the $Ti^{3+}$ ion have been detected by workers who have used e.s.r.

techniques to study analogous solution phase reactions [65,66].

The role of water in photocatalytic oxidation reactions has not been taken full account of in the past. This work clearly demonstrated that in the absence of $H_2O$ , no reaction took place. It is proposed that it is involved in the next stage , thus ,

$$Ti^{4+}[OH^{\cdot},O_2^{-}]_S + H_2O \longrightarrow Ti^{4+}[OH^{\cdot},HO_2^{\cdot},OH^{-}]_S \quad (2.20)$$

E.s.r. has also been used to detect the presence of the perhydroxyl radical at the photoactivated $TiO_2$ surface [67] and several workers have reported that hydroxyl and perhydroxyl radicals can be stabilised in the presence of $Ti^{4+}$ ions [68,69]. Note that the hydroxide ion formed in this step will replace that which was involved in the hole trapping step.

The substrate molecules are continually absorbing and desorbing on the pigment surface , the rate being determined primarily by the reaction temperature. The net effect of the proposed mechanism thus far is to have converted one molecule of $O_2$ and one of $H_2O$ to $HO_2^{\cdot}$ and $HO^{\cdot}$ free radical species. The next steps in the reaction sequence involve the reaction of the substrate , with the subsequent formation of the carbonyl containing product and hydrogen peroxide :

$$Ti^{4+}[OH^{\cdot},HO_2^{\cdot},OH^{-}]_S + HOCHRR' \longrightarrow Ti^{4+}[OH^{\cdot},HO\dot{C}RR',OH^{-}]_S + H_2O_2 \quad (2.21)$$

$$Ti^{4+}[OH^{\cdot},HO\dot{C}RR',OH^{-}]_S \longrightarrow Ti^{4+}[OH^{-}]_S + H_2O + O{=}CRR' \quad (2.22)$$

The substrate is depicted as having a hydrogen on the same carbon as the hydroxyl function , one of the requirements identified for dehydrogenation to occur (see section 2.8). It should also be noted that the pigment surface has returned to its initial state (cf. eqn. 2.22 with eqn. 2.18) suggesting that the whole oxidative process is cyclical and that the original active sites are regenerated.

So far , oxygen has been considered as the oxidising agent in the reaction. It is believed , however , that hydrogen peroxide may be involved in a competing oxidative pathway [40]. It is possible that $H_2O_2$ molecules , if adsorbed on the pigment surface may have the opportunity to oxidise $Ti^{3+}$ to $Ti^{4+}$ via a Fenton type reaction :

$$Ti^{3+}[H_2O_2]_S \longrightarrow Ti^{4+}[OH^{\cdot},OH^{-}]_S \quad (2.23)$$

The $E^{\ominus}$ for this reaction is +1.57V which compares favourably , in terms of energetics , with the well established $Fe^{2+} \rightarrow Fe^{3+}$ oxidation mediated by $H_2O_2$ ($E^{\ominus}$ = +0.25V) [70].

$$Fe^{2+}_{(aq)} + H_2O_{2(l)} \rightarrow Fe^{3+}_{(aq)} + OH^{\cdot}_{(aq)} + OH^{-}_{(aq)} \quad (2.24)$$

If at equation 2.19 , addition of $O_2$ is replaced by $H_2O_2$ , the following sequence may be envisaged :

$$Ti^{3+}[OH^{\cdot},H_2O_2]_S \longrightarrow Ti^{4+}[OH^{\cdot},OH^{\cdot},OH^{-}]_S \quad (2.25)$$

$$Ti^{4+}[OH\cdot, OH\cdot, OH^{-}, HOCHRR']_S \rightarrow Ti^{4+}[OH\cdot, HO\dot{C}RR', OH^{-}] + H_2O \quad (2.26)$$

$$Ti^{4+}[OH\cdot, HO\dot{C}RR', OH^{-}]_S \rightarrow Ti^{4+}[OH^{-}]_S + O{=}CRR' + H_2O \quad (2.27)$$

Once again a cyclical process is envisaged resulting in the formation of a carbonyl containing species with the $TiO_2$ surface restored to its original state. The net result is that there are two competing oxidative cycles , one involving $O_2$ and the other involving $H_2O_2$. This is in good agreement with the findings of Fraser [40,41]. These schemes have been depicted schematically in figure 2.20.

One important observation which was made for the photo-oxidation of 1,3-propanediol , 1,4-butanediol and 1,3-butanediol was the marked rate dependence on oxygen partial pressure. Previous studies carried out on the propan-2-ol / $TiO_2$ system have been contradictory in this respect [27,40]. Harvey et. al. witnessed an increase in the rate of propanone formation as the partial pressure of oxygen in the reaction vessel was increased. Fraser et. al. saw no such increase.

In the above mechanism it is assumed that all reaction takes place on the surface of the pigment. Studies carried out looking at the effect of light intensity on rate of reaction [23] have suggested that electron / hole recombination is the dominant process at the sort of light intensity used in this work. If

SURFACE PHOTOCATALYTIC OXIDATION CYCLE

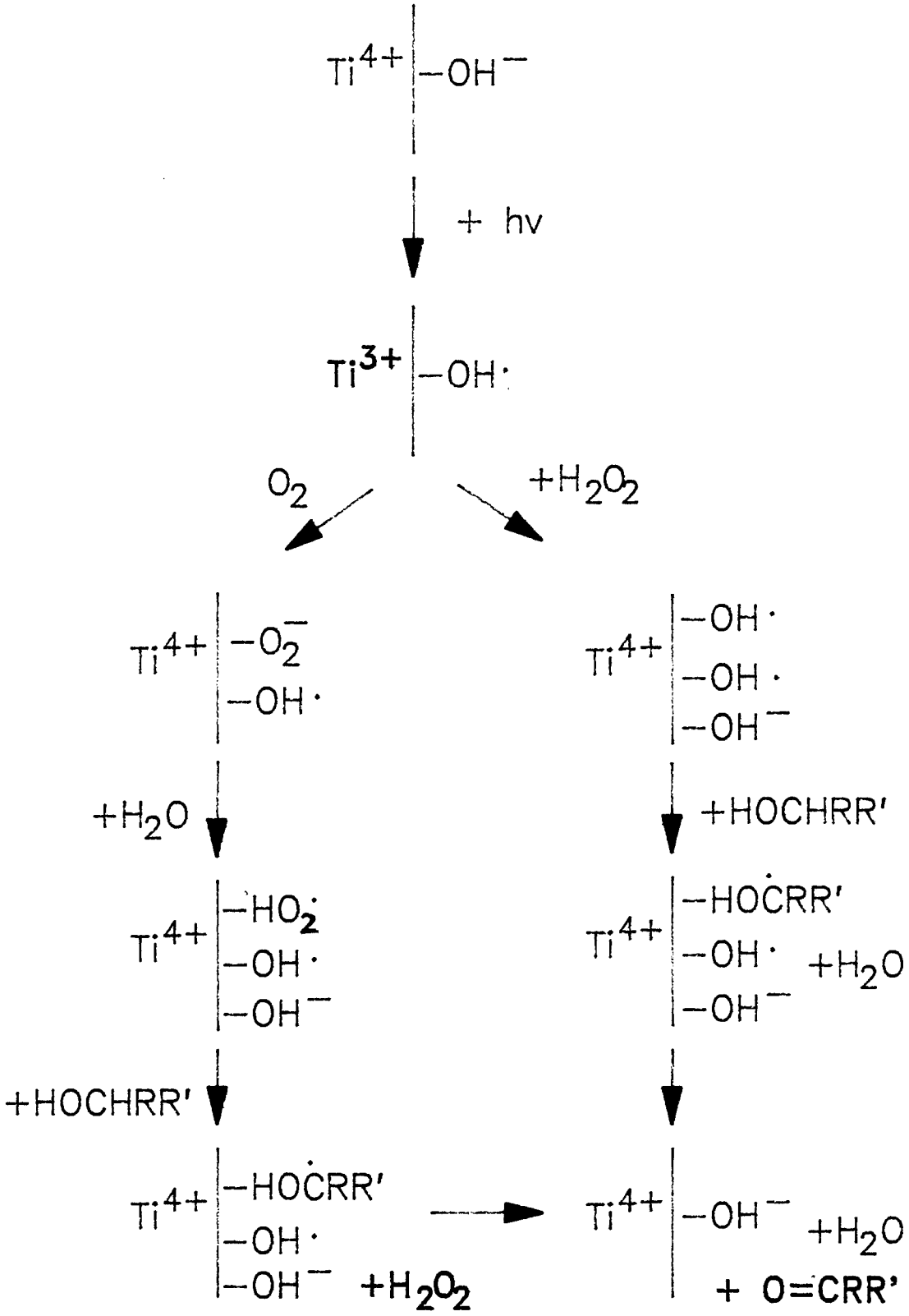


Figure 2.20

this is the case , then the number of active sites on the rutile surface will be low , relative to the number of oxygen molecules available for reaction. In this scenario it would be anticipated that the rate determining factor would be the concentration of active sites and that changing the oxygen partial pressure would not influence the rate.

It is possible that if the substrate radical species , $HO\dot{C}RR'$ , were desorbed from the surface into the bulk liquid then it would be possible for dissolved oxygen to react directly with this species :

$$HO\dot{C}RR'_{(b)} + O_{2(dis)} \longrightarrow HOC(OO^{\cdot})RR'_{(b)} \qquad (2.28)$$

$$HOC(OO^{\cdot})RR'_{(b)} \longrightarrow O{=}CRR'_{(b)} + HO_2{}^{\cdot}{}_{(b)} \qquad (2.29)$$

$$HO_2{}^{\cdot}{}_{(b)} + HO\dot{C}HRR'_{(b)} \longrightarrow HO\dot{C}RR'_{(b)} + H_2O_{2(b)} \qquad (2.30)$$

The $H_2O_2$ produced can then go on to take part in the surface reaction ( eqn 2.25 ). The rate constant for such additions will be high.

In pigmented polymer systems , for example paints and plastics , the substrates ( i.e. the polymers , binders etc. ) are much less mobile than the model compounds used in the present study. In these "real" situations it is likely that reactive species such as hydroxyl and perhydroxyl radicals are generated on the pigment surface and subsequently migrate through the polymeric media. They can then react , abstracting

hydrogen , ultimately leading to degradation of the system.

The main conclusion from the oxygen-uptake work is, therefore , that a complex series of competing reactions is taking place , the net result of which is the formation of an oxidised substrate and hydrogen peroxide.

# CHAPTER 3

## SELF-ASSOCIATION IN DIOL SYSTEMS

## 3.0 INTRODUCTION

One very important phenomenon which is displayed by molecules containing the hydroxyl function is that of self association [71]. This process involves the formation of chain or cyclic poly-molecular structures via hydrogen bonding [62] i.e.

$$ROH + ROH \rightleftharpoons \cdots O(R)-H \cdots O(R)-H \qquad (3.1)$$

This type of interaction , whereby molecules withcertain functional groups ( e.g. OH and $NH_2$ ) form associated complexes , is extremely common , of great significance , and has received a great deal of attention in scientific literature [72-76]. Indeed , two of nature's most important phenomena are governed by such associative interactions , namely the structure and formation of ice [77] and the double helical conformation of DNA [78].

Several techniques have been used to investigate the molecular association of alcohols e.g. infra-red and Raman spectroscopy [79-81]. In both of these methods , particular functional groups within molecules give rise to characteristic peaks in their spectra. If hydrogen bonding occurs , these spectra will be distorted and often a separate peak corresponding to the hydrogen bonded complex can appear. If this occurs, quantitative information about the concentrations of free and bound alcohol molecules can be calculated from the relative intensities of the two peaks.

Alternatively , a peak shift may be observed , the magnitude of which is related to the extent of association. Concentration and / or temperature dependence measurements on these spectroscopic shifts can lead to values for the equilibrium constants of self-association and heats of hydrogen bond formation.

Several other techniques have also been applied to the study of molecular association , e.g. dielectric constant measurements [82] , vapour pressure measurements [83] , surface tension effects [84] and thermodynamic measurements [85].

Recently however , proton nuclear magnetic resonance spectroscopy ( $^1$H n.m.r. ) has been employed in the study of self-associating alcohol systems [86-90]. This technique is capable of extremely high degrees of sensitivity in the detection of hydrogen bonding effects. Indeed , in recent years the power of n.m.r. spectrometers has increased dramatically , 500 MHz machines now being relatively commonplace.

Whilst previous studies of self-association in alcohols have provided important information , detailed knowledge of the phenomenon is still inadequate. On top of this , very little work has been carried out looking at the self-association of diols. For this reason it was decided to carry out an investigation into the hydrogen bonding effects in 1,3-butanediol and 2,3-butanediol using the $^1$H n.m.r. technique. It was also

hoped that the information obtained from this work would perhaps reveal whether or not the self-association properties of these diols influenced the oxygen-uptake results shown previously.

## 3.1 PROTON N.M.R. SPECTROSCOPY

The hydrogen nucleus , or proton , is spin active with a spin quantum number (I) of 1/2. It can assume either one of two spin states : +1/2 or -1/2. Since the proton is electrically charged , when it spins a magnetic moment is generated which coincides with the axis of spin. Thus a spinning proton behaves as a tiny bar magnet.

When a proton is subjected to an external magnetic field , it may assume one of two possible orientations with respect to the magnetic field. It may be aligned with the field ( $\alpha$ -state ) or against the field ( $\beta$ -state ) as represented in figure 3.1.

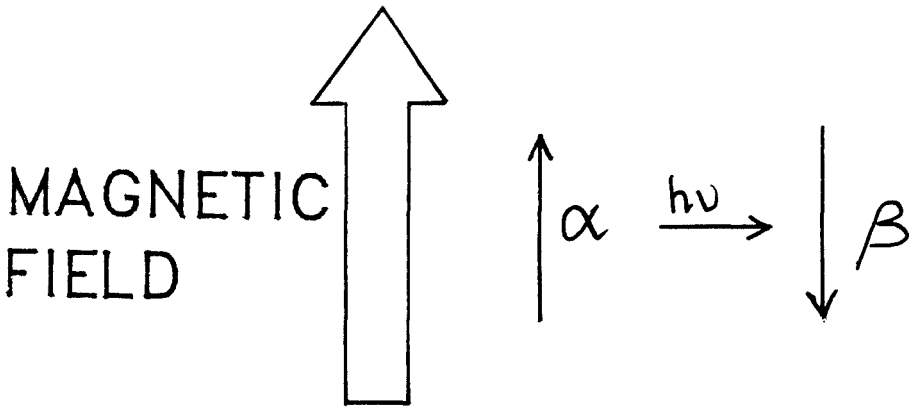


Figure 3.1

It is possible to "flip" the proton from the lower energy $\alpha$-state to the higher energy $\beta$-state by supplying the appropriate frequency of electromagnetic radiation. In nuclear magnetic resonance spectroscopy , the energy is supplied by electromagnetic radiation in the radio frequency region , the energy required being proportional to the magnetic field strength. N.m.r. spectrometers are designed so that the radio frequency is kept constant and the magnetic field is varied. When the magnetic field is tuned to precisely the right strength , the protons of a particular set in the molecule flip from one state to the other. In doing so, they absorb radio frequency energy. This "flipping" of protons generates a small electric current in a coil of wire surrounding the sample which on amplification , appears as a peak in the spectrum.

In a molecule the situation is complicated by the fact that all nuclei are surrounded by electrons. When placed in a magnetic field , the electron clouds tend to circulate in such a direction as to induce a magnetic field opposing that applied , thus

$$B_{effective} = B_{applied} - B_{induced}$$

B being the magnetic field strength.

The strength of the induced field is dependent upon the electron density surrounding the nucleus. Thus for protons bondeed to oxygen atoms , the electron density surrounding the proton will be reduced relative

to a proton attached to a carbon atom. $B_{induced}$ for protons bonded to oxygen is thus less and these protons will experience a greater effective magnetic field. These protons are said to be deshielded. The net effect of this is that protons in different chemical environments resonate at different frequencies , and thus produce peaks in different positions in the n.m.r. spectrum.

From this it can be deduced that , since alcohol protons involved in self-association exist in a different environment to the non-associated species , the resonance frequencies , or chemical shifts of the two will be different. More specifically , the former will be more deshielded than the latter and hence will resonate at higher frequencies.

Chemical shifts are measured with reference to the absorption of protons of reference compounds , the most common of which is tetramethylsilane (TMS). These chemical shifts are measured in Hertz (Hz) and are proportional to the strength of the external magnetic field. However , since spectrometers with different magnetic field strengths are commonly used , it is desirable to express chemical shifts in a form that is independent of field strength. This is done by quoting chemical shifts in parts per million ( $\delta$ ) relative to TMS. Thus,

$$\delta = \frac{\text{chemical shift in Hz from TMS} \times 10^6}{\text{operating frequency of spectrometer (Hz)}}$$

In the following sections , the effects of concentration and temperature in 1,3-butanediol/solvent 2,3-butanediol/solvent systems are detailed. In each case the chemical shifts are quoted in Hertz ; reasons for which will be explained in the relevant section.

## 3.2 VARIABLE CONCENTRATION MODEL

In this section the effect of concentration on the chemical shifts of the hydroxyl protons in 1,3-butanediol and 2,3-butanediol is dicussed. In order to interpret the chemical shift data obtained , however , a self-association model must first of all be proposed.

If we consider the molecules under study , it is not unreasonable to suppose that they may exist in a monomer-dimer equilibrium ( see figure 3.2 ) in solution. Indeed , it has been found previously by several workers , studying various alcohol / solvent systems using the $^1H$ n.m.r. technique , that monomer-dimer equilibria do exist in such systems [79,91,92]. The following model is based on that proposed by Chen and Shirts [93].

In a monomer - dimer equilibrium , at temperatures where there is rapid interconversion ,

$$A + A \rightleftharpoons A_2 \qquad (3.1)$$

the observed chemical shift , $d_{obs}$ , is the weighted average of the shifts of monomer and dimer and was given by Gutowsky and Saika [94] as ,

$$d_{obs} = x_m d_m + x_d d_d \qquad (3.2)$$

or $$d_{obs} = ([A]/[A]_o)d_m + (2[A_2]/[A]_o)d_d \qquad (3.3)$$

where $d_m$ is the monomer shift , $d_d$ the dimer shift , $[A]$ , $[A_2]$ and $[A]_o$ the monomer , dimer and total diol

# POSSIBLE DIMER STRUCTURE
# 2,3–BUTANEDIOL

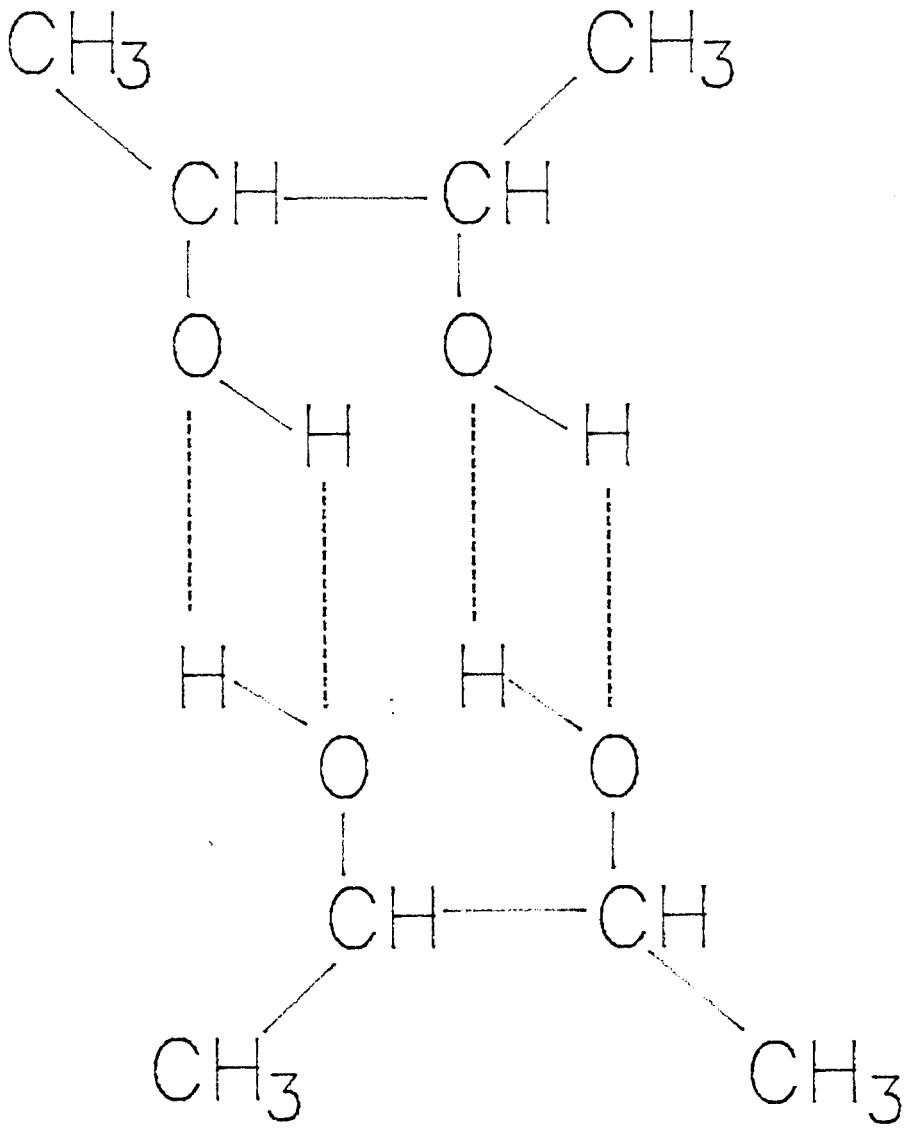


Figure 3.2

concentrations respectively ; $x_m$ is the monomer mole fraction and $x_d$ is the dimer mole fraction and obviously ,

$$x_m + x_d = 1 \qquad (3.4)$$

These mole fractions can readily be expressed in terms of chemical shift parameters , thus

$$x_m = (d_d - d_{obs})/(d_d - d_m) \qquad (3.5)$$

$$x_d = (d_{obs} - d_m)/(d_d - d_m) \qquad (3.6)$$

The dimerisation constant , $K_2$ , can be expressed as

$$K_2 = [A_2]/[A]^2 \qquad (3.7)$$

or if equations 3.2 and 3.3 are substituted in ,

$$K_2 = x_d/2[A]_o x_m \qquad (3.8)$$

If equations 3.5 and 3.6 are substituted into equation 3.8 and the square root is taken , we have

$$d_{obs} = d_d +/- \left[\frac{d_d - d_m}{2K}\right]^{0.5} \left[\frac{d_{obs} - d_m}{[A]_o}\right]^{0.5} \qquad (3.9)$$

For later convenience the latter square root term will be denoted by X ,

$$X = \left[\frac{d_{obs} - d_m}{[A]_o}\right]^{0.5} \qquad (3.10)$$

It is easy to see that , for a given set of $d_{obs}$ / concentration data , by substituting in an accurate value for $d_m$ into equation 3.10 , a plot of $d_{obs}$ v X

should give a linear plot whose intercept and slope can provide a value for $d_d$ , the dimer shift , and $K_2$ the dimerisation constant.

Replacing $1 - x_d$ for $x_m$ in equation 3.8 and solving for $x_d$ gives ,

$$x_d = \frac{(1 + 8K_2[A]_o)^{0.5} - 1}{(1 + 8K_2[A]_o)^{0.5} + 1} \qquad (3.11)$$

We can then use this equation to express $d_{obs}$ in terms of $K_2$ , $[A]_o$ and $d_m$ :

$$d_{obs} = d_m + x_d(d_d - d_m) \qquad (3.12)$$

$$d_{obs} = d_m + \frac{(d_d - d_m)(1 + 8K_2[A]_o)^{0.5} - 1}{(1 + 8K_2[A]_o)^{0.5} + 1} \qquad (3.13)$$

From equation 3.13 it is apparent that if one has an accurate value for $K_2$ , a plot of $d_{obs}$ v $x_d$ will give a straight line whose intercept is the monomer shift.

It would appear , therefore , that by using equations 3.9 and 3.13 in conjunction , an iterative algorithm to determine $d_m$ , $d_d$ and $K_2$ self consistently from chemical shift / concentration data could be devised.

One problem with this is that unless the initial trial monomer shift , $d_m^{(o)}$ , used in equation 3.10 is the true monomer shift , a plot of $d_{obs}$ v X will not necessarily give a straight line. Nevertheless , the intercept and limiting slope of a quadratic polynomial

( see Appendix II ) can be used to calculate a dimer shift and dimerisation constant. This $K_{2}$ is then used in equation 3.11 to calculate $x_{d}$. A plot of $x_{d}$ v $d_{obs}$ will probably also be non-linear but a new monomer shift , $d_{m}^{(1)}$ , can again be extracted from the intercept of a quadratic polynomial. This fitting cycle can be repeated until $d_{m}^{(N)} - d_{m}^{(N-1)} <= D$ , where D is an arbitrary tolerance limit for converggence.

A computer program to impliment this iterative algorithm ( NMR2.FOR ) was written in FORTRAN 77 and run on the St. Andrews University VAX mainframe. The program is shown in Appendix III.

Having calculated $d_{m}$ , $d_{d}$ and $K_{2}$ using this iterative technique , it is easy to see that for any given concentration , a predicted value for the observed chemical shift can be obtained. In order to enable this , another FORTRAN 77 program was written and employed on the VAX mainframe.

## 3.3 VARIABLE CONCENTRATION STUDIES OF DIOLS

Having set up the proposed model , it was decided to implement it using data obtained from variable concentration $^{1}H$ n.m.r. studies on 1,3-butanediol and 2,3-butanediol in a suitable solvent. These compounds were chosen because of their previous usage in the

oxygen-uptake work and because of the differences in behaviour shown by them in that work. It was hoped that the following n.m.r. studies might shed some light on these differences.

## 3.3.1 EXPERIMENTAL

1,3-butanediol and 2,3-butanediol ( Aldrich ) were distilled onto molecular seive (4A) in order to obtain pure , dry samples. A range of solutions of each diol in $CDCl_3$ were prepared. $^1H$ n.m.r. spectra of each of the solutions were run on a Bruker 300MHz spectrometer at a temperature of 298K.

## 3.3.2 RESULTS FOR 2,3-BUTANEDIOL

A typical n.m.r. spectrum for a solution of 2,3-butanediol in $CDCl_3$ is shown in figure 3.3 ( 2.21M @ 298K ). Since both hydroxyls in this molecule are chemically equivalent , only one hydroxyl peak appears in each spectrum ( at $\delta$ = 4.35 p.p.m. for the spectrum shown ). In this instance , 16 solutions were prepared, their n.m.r. spectra obtained at 298K , and the observed chemical shift of the hydroxyl peak measured. These measurements are shown in table 3.1 below.

It should be noted that , due to the difficulty in dissolving TMS in these solutions , there were no

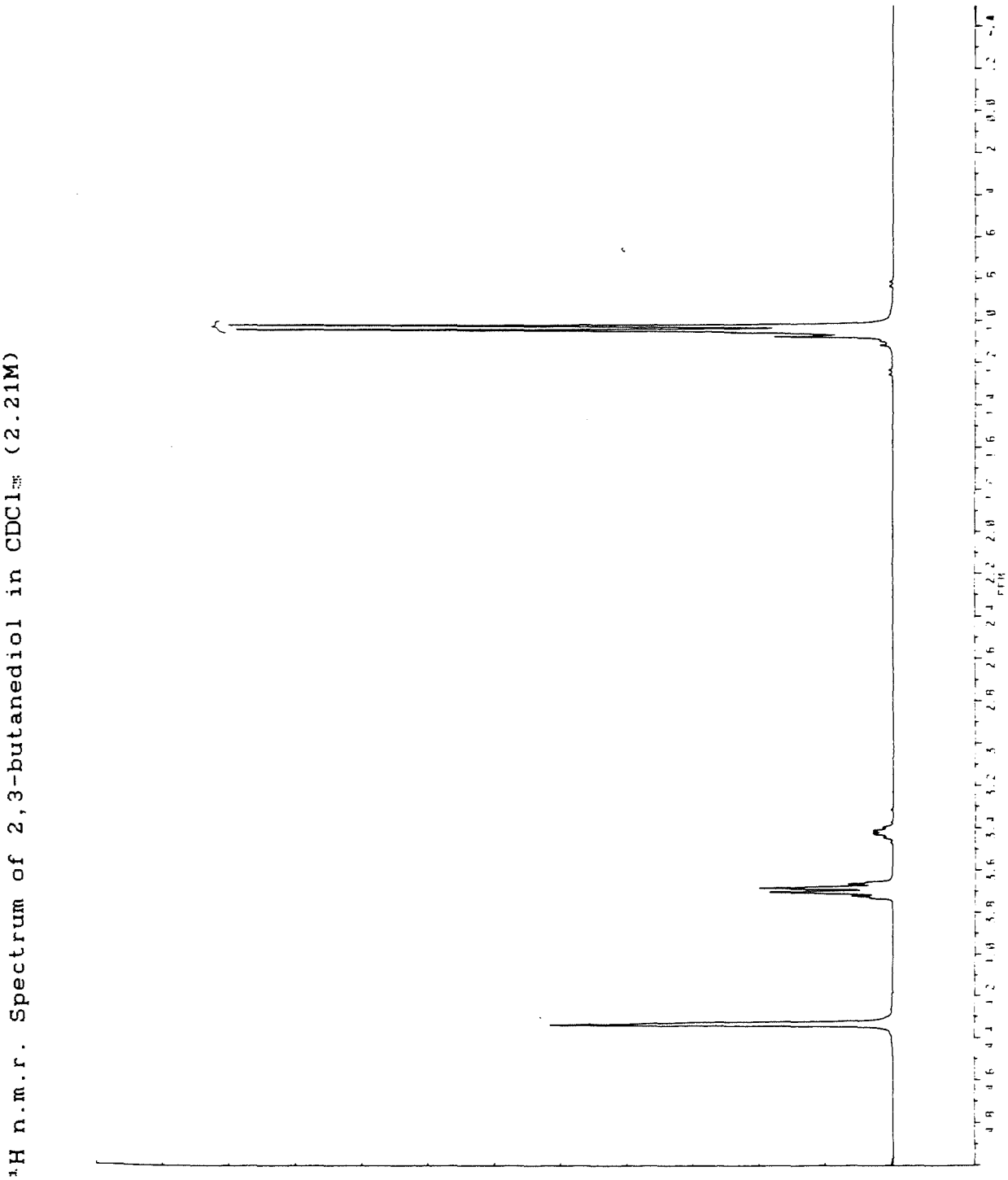


Figure 3.3

reference peaks at $\delta$ = 0 in any of the spectra. The observed shifts shown are the differences between the chemical shifts of the hydoxyl peaks and the chemical shifts of the methyl peaks ( $\delta$ = 1.0 ). This is justifiable , since the position of the methyl peak in the spectrum is not temperature or concentration dependent and was assumed to be constant over the experimental range used [71].

| $[A]_o$ (mol/l) | $d_{obs}$ (Hz) | $[A]_o$ (mol/l) | $d_{obs}$ (Hz) |
|---|---|---|---|
| 0.069 | 370.0 | 1.327 | 787.5 |
| 0.089 | 385.0 | 2.211 | 857.5 |
| 0.106 | 395.0 | 3.538 | 927.5 |
| 0.221 | 470.0 | 4.422 | 970.0 |
| 0.442 | 605.0 | 6.634 | 980.0 |
| 0.690 | 667.5 | 8.845 | 1027.5 |
| 0.885 | 707.5 | 9.729 | 1044.0 |
| 1.061 | 725.0 | 10.614 | 1072.5 |

Table 3.1

The role of the solvent should also be considered at this point. In an ideal situation it would be desirable to have a completely inert solvent i.e. one which did not itself participate in the self-associating system. For this reason previous workers have thus used cyclohexane [41] and carbon tetrachloride [71,95] as solvents. However, due to the nature of the compounds under study here, namely 1,3-butanediol and 2,3-butanediol, it was very difficult to find a suitable non-polar solvent. $CDCl_3$ was chosen for its convenience and also because it had also been used by others [93,96]. It was also felt that the

solvent-diol interaction would be much less significant than the diol-diol interaction.

The chemical shift-concentration data for the 2,3-butanediol-$CDCl_3$ system were processed using the previously described iterative procedure. Table 3.2 demonstrates the convergence of the algorithm, in this case having assumed an initial monomer shift ($d_m^{(0)}$) of 0 Hz. $d_m$ can be estimated from a plot of $d_{obs}$ v $[A]_o$. As $[A]_o$ -> 0 then $d_{obs}$ -> $d_m$. In practice, convergance occurred when -400 Hz < $d_m^{(0)}$ < 350 Hz.

| Iteration | $d_m$ (Hz) | $d_d$ (Hz) | $K_2$ (l/mol) |
|---|---|---|---|
| 0 | 0 | | |
| 1 | | 1294.04 | 0.975 |
| | 269.77 | | |
| 2 | | 1300.22 | 0.609 |
| | 282.38 | | |
| 3 | | 1275.30 | 0.749 |
| | 275.77 | | |
| 4 | | 1289.98 | 0.659 |
| | 279.69 | | |
| 5 | | 1281.75 | 0.707 |

Table 3.2

Figure 3.4 shows a plot of X versus observed chemical shift based on equation 3.9. There are 3 curves representing the first three iterations and it can be seen that curves 2 and 3 are almost superimposed, demonstrating the rapidity of the convergence.

The results obtained were as follows :

$$d_m = 278.3 \text{ Hz}$$

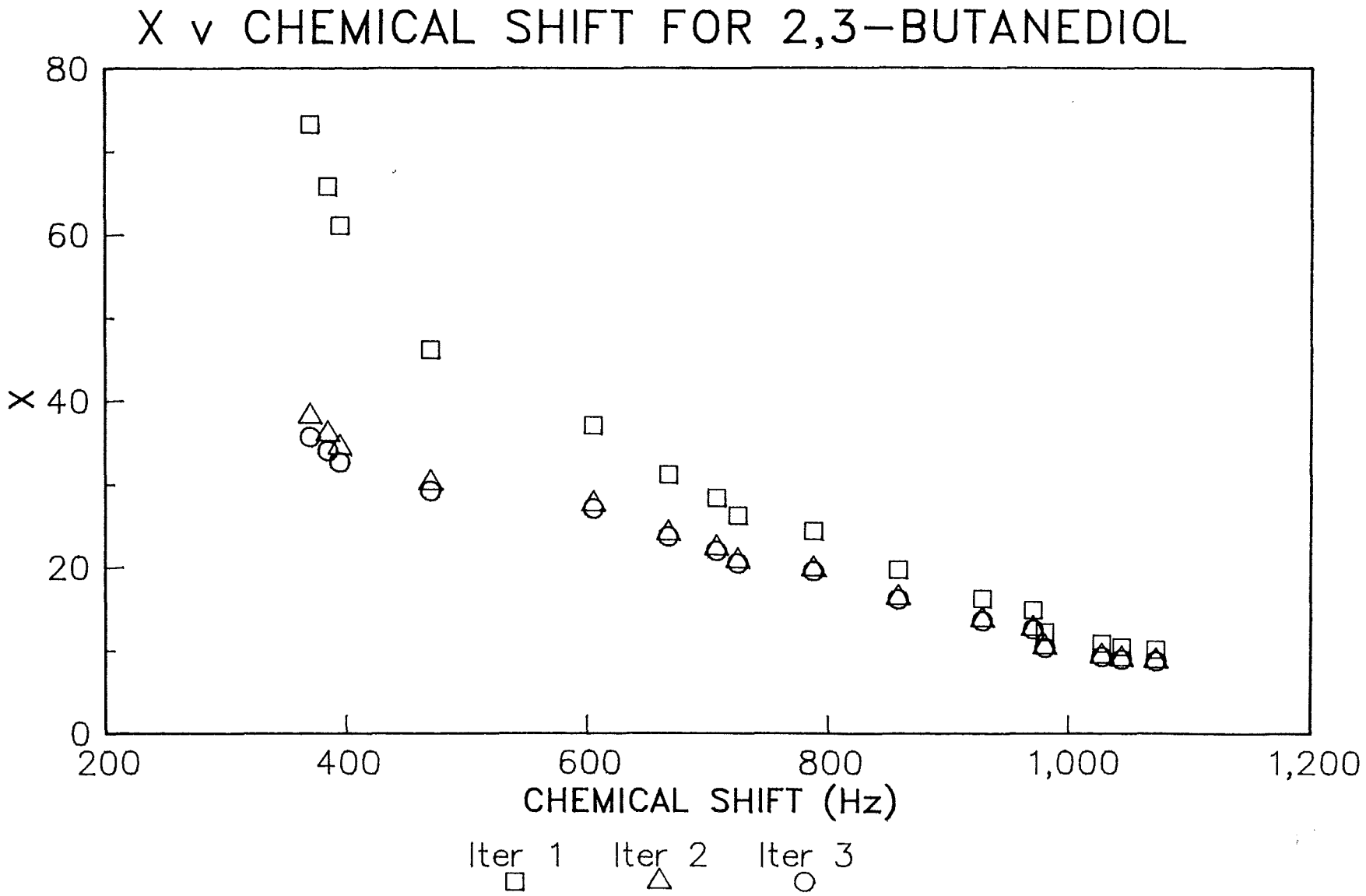
X v CHEMICAL SHIFT FOR 2,3-BUTANEDIOL
80
60
40
20
0
X
200
400
600
800
1,000
1,200
CHEMICAL SHIFT (Hz)
Iter 1
Iter 2
Iter 3

Figure 3.4

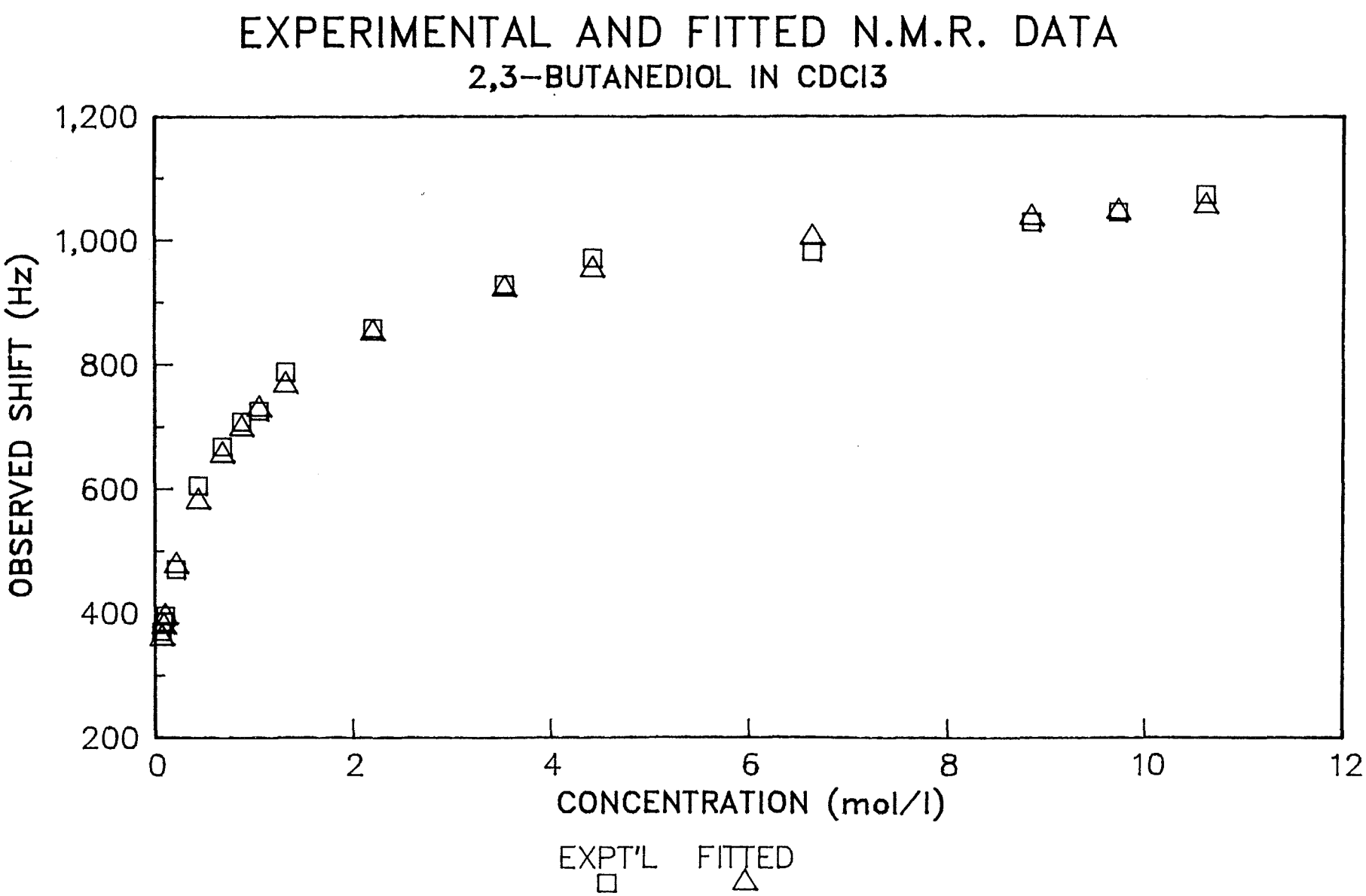
EXPERIMENTAL AND FITTED N.M.R. DATA
2,3-BUTANEDIOL IN CDCl3
OBSERVED SHIFT (Hz)
1,200
1,000
800
600
400
200
0
2
4
6
8
10
12
CONCENTRATION (mol/l)
EXPT'L
FITTED

Figure 3.5

$d_d$ = 1284.8 Hz

$K_2$ = 0.688 $lmol^{-1}$

These figures were obtained regardless of the initial monomer shift input, provided it was in the range quoted earlier.

These data were then fed into the computer program NMR.FOR ( Appendix IV ) in order to calculate observed chemical shifts for any given concentration. The experimental and fitted concentration / chemical shift data are shown in figure 3.5. As can be seen, an excellent fit was obtained.

## 3.3.3 RESULTS FOR 1,3-BUTANEDIOL

The $^1H$ nmr spectrum of a 2.23 M solution of 1,3-butanediol in $CDCl_3$ at 298K is shown in figure 3.6. In this molecule, the two hydroxyls are in different chemical environments and as a result there are two -OH peaks in the spectrum. ( $\delta$ = 4.6 p.p.m. and $\delta$ = 4.7 p.p.m. ). This made the analysis of data obtained slightly more complex; both hydroxyls were treated separately. In order to identify them, one was denoted -OH(A) and the other -OH(B) (see below).

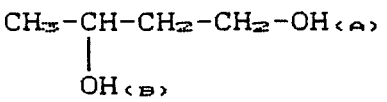

$^1$H n.m.r. Spectrum of 1,3-butanediol in $CDCl_3$ (2.23M)

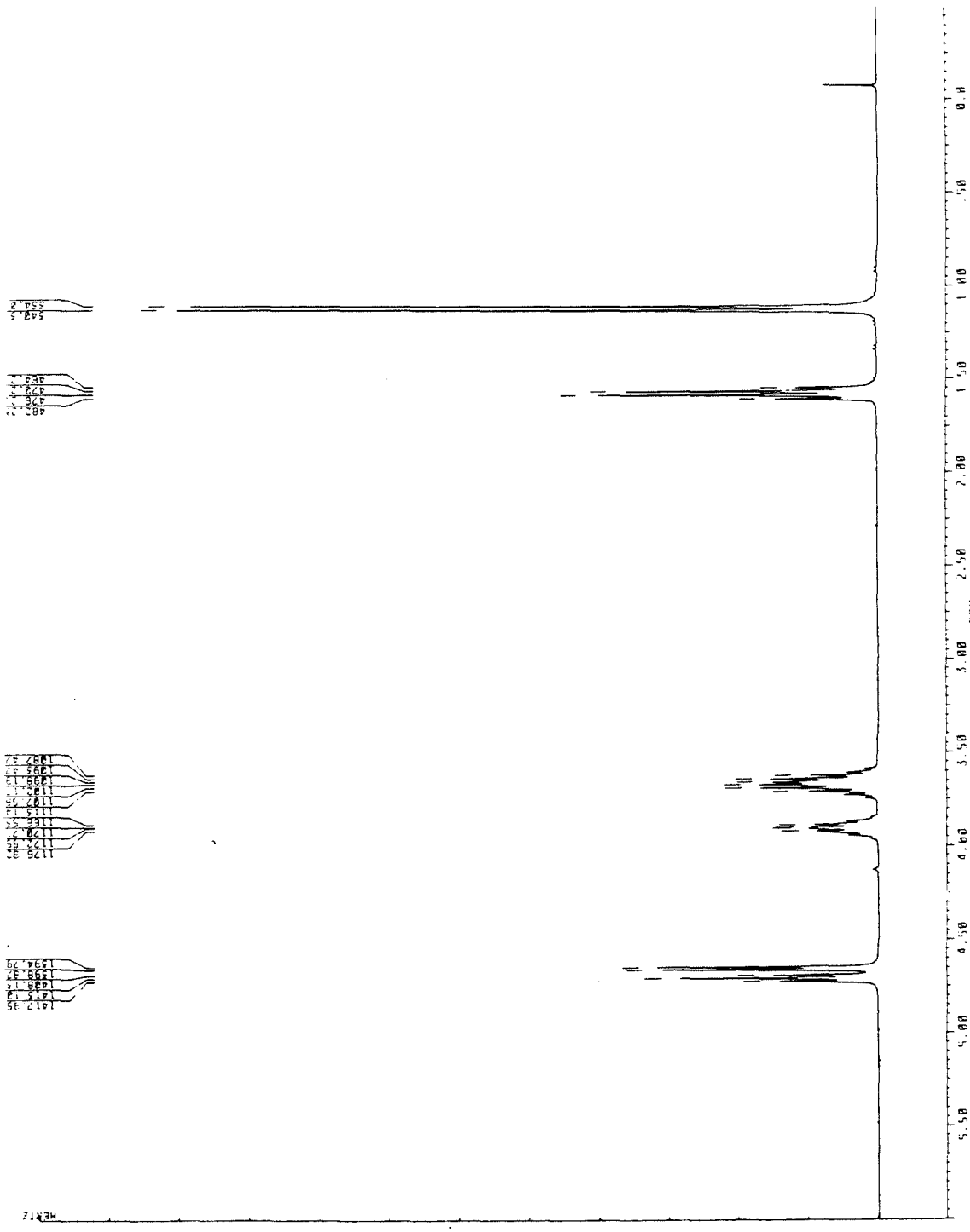

Figure 3.6

12 solutions were prepared and $^1H$ n.m.r. spectra of each were run. The results are shown in table 3.3. Again, due to the difficulty of dissolving a T.M.S. standard in these solutions, the chemical shift of the hydroxyl peaks was noted relative to one of the other peaks in the spectrum. In this case, the $CH_3$ peak was chosen. The ( reasonable ) assumption that its shift was unaffected by concentration was made.

| $[A]_o$ (mol/l) | $d_{obs}$ $OH_A$ (Hz) | $d_{obs}$ $OH_B$ (Hz) |
|---|---|---|
| 0.13 | 535.0 | 520.0 |
| 0.22 | 572.5 | 565.0 |
| 0.45 | 697.5 | 697.0 |
| 0.89 | 810.0 | 810.0 |
| 1.34 | 870.0 | 850.0 |
| 2.23 | 955.0 | 930.0 |
| 3.57 | 1022.0 | 997.5 |
| 4.47 | 1055.0 | 1030.0 |
| 6.70 | 1122.5 | 1097.5 |
| 8.93 | 1180.0 | 1157.5 |
| 9.83 | 1200.0 | 1180.0 |
| 10.72 | 1210.0 | 1195.0 |

Table 3.3

The data for each hydroxyl, A and B, was processed via the iterative procedure. Table 3.4 demonstrates once again the rapid convergence of the algorithm, using the first five iterations from the $-OH_B$ data set. Figures 3.7 and 3.8 show plots of Chemical Shift v X for the first three iterations from both sets of data. In both cases , iterations 2 and 3 virtually overlap. The converged values of $d_m$ , $d_d$ and $K_a$ for both $OH_A$ and $OH_B$ are shown in table 3.5.

In both cases , the algorithm converged to the same values so long as the initial trial monomer shift was in the range $-300\ Hz < d_m^{(0)} < 450\ Hz$.

These $d_m$ , $d_d$ and $K_2$ values were used to predict the chemical shift at each concentration , using the program NMR.FOR as mentioned previously. Experimental and predicted plots for $OH_A$ and $OH_B$ are shown in figures 3.9 and 3.10 respectively. once again , excellent fits to the experimental data were obtained.

| Iteration | $d_m$ (Hz) | $d_d$ (Hz) | $K_2$ (l/mol) |
|---|---|---|---|
| 0 | 0 | | |
| 1 | | 1436.20 | 0.909 |
| | 419.46 | | |
| 2 | | 1460.23 | 0.428 |
| | 436.94 | | |
| 3 | | 1456.83 | 0.449 |
| | 434.98 | | |
| 4 | | 1455.32 | 0.453 |
| | 434.67 | | |
| 5 | | 1455.15 | 0.453 |

Table 3.4

| | $OH_A$ | $OH_B$ |
|---|---|---|
| $d_m$ (Hz) | 437.49 | 434.64 |
| $d_d$ (Hz) | 1482.58 | 1455.14 |
| $K_2$ (l/mol) | 0.462 | 0.453 |

Table 3.5

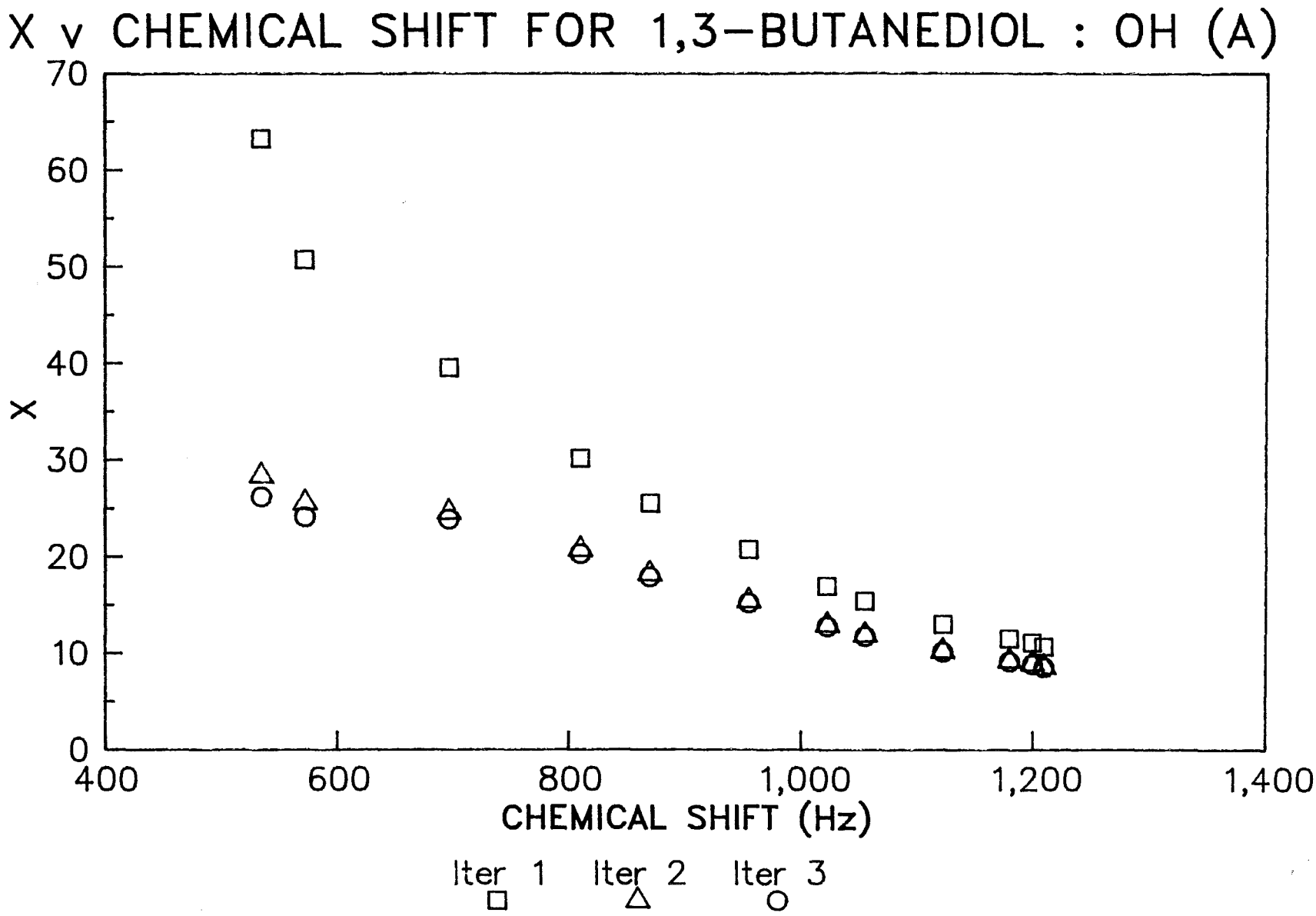
X v CHEMICAL SHIFT FOR 1,3-BUTANEDIOL : OH (A)
X
70
60
50
40
30
20
10
0
400
600
800
1,000
1,200
1,400
CHEMICAL SHIFT (Hz)
Iter 1
Iter 2
Iter 3

Figure 3.7

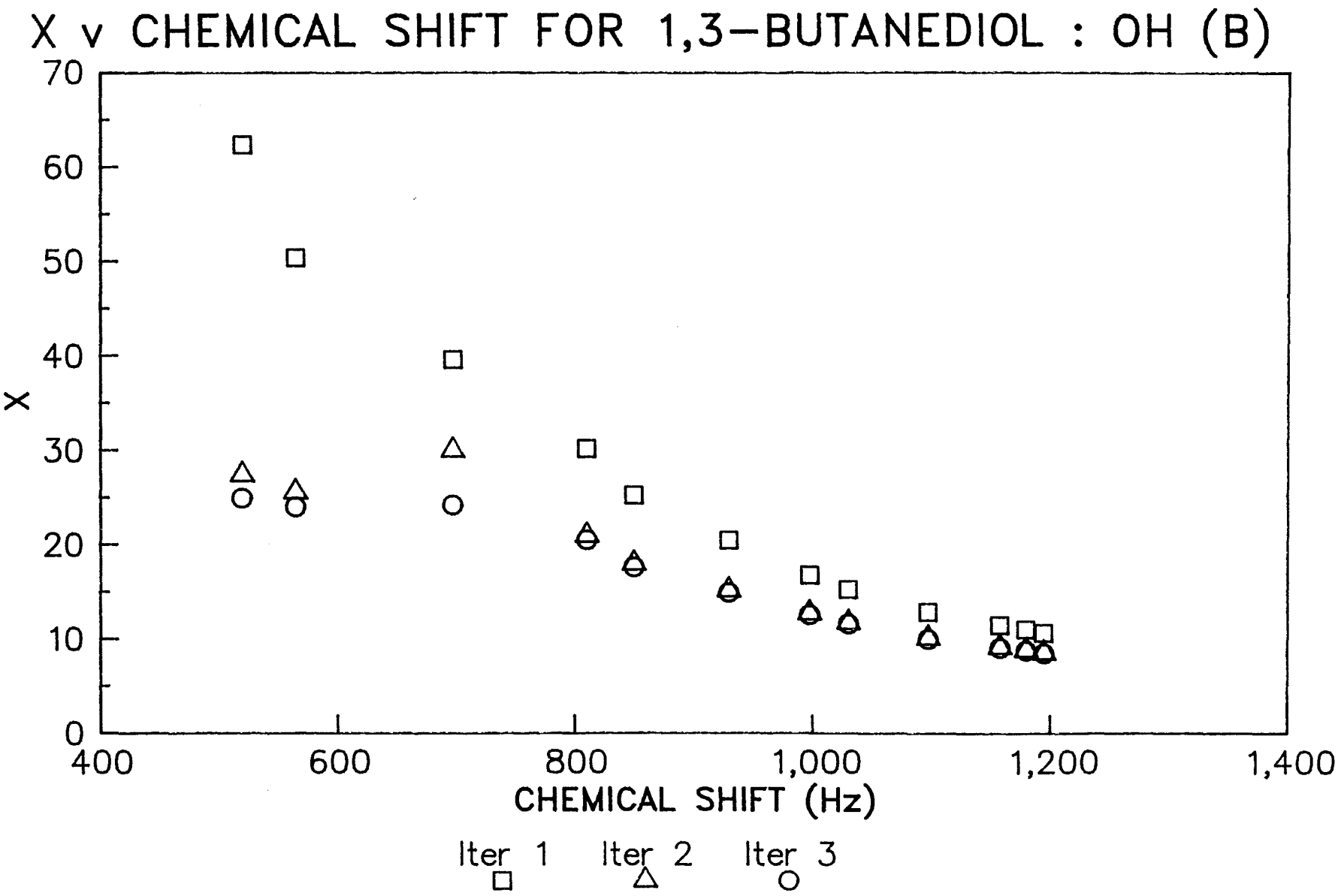
X v CHEMICAL SHIFT FOR 1,3-BUTANEDIOL : OH (B)
X
70
60
50
40
30
20
10
0
400
600
800
1,000
1,200
1,400
CHEMICAL SHIFT (Hz)
Iter 1
Iter 2
Iter 3

Figure 3.8

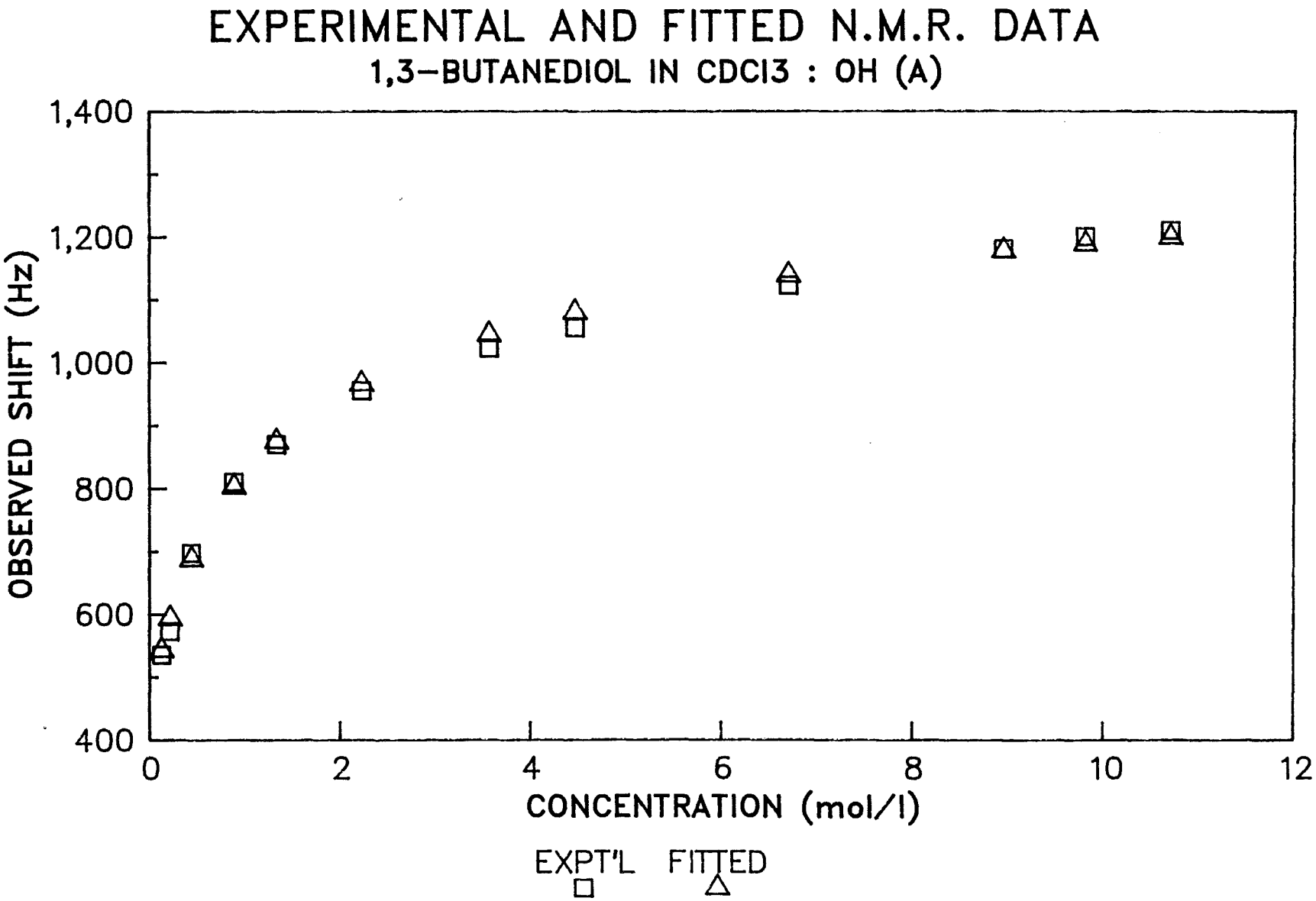
EXPERIMENTAL AND FITTED N.M.R. DATA
1,3–BUTANEDIOL IN CDCl3 : OH (A)
OBSERVED SHIFT (Hz)
1,400
1,200
1,000
800
600
400
0
2
4
6
8
10
12
CONCENTRATION (mol/l)
EXPT'L
FITTED

Figure 3.9

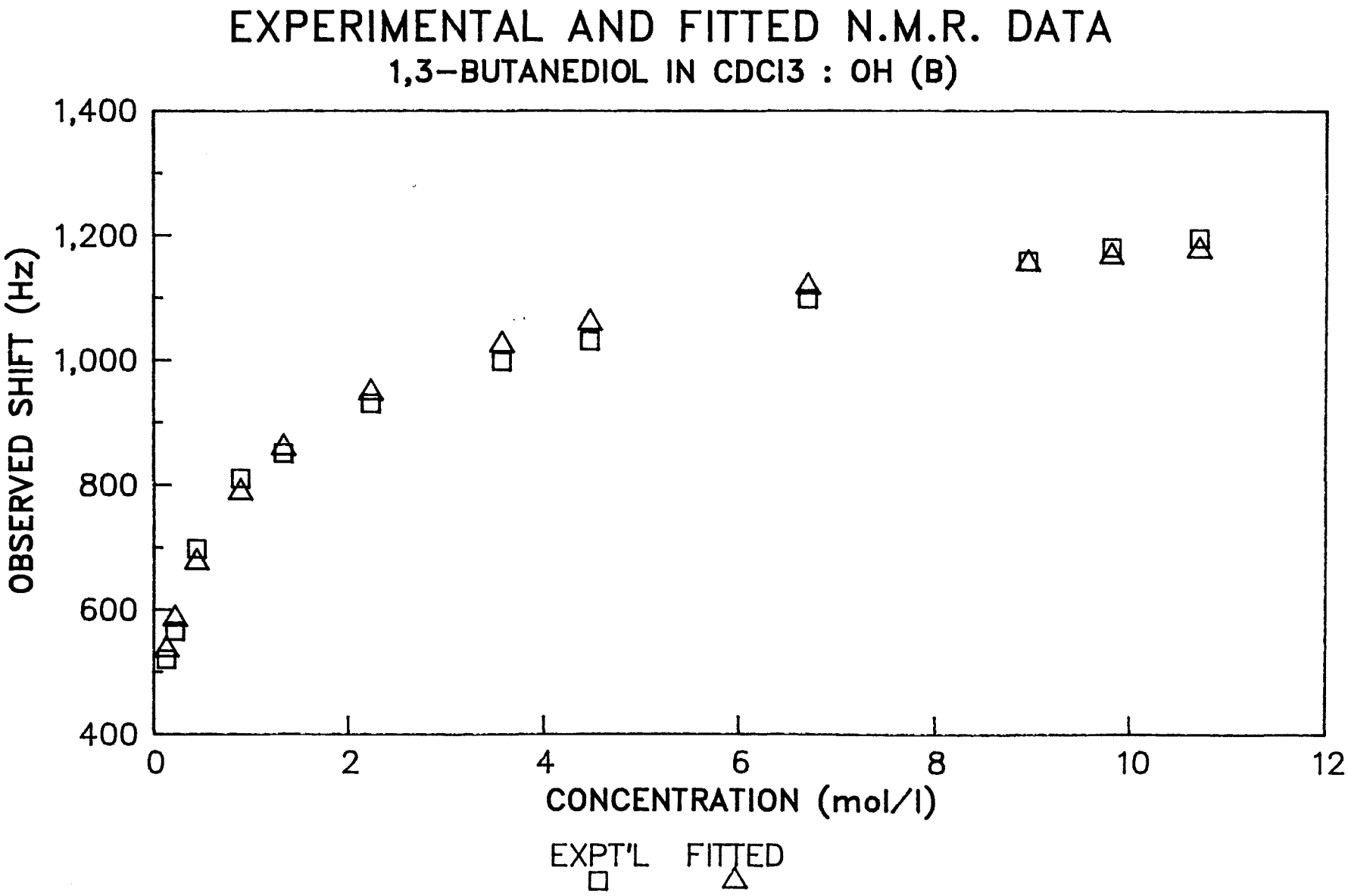
EXPERIMENTAL AND FITTED N.M.R. DATA
1,3–BUTANEDIOL IN CDCl3 : OH (B)
OBSERVED SHIFT (Hz)
1,400
1,200
1,000
800
600
400
0
2
4
6
8
10
12
CONCENTRATION (mol/l)
EXPT'L
FITTED

Figure 3.10

## 3.4 VARIABLE TEMPERATURE $^1$H N.M.R. STUDIES

It has now been established that self-association in both 1,3-butanediol / $CDCl_3$ and 2,3-butanediol / $CDCl_3$ systems leads to the formation , predominantly , of monomer - dimer equilibria. The aim of the work in this section was to obtain thermodynamic data about these equilibria. With this in mind , a series of diol solutions were prepared using $CDCl_3$ as the solvent and the hydroxyl chemical shifts were determined for each solution over the temperature range 283K to 313K. The data obtained and subsequent analyses are described in the following sections.

### 3.4.1 INTERPRETATION OF DATA

Once again a method with which to usefully interpret the data had to be devised. To this end a second self-association model was constructed. As a useful guide , the nomenclature used in the subsequent equations is as follows :

$[A]_o$ = total diol concentration
$[A]$ = monomer concentration
$[A_2]$ = dimer concentration
$[A_F]$ = "free" hydroxyl concentration
$K_2$ = self-association constant
$d_{obs}$ = observed chemical shift
$d_m$ = monomer shift
$d_d$ = dimer shift

It has already been shown that a monomer - dimer equilibrium system exists in both cases under study.

Let us assume that when dimers form , both hydroxyls are involved in the associative process i.e. cyclic dimers are formed ( figure 3.11 ). This simplifies the analysis considerably.

This equilibrium can be written ,

$$A + A \rightleftharpoons A_2 \qquad (3.14)$$

and therefore the dimerisation constant can be expressed ,

$$K_2 = [A_2]/[A]^2 \qquad (3.15)$$

The total diol concentration and "free" hydroxyl concentration can be written in terms of the monomer and dimer concentrations as follows ,

$$[A]_o = \sum i[A_i] = [A] + 2[A_2] \qquad (3.16)$$

and

$$[A_F] = 2[A] \qquad (3.17)$$

From equations 3.15 and 3.16 we have ,

$$[A]_o = [A] + 2K_2[A]^2 \qquad (3.18)$$

and by combining 3.17 with 3.18 , $K_2$ can be expressed in terms of $[A]_o$ and $[A_F]$ , thus ,

$$K_2 = (2[A]_o - [A_F])/[A_F]^2 \qquad (3.19)$$

Thus , the self-association constant , which is temperature dependent , can be calculated provided that

$[A_F]$ , the "free" hydroxyl concentration is known at any given temperature.

A fundamental expression , relating an observed chemical shift to a particular alcohol concentration , has been established by Pople et. al [97].

$$\frac{d_{obs} - d_m}{d_d - d_{obs}} = \frac{[A]_o - [A_F]}{[A_F]} \qquad (3.20)$$

This can easily be rearranged to yield an expression in $[A_F]$ ,

$$[A_F] = [A]_o(d_d - d_{obs})/(d_d - d_m) \qquad (3.21)$$

If $d_m$ and $d_d$ , the theoretical minimum and maximum self-association limits , are known , $[A_F]$ may be calculated for any diol concentration. These limits were , of course , obtained from the variable concentration work described previously.

## 3.4.2 RESULTS FOR 2,3-BUTANEDIOL

5 solutions of 2,3-butanediol in $CDCl_3$ were made up spanning the range from 11.04 mol/l (i.e. neat 2,3-butanediol ) down to 2.21 mol/l. Chemical shifts were measured in Hertz with respect to the methyl peak in the spectrum , as previously. The data obtained for the variable temperature experiments are shown in table 3.6.

**Chemical Shift (Hz) versus Temperature : 2,3-butanediol**

| | Concentration (mol/l) | | | | |
|---|---|---|---|---|---|
| T (K) | 2.21 | 4.42 | 6.62 | 8.83 | 11.04 |
| 283 | 991.5 | 1054.5 | 1100.0 | 1160.0 | 1170.8 |
| 288 | 948.3 | 1029.3 | 1078.3 | 1132.5 | 1137.9 |
| 293 | 906.4 | 977.0 | 1054.1 | 1105.9 | 1125.9 |
| 298 | 869.8 | 952.9 | 1024.3 | 1076.7 | 1100.5 |
| 303 | 840.1 | 920.4 | 1009.5 | 1051.5 | 1075.8 |
| 308 | 794.9 | 890.0 | 976.8 | 1027.8 | 1048.4 |
| 313 | 767.5 | 866.3 | 940.6 | 1004.0 | 1014.3 |

Table 3.6

This data , in conjunction with $d_m$ and $d_d$ ( 278.3 Hz and 1284.8 Hz respectively ) was used to calculate $[A_F]$ for each concentration and temperature.

**$[A_F]$ for 2,3-butanediol : function of temp. and conc.**

| | Concentration (mol/l) | | | | |
|---|---|---|---|---|---|
| T (K) | 2.21 | 4.42 | 6.62 | 8.83 | 11.04 |
| 283 | 0.64 | 1.01 | 1.22 | 1.09 | 1.25 |
| 288 | 0.74 | 1.12 | 1.36 | 1.34 | 1.61 |
| 293 | 0.83 | 1.35 | 1.52 | 1.57 | 1.74 |
| 298 | 0.91 | 1.46 | 1.71 | 1.83 | 2.02 |
| 303 | 0.98 | 1.60 | 1.81 | 2.05 | 2.29 |
| 308 | 1.08 | 1.73 | 2.03 | 2.25 | 2.59 |
| 313 | 1.14 | 1.84 | 2.26 | 2.46 | 2.97 |

Table 3.7

The data contained in table 3.7 may be interpreted in a physical sense by considering the temperature effect. An increase in temperature will increase the thermal motion of the 2,3-butanediol molecules. There will be less opportunity to undergo any self-association and any associated structures which have been formed will break up much more readily as the temperature is raised. Therefore , increasing

temperature will disfavour self-association and this is reflected in the increase in $[A_F]$ with temperature. Also , if $[A_F]$ is considered as a percentage of the total alcohol concentration , $[A]_o$ , there is an increase with decreasing concentration. This is to be expected since , at lower concentrations , there will be less tendency for association to occur due to intervening solvent molecules.

These calculated $[A_F]$ values may now be used in the calculation of self-association constant data and table 3.8 shows the effect of temperature and total alcohol concentration on this variable.

**$K_2$ for 2,3-butanediol : function of temp. and conc.**

| | Concentration (mol/l) | | | | |
|---|---|---|---|---|---|
| T (K) | 2.21 | 4.42 | 6.62 | 8.83 | 11.04 |
| 283 | 9.23 | 7.68 | 8.08 | 13.95 | 13.33 |
| 288 | 6.72 | 6.15 | 6.42 | 9.09 | 7.90 |
| 293 | 5.21 | 4.11 | 5.07 | 6.53 | 6.72 |
| 298 | 4.24 | 3.46 | 3.94 | 4.73 | 4.92 |
| 303 | 3.58 | 2.83 | 3.49 | 3.71 | 3.77 |
| 308 | 2.86 | 2.37 | 2.72 | 3.04 | 2.91 |
| 313 | 2.52 | 2.07 | 2.15 | 2.51 | 2.17 |

Table 3.8

The influence of temperature is as would be expected , i.e. as the temperature increases there is a diminished tendency for the diol to self-associate , leading to a decrease in dimerisation constant.

The effect of $[A]_o$ on $K_2$ is not easy to explain. If the 2,3-butanediol / $CDCl_3$ solution were ideal and if cyclic dimers were the only self-associated

structures formed , then one would expect $K_2$ to be dependent only on temperature. For higher temperatures there is indeed only a small variation in $K_2$ with $[A]_o$. It is apparent from table 3.8 that at lower temperatures there is far greater variation and it is at these temperatures that the tendency for self-association would be greatest. It is probable that the contribution to association by other mechanisms e.g. chains or larger cyclic structures , is at the root of this variation.

### 3.4.2.1 ENTHALPY OF H-BONDING IN 2,3-BUTANEDIOL

Having obtained self-association constant data over a range of temperatures it should now be possible to calculate the enthalpy of hydrogen bonding , $\Delta H^o$. This can be done quite simply by using the Van't Hoff equation :

$$\frac{d\ ln(K)}{d\ (1/T)} = \frac{-\Delta H^o}{R} \qquad (3.22)$$

where R is the universal gas constant (8.314 $Jmol^{-1}K^{-1}$) and $\Delta H^o$ can be calculated from the slope of a plot of ln (K) versus 1/T.

This equation will only be relevant if reliable association constant data are used. Consequently the low temperature data from table 3.8 ( 283K and 288K ) were omitted from the plot. Average values of $K_2$ were calculated at each temperature and are shown in table

3.9. The resultant Van't Hoff plot is shown in figure 3.11.

| T (K) | $K_{assoc}$ (avg) | 1/T ($K^{-1}/10^{-3}$) | ln ($K_{assoc}$) |
|---|---|---|---|
| 293 | 5.53 | 3.41 | 1.71 |
| 298 | 4.26 | 3.36 | 1.45 |
| 303 | 3.48 | 3.30 | 1.25 |
| 308 | 2.78 | 3.25 | 1.02 |
| 313 | 2.28 | 3.19 | 0.82 |

Table 3.9

It is immediately obvious from figure 3.11 that a highly linear relationship exists between ln ($K_{assoc}$) and 1/T ( r = 0.997 ). From the slope a value of -33.3 $kJmol^{-1}$ is obtained for $\Delta H^{\ominus}$.

## 3.4.3 RESULTS FOR 1,3-BUTANEDIOL

5 solutions of 1,3-butanediol in $CDCl_3$ , ranging from 11.17 mol/l ( neat 1,3-butanediol ) to 2.23 mol/l, were made up and $^1H$ n.m.r. spectra run in the usual manner. As in the variable concentration work ( section 3.3.3 ) two sets of hydroxyl peaks were obtained. The spectra were analysed in terms of both hydroxyl shifts separately ; the data obtained from the variable temperature experiments are shown in tables 3.10 and 3.11 respectively.

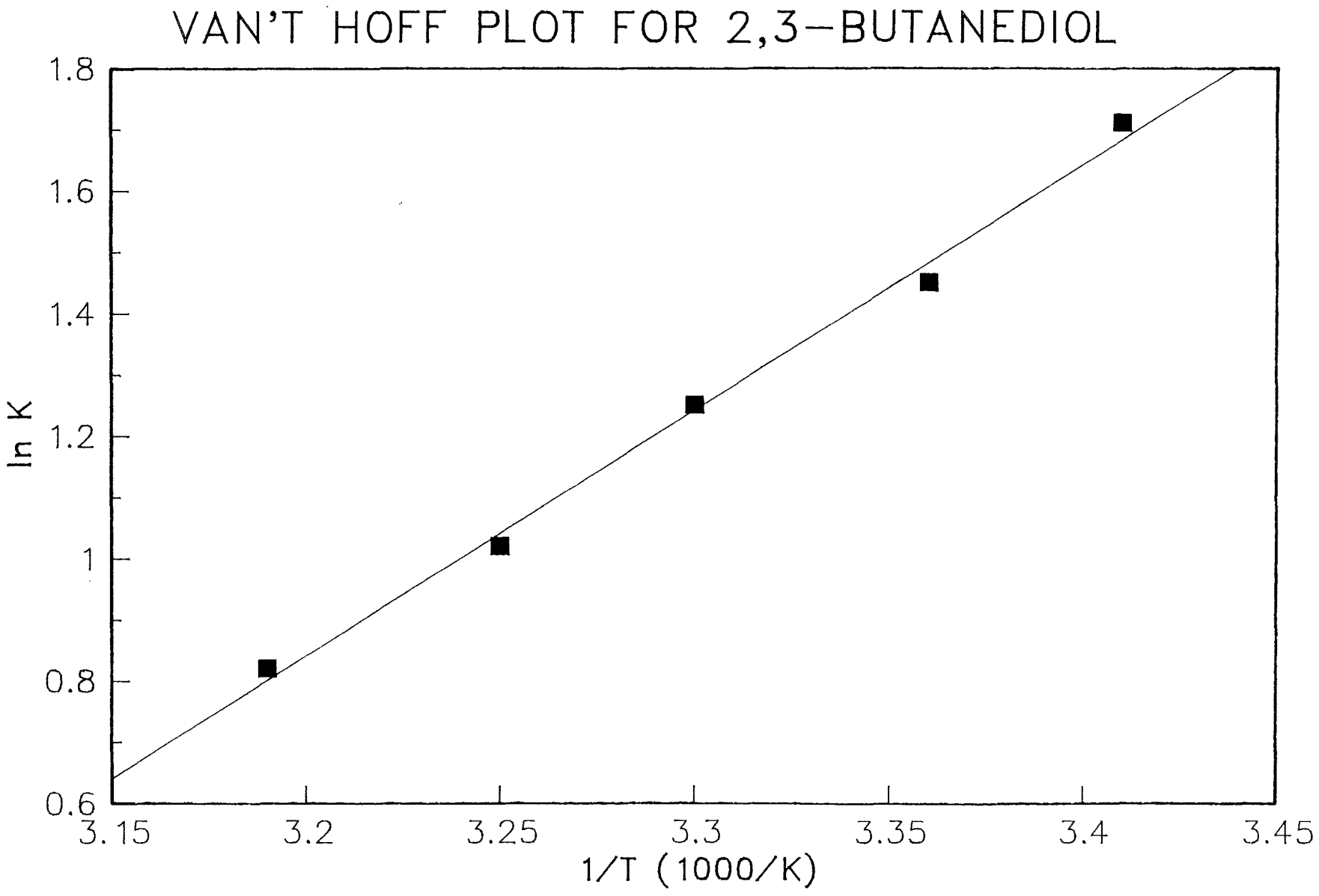
VAN'T HOFF PLOT FOR 2,3-BUTANEDIOL
ln K
1.8
1.6
1.4
1.2
1
0.8
0.6
3.15
3.2
3.25
3.3
3.35
3.4
3.45
1/T (1000/K)

Figure 3.11

Chemical Shift (Hz) v. Temperature : $OH_A$

| | Concentration (mol/l) | | | | |
|---|---|---|---|---|---|
| T (K) | 2.23 | 4.47 | 6.70 | 8.93 | 11.17 |
| 283 | 1059.6 | 1139.3 | 1182.1 | 1241.5 | 1261.7 |
| 288 | 1021.1 | 1113.3 | 1156.0 | 1222.1 | 1237.5 |
| 293 | 985.6 | 1084.5 | 1129.9 | 1196.0 | 1223.6 |
| 298 | 960.8 | 1062.1 | 1105.9 | 1176.8 | 1198.0 |
| 303 | 922.6 | 1028.2 | 1088.8 | 1153.3 | 1179.9 |
| 308 | 885.6 | 1006.2 | 1061.2 | 1128.9 | 1154.8 |
| 313 | 856.7 | 969.6 | 1036.8 | 1097.9 | 1137.5 |

Table 3.10

Chemical Shift (Hz) v. Temperature : $OH_B$

| | Concentration (mol/l) | | | | |
|---|---|---|---|---|---|
| T (K) | 2.23 | 4.47 | 6.70 | 8.93 | 11.17 |
| 283 | 1075.9 | 1153.8 | 1193.2 | 1241.5 | 1265.4 |
| 288 | 1038.2 | 1128.5 | 1168.0 | 1222.1 | 1241.2 |
| 293 | 1003.4 | 1100.8 | 1141.5 | 1196.0 | 1227.0 |
| 298 | 978.9 | 1079.1 | 1120.4 | 1183.8 | 1202.0 |
| 303 | 941.7 | 1046.1 | 1103.3 | 1161.0 | 1183.9 |
| 308 | 904.5 | 1024.7 | 1076.6 | 1138.2 | 1154.8 |
| 313 | 876.8 | 988.9 | 1053.1 | 1108.1 | 1137.5 |

Table 3.11

Knowing $d_m$ and $d_d$ from the variable concentration work ( $OH_A$ : $d_m$ = 437.49 Hz , $d_d$ = 1482.58 Hz. $OH_B$ : $d_m$ = 434.64 Hz , $d_d$ = 1455.14 Hz ) and using equation 3.21, $[A_F]$ was calculated for each concentration and temperature.

[$A_F$] for $OH_\alpha$ : function of temp. and conc.

| | Concentration (mol/l) | | | | |
|---|---|---|---|---|---|
| | 2.23 | 4.47 | 6.70 | 8.93 | 11.17 |
| T (K) | | | | | |
| 283 | 0.90 | 1.47 | 1.93 | 2.06 | 2.36 |
| 288 | 0.93 | 1.58 | 2.09 | 2.23 | 2.62 |
| 293 | 1.06 | 1.70 | 2.26 | 2.45 | 2.77 |
| 298 | 1.11 | 1.80 | 2.41 | 2.61 | 3.04 |
| 303 | 1.19 | 1.94 | 2.52 | 2.81 | 3.24 |
| 308 | 1.27 | 2.04 | 2.70 | 3.02 | 3.50 |
| 313 | 1.34 | 2.19 | 2.86 | 3.29 | 3.69 |

Table 3.12

[$A_F$] for $OH_\beta$ : function of temp. and conc.

| | Concentration (mol/l) | | | | |
|---|---|---|---|---|---|
| | 2.23 | 4.47 | 6.70 | 8.93 | 11.17 |
| T (K) | | | | | |
| 283 | 0.83 | 1.32 | 1.72 | 1.87 | 2.08 |
| 288 | 0.91 | 1.43 | 1.88 | 2.02 | 2.34 |
| 293 | 0.99 | 1.55 | 2.06 | 2.27 | 2.50 |
| 298 | 1.04 | 1.65 | 2.20 | 2.37 | 2.77 |
| 303 | 1.12 | 1.79 | 2.31 | 2.57 | 2.97 |
| 308 | 1.20 | 1.88 | 2.49 | 2.77 | 3.29 |
| 313 | 1.26 | 2.04 | 2.64 | 3.04 | 3.48 |

Table 3.13

As in table 3.7 ( showing the [$A_F$] data for 2,3-butanediol ) the "free" hydroxyl concentration increases with increasing temperature. Also the percentage of "free" hydroxyls increases with increasing concentration due to the reduced opportunity for association at these lower concentrations.

These [$A_F$] values were used to calculate $K_\alpha$ for each concentration by implementing equation 3.19. The resulting self-association constant data for $OH_\alpha$ and $OH_\beta$ are presented in tables 3.14 and 3.15 respectively.

As was the case for 2,3-butanediol , the self association constants decrease as the temperature increases. Again there is a certain amount of variability in $K_2$ with concentration at each temperature although much less than for 2,3-butanediol ( < 15% compared with ca. 20-30%).

$K_2$ (mol/l) for $OH_a$ : function of temp. and conc.

| | Concentration (mol/l) | | | | |
|---|---|---|---|---|---|
| | 2.23 | 4.47 | 6.70 | 8.93 | 11.17 |
| T (K) | | | | | |
| 283 | 4.40 | 3.46 | 3.08 | 3.72 | 3.59 |
| 288 | 3.62 | 2.95 | 2.59 | 3.14 | 2.87 |
| 293 | 3.03 | 2.51 | 2.18 | 2.56 | 2.55 |
| 298 | 2.72 | 2.20 | 1.89 | 2.24 | 2.09 |
| 303 | 2.31 | 1.86 | 1.71 | 1.91 | 1.82 |
| 308 | 1.98 | 1.66 | 1.47 | 1.63 | 1.54 |
| 313 | 1.74 | 1.41 | 1.29 | 1.35 | 1.37 |

Table 3.14

$K_2$ (mol/l) for $OH_b$ : function of temp. and conc.

| | Concentration (mol/l) | | | | |
|---|---|---|---|---|---|
| | 2.23 | 4.47 | 6.70 | 8.93 | 11.17 |
| T (K) | | | | | |
| 283 | 5.27 | 4.37 | 3.95 | 4.57 | 4.68 |
| 288 | 4.29 | 3.67 | 3.26 | 3.88 | 3.65 |
| 293 | 3.54 | 3.08 | 2.67 | 3.03 | 3.17 |
| 298 | 3.16 | 2.68 | 2.31 | 2.76 | 2.55 |
| 303 | 2.66 | 2.23 | 2.08 | 2.31 | 2.20 |
| 308 | 2.26 | 2.00 | 1.76 | 1.97 | 1.76 |
| 313 | 2.02 | 1.66 | 1.54 | 1.60 | 1.56 |

Table 3.15

### 3.4.3.1 ENTHALPY OF H-BONDING IN 1,3-BUTANEDIOL

$\Delta H^{\circ}$ for self-association in 1,3-butanediol was calculated from a plot of ln ($K_2$) against 1/T by measuring the slope , again using the Van't Hoff equation (eqn. 3.22 ) . The analysis was carried out for both $OH_A$ and $OH_B$ data, taking the average $K_2$ at each temperature. In this instance , due to the lower variability of $K_2$ with concentration , even at lower temperatures , all of the points were used. The Van't Hoff plots are shown infigures 3.12 and 3.13 with the corresponding data in tables 3.16 and 3.17.

**Van't Hoff data : $OH_A$**

| T (K) | $K_2$(avg) | 1/T ($K^{-1}/10^{-3}$) | ln ($K_2$) |
|---|---|---|---|
| 283 | 3.65 | 3.53 | 1.29 |
| 288 | 3.03 | 3.47 | 1.11 |
| 293 | 2.57 | 3.41 | 0.94 |
| 298 | 2.23 | 3.36 | 0.80 |
| 303 | 1.92 | 3.30 | 0.65 |
| 308 | 1.66 | 3.25 | 0.50 |
| 313 | 1.43 | 3.19 | 0.36 |

Table 3.16

**Van't Hoff data : $OH_B$**

| T (K) | $K_2$(avg) | 1/T ($K^{-1}/10^{-3}$) | ln ($K_2$) |
|---|---|---|---|
| 283 | 4.57 | 3.53 | 1.52 |
| 288 | 3.75 | 3.47 | 1.32 |
| 293 | 3.10 | 3.41 | 1.13 |
| 298 | 2.69 | 3.36 | 0.99 |
| 303 | 2.30 | 3.30 | 0.83 |
| 308 | 1.95 | 3.25 | 0.67 |
| 313 | 1.68 | 3.19 | 0.52 |

Table 3.17

The results obtained from the analysis of these plots are summarised below.

| | $\Delta H^{o}$ (kJmol$^{-1}$) | r |
|---|---|---|
| $OH_{\alpha}$ | -22.8 | 1.00 |
| $OH_{\beta}$ | -24.4 | 1.00 |

Table 3.18

## 3.5 DISCUSSION OF RESULTS

Two separate approaches have been used in this chapter to study hydrogen-bonding within 1,3-butanediol and 2,3-butanediol , i.e. variable concentration and variable temperature $^{1}H$ n.m.r. spectroscopy. The purpose of the variable concentration work was twofold. Firstly , it was used to calculate values for $d_m$ and $d_d$, the monomer shift and dimer shift of each of the diols respectively. This information was important since it was then used to generate thermodynamic parameters for self-association in conjunction with the variable temperature data obtained. Previous workers in this field have used alternative methods of calculating $d_m$ and $d_d$. For example , Davis et. al. [79] obtained $d_m$ by extrapolating to $[A]_o = 0$ from a plot of chemical shift vs. concentration. If we refer to figures 3.5 , 3.9 and 3.10 , it is fairly obvious that there is considerable room for error in doing it this way since the curves approach the y-axis almost asymptotically. Fraser et. al. [40,48] and Littlewood and Willmott [88] plotted chemical shift vs. $1/C^{0.5}$ at various

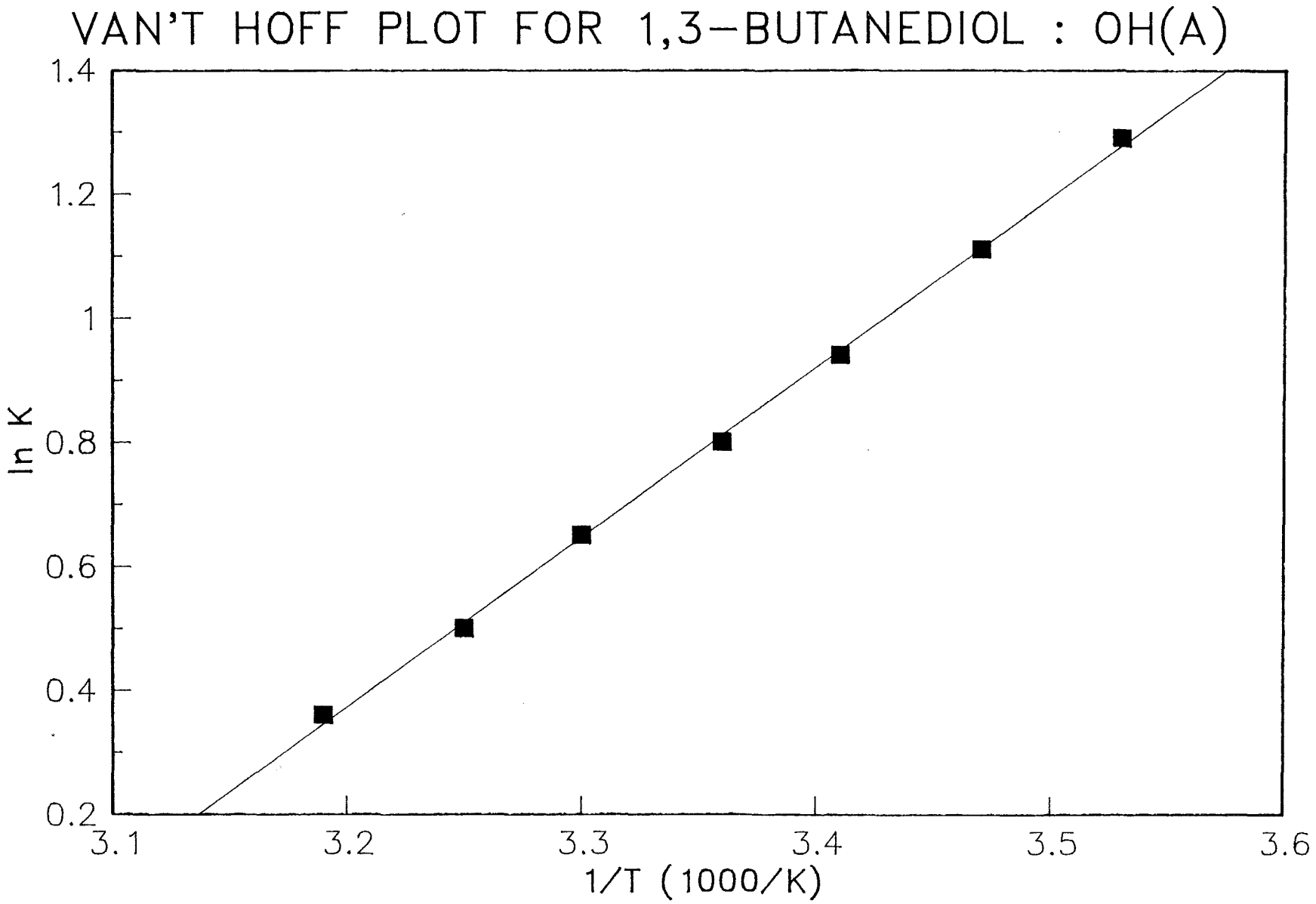
VAN'T HOFF PLOT FOR 1,3-BUTANEDIOL : OH(A)
ln K
1.4
1.2
1
0.8
0.6
0.4
0.2
3.1
3.2
3.3
3.4
3.5
3.6
1/T (1000/K)

Figure 3.12

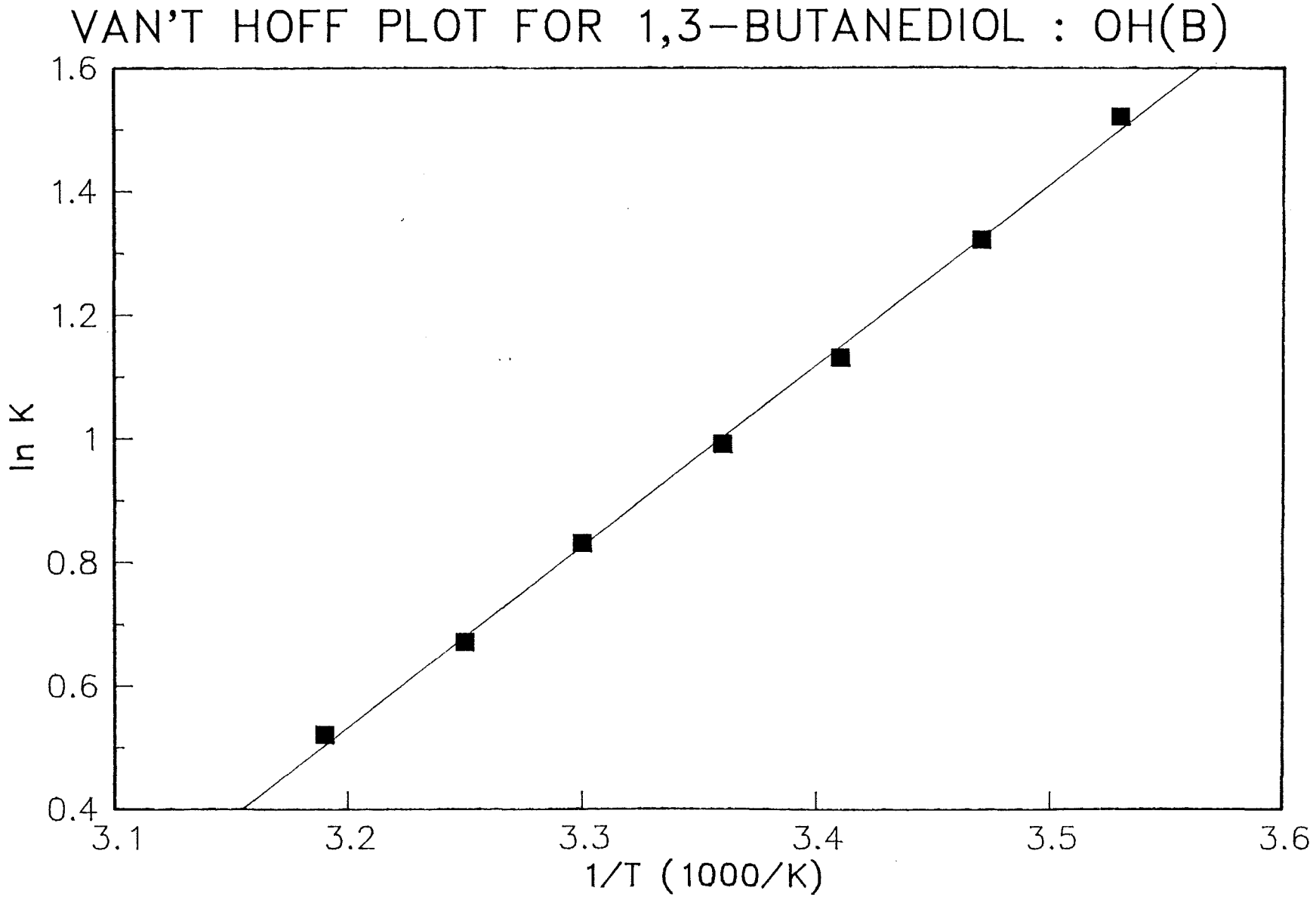
VAN'T HOFF PLOT FOR 1,3-BUTANEDIOL : OH(B)
ln K
1.6
1.4
1.2
1
0.8
0.6
0.4
3.1
3.2
3.3
3.4
3.5
3.6
1/T (1000/K)

Figure 3.13

temperatures and obtained $d_m$ from the y-axis intercept. $d_d$ was calculated from the relationship $d_d - d_m = 4.5$ p.p.m. [98,99]. In both cases $d_m$ was found to be variable over the temperature range studied and was therefore not an accurate measure of the monomer shift. The hydroxyl proton chemical shift of a monomeric alcohol species should be independent of temperature over the range involved in these experiments (283K - 313K). In our opinion , using the variable concentration data in conjunction with the iterative algorithm derived from the dimer model is a more accurate way of determining the monomer and dimer shifts than either of the above methods.

Secondly the data obtained was used to confirm that the proposed dimer model was a reasonable one. Having obtained $d_m$ , $d_d$ and $K_2$ via the algorithm for each of the diols , it was then a trivial exercise to calculate predicted chemical shift for a given concentration. Figures 3.5 , 3.9 and 3.10 show plots of experimental data alongside the predicted data and it is clear that the correlation between the two is extremely high. It would appear , therefore , that in both diol / solvent systems , over the concentration range studied , the diols exist primarily in a monomer - dimer equilibrium.

There was no indication as to what form these dimers took. For example , the dimer species may adopt a symmetrical cyclic structure involving four non-

linear hydrogen bonds as in figure 3.2. Alternatively , there are a number of possible asymmetrical open chain dimer structures involving 1 or 2 hydrogen bonds. In the second part of this chapter , variable temperature studies were carried out. One of the major assumptions made , prior to the formulation of a model with which to analyse the data , was that the dimers were in fact closed cyclic species. This assumption was made primarily to simplify the analysis. However in Chapter 4 , theoretical studies have been carried out which go some way to justifying this assumption.

The purpose of the variable temperature work was to calculate the heat of association , $\Delta H^{\circ}$ , for these diol dimers. The results are summarised below and compared with data for other alcohol/solvent systems obtained by others using the $^{1}H$ n.m.r. technique.

| System | $\Delta H^{\circ}$ (kJmol$^{-1}$) | Ref. |
|---|---|---|
| 2,3-butanediol/ $CDCl_3$ | -33.3 | ---- |
| 1,3-butanediol/ $CDCl_3$ | -22.8 ($OH_A$) | ---- |
| | -24.4 ($OH_B$) | ---- |
| 1-dodecanol/ squalane | -42.2 | [88] |
| propan-2-ol/ cyclohexane | -53.6 | [40] |
| methanol/$CCl_4$ | -38.6 | [79] |
| 2-pentanol/ n-heptane | -34.4 | [86] |
| t-pentanol/ n-heptane | -58.3 | [86] |

Table 3.19

It is fairly obvious that a wide range of values have been determined for hydrogen bond strengths and much is dependent upon the system under study. It is apparent , however , that the values obtained for the diol / $CDCl_3$ systems are , in general , lower than those quoted for the others. It is not clear as to why this should be. It may be the fact that diols are being compared with mono-functional alcohols. Alternatively the solvent may be interfering to a certain extent in the hydrogen bonding or other associative mechanisms may be contributing , leading to a distorted $\Delta H^{\circ}$ value.

It is much more interesting and useful to compare the results for the two diols. First of all , let us consider the relative heats of association i.e. -33.3 $kJmol^{-1}$ for 2,3-butanediol and ca. -23.6 $kJmol^{-1}$ for 1,3-butanediol. If we assume that the changes in entropy ( $\Delta S^{\circ}$) involved in the formation of both dimers are roughly the same , then the Gibbs free energy ,which is given by ,

$$\Delta G^{\circ} = \Delta H^{\circ} - T \Delta S^{\circ} \qquad (3.23)$$

will be more negative for the formation of a 2,3-butanediol dimer than for a 1,3-butanediol dimer. In other words , self-association will be more favourable in the former than in the latter.

Another aspect to consider is the fraction of 'free' hydroxyls present in the various solutions

studied i.e. the 'free' hydroxyl concentration as a percentage of the total diol concentration. Tables 3.20 and 3.21 show this data as a function of concentration and temperature for both diols ( only $OH_a$ of 1,3-butanediol is considered ). The figures are calculated directly from tables 3.7 and 3.12 respectively.

**Fraction of 'free' hydroxyls in 2,3-butanediol**

| | Concentration | | | | |
|---|---|---|---|---|---|
| | 2.21 | 4.42 | 6.62 | 8.83 | 11.04 |
| T (K) | | | | | |
| 283 | 0.29 | 0.23 | 0.18 | 0.12 | 0.11 |
| 288 | 0.33 | 0.25 | 0.21 | 0.15 | 0.15 |
| 293 | 0.38 | 0.31 | 0.23 | 0.18 | 0.16 |
| 298 | 0.41 | 0.33 | 0.26 | 0.21 | 0.18 |
| 303 | 0.44 | 0.36 | 0.27 | 0.23 | 0.21 |
| 308 | 0.49 | 0.39 | 0.31 | 0.25 | 0.23 |
| 313 | 0.52 | 0.42 | 0.34 | 0.28 | 0.27 |

Table 3.20

**Fraction of 'free' hydroxyls in 1,3-butanediol ($OH_a$)**

| | Concentration | | | | |
|---|---|---|---|---|---|
| | 2.23 | 4.47 | 6.70 | 8.93 | 11.17 |
| T (K) | | | | | |
| 283 | 0.40 | 0.33 | 0.29 | 0.23 | 0.21 |
| 288 | 0.42 | 0.35 | 0.31 | 0.25 | 0.23 |
| 293 | 0.48 | 0.38 | 0.34 | 0.27 | 0.25 |
| 298 | 0.50 | 0.40 | 0.36 | 0.29 | 0.27 |
| 303 | 0.53 | 0.43 | 0.38 | 0.31 | 0.29 |
| 308 | 0.57 | 0.46 | 0.40 | 0.34 | 0.31 |
| 313 | 0.60 | 0.49 | 0.43 | 0.37 | 0.33 |

Table 3.21

Both tables show that , as the temperature increases or as the concentration decreases , the fraction of 'free' hydroxyls increases , as would be expected. The interesting thing to note is the fact that , at similar conditions of concentration and

temperature , there is a greater percentage of 'free' hydroxyls in the 1,3-butanediol solutions.

The question which must now be addressed is how this information fits in with the results of the oxygen-uptake work described in the previous chapter. 1,3-butanediol was found to oxidise readily whereas , under standard conditions , 2,3-butanediol did not react at all.

From the $^{1}H$ n.m.r. studies it has been established that

i) the free energy for hydrogen bond formation is greater for 2,3-butanediol than for 1,3-butanediol.

ii) there are fewer 'free' hydroxyls in 2,3-butanediol than in 1,3-butanediol.

In addition to this , Rochester et. al. have established that 2,3-butanediol binds less firmly to the surface of silica than 1,3-butanediol [53] (see section 2.6.1). Given that for oxidation to begin , there must be some interaction of the substrate with the pigment surface , in this case via a 'free' hydroxyl group , these results may go some way to explaining the non-reactivity of 2,3-butanediol.

# CHAPTER 4

## THEORETICAL STUDIES OF DIOL SYSTEMS

## 4.1 INTRODUCTION

The results obtained in the previous chapter indicated that 1,3-butanediol and 2,3-butanediol existed primarily as dimers in the liquid phase. The $^1H$ n.m.r. results did not , however , reveal any information about the possible structures and conformations of these dimer species. In this chapter, quantum mechanical calculations are carried out on these diols in an attempt to elucidate possible monomer and dimer structures.

Because of the importance of the phenomenon of hydrogen-bonding , a great deal of theoretical work has been carried out in an attempt to gain a better understanding of it at the atomic and molecular level [100 - 103]. In the past , ab initio methods have yielded reliable quantitative results for hydrogen-bonding interactions [104,105]. However these calculations are extremely time consuming and expensive because of the amount of computing time required.

This chapter describes the use of a semi-empirical molecular orbital technique to study possible monomer and dimer structures for both 1,3-butanediol and 2,3-butanediol. Semi-empirical quantum mechanical methods are used to reduce the amount of time spent carrying out theoretical calculations. Rather than calculating molecular properties from first principles , as in ab initio methods , results of 'crude' initial calculations on small molecules are compared with

experimentally measurable properties. The initial values used in the calculations are then modified and refined until there is good agreement between computed and measured values. After this procedure has been carried out for several small molecules (>100) , specific atoms can be assigned parameters. The experimental quantities used to determine these parameters are , for example , heats of formation , geometries , dipole moments and ionisation energies. Having established parameters for specific atoms , these can then be used to carry out calculations on larger and more complex molecules and systems.

## 4.2 EXPERIMENTAL SECTION

The calculations reported on in subsequent sections were carried out on the St. Andrews University VAX/VMS mainframe using the semi-empirical quantum mechanical package , MOPAC (Molecular Orbital Package). For this work the AM1 (Austin Model 1) Hamiltonian was used. AM1 is a general purpose quantum mechanical model which has recently been developed by Dewar et. al. [106,107] , and has the advantage over previously developed models such as MINDO/3 [108] and MNDO [109] that it is a better predictor of heats of formation of hydrogen bonded molecules. It was therefore felt that it was the best Hamiltonian to use , bearing in mind

that the aim of this work was to model hydrogen bonding in diol systems.

## 4.2.1 INPUT OF DATA TO MOPAC

In order to use MOPAC to determine molecular structures , data had to be input in an acceptable format. The standard method was to use a z-matrix , an example of which is given below.

```
CHEMX=I ZMAT=M GRADIENTS AM1
DATA FOR MOPAC
1,3-BUTANEDIOL
1  H
2  C   1.11  1
3  C   1.45  1  110.0  1
4  H   1.11  1  110.0  1  120.0  1    2   3   1
5  H   1.11  1  110.0  1  240.0  1    2   3   1
6  H   1.11  1  110.0  1  300.0  1    3   2   1
7  O   1.35  1  110.0  1   60.0  1    3   2   1
8  H   0.98  1  110.0  1   60.0  1    7   3   2
9  C   1.45  1  110.0  1  180.0  1    3   2   1
10 H   1.11  1  110.0  1   60.0  1    9   3   2
11 H   1.11  1  110.0  1  300.0  1    9   3   2
12 C   1.45  1  110.0  1  180.0  1    9   3   2
13 H   1.11  1  110.0  1  240.0  1   12   9   3
14 H   1.35  1  110.0  1  180.0  1   12   9   3
15 O   1.35  1  110.0  1   60.0  1   12   9   3
16 H   0.98  1  110.0  1  240.0  1   12   9   3
```

Z-matrix for 1,3-butanediol

There are three lines at the beginning of the data file , the first of which contains keywords which specify what type of calculation is required , what to do with the output etc. The second two lines are comment lines which act as an aide memoire for future identification. The remainder of the data file is used to specify the geometry of the molecule ; the example

showing the initial geometry of 1,3-butanediol (see figure 4.1).

To explain briefly the meaning of the various numbers consider , for example , the line corresponding to atom 9 i.e. ,

9 C 1.45 1 110.0 1 180.0 1 3 2 1

The three numbers at the end of the line describe the relationship of the particular atom to those it can be geometrically related to. In this case , atom 9 (C) is linked directly to atom 3 (C) with a bond length of 1.54 A ; atoms 9 (C) , 3 (C) and 2 (C) describe an angle of 110.0° ; and if we consider a Newman projection of atoms 9 (C) , 3 (C) , 2 (C) and 1 (H) , looking along the C3-C2 bond , there is a dihedral angle of 180° between C9 and H1 (see figure 4.1). The 1's after each bond length , angle and dihedral tell the program to optimise these parameters. A zero would mean that the parameter did not require optimising.

Values for initial bond lengths and angles were taken from Pople and Beveridge [110].

## 4.2.2 GRAPHICAL DISPLAY

In order to get a visual perception of the various structures generated , a graphics package , CHEMX (Chemical Design Ltd. , Oxford) was used. Suitable

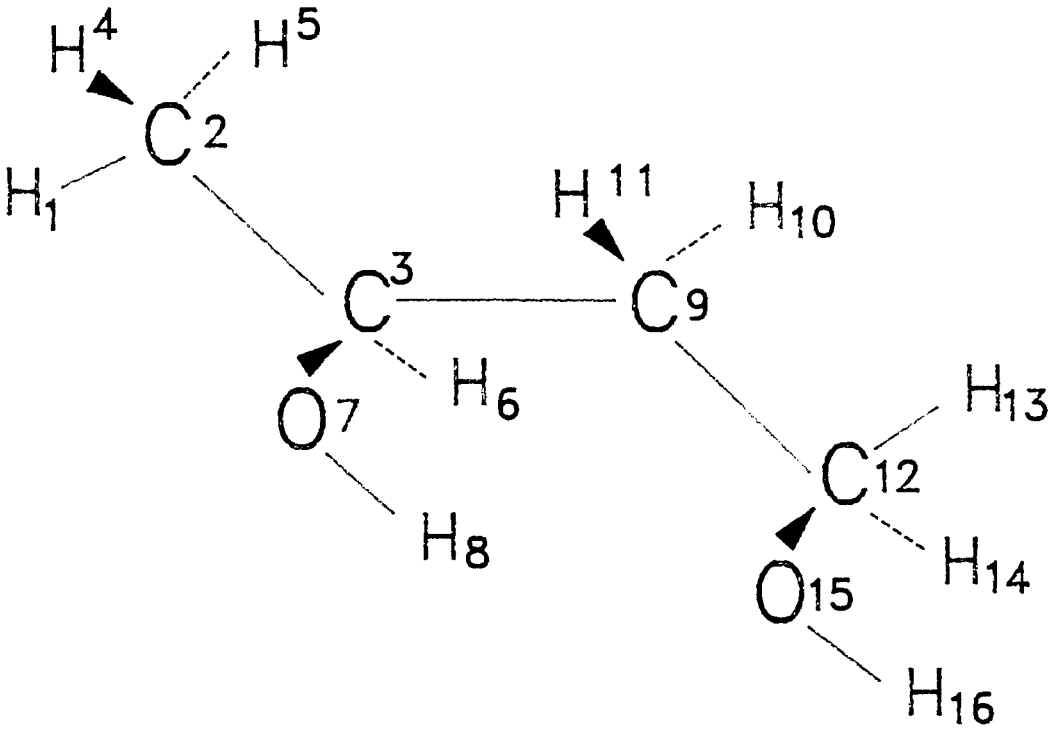


1,3–BUTANEDIOL : CONFORMATION 1

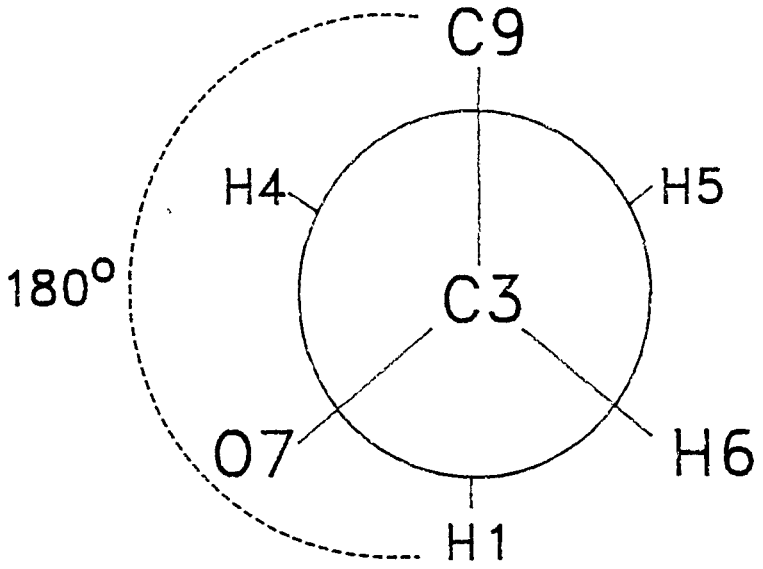


NEWMAN PROJECTION

Figure 4.1

graphics files were generated by MOPAC by entering the appropriate keyword in the first line of the z-matrix. The CHEMX package had the facility to view the molecule from any angle and to vary the sizes and colours of the atoms and bonds in the molecules. Hard copies of these images were obtained by using an EPSON inkjet plotter. Several examples are included in this chapter.

Contour diagrams resulting from rotation calculations were generated by the graphics package SURFACE on the VAX mainframe.

## 4.3 OPTIMISATION OF MONOMERS

Before any attempt was made to look at possible dimer structures for 1,3-butanediol and 2,3-butanediol, the monomers were first considered. The approach taken was to attempt to find the lowest energy configuration for each diol , using the AM1 Hamiltonian. Having achieved an optimum monomer structure , then possible dimer structures were looked at based on the monomer.

It should be noted at this point that both 1,3-butanediol and 2,3-butanediol are chiral molecules. The former has one chiral centre , the latter 2 (see below).

For this work only one enantiomer of each diol was considered ; for 1,3-butanediol the R form and for 2,3-butanediol , the R,S form. This cut down the amount of computing time required considerably.

For each of the two diols , z-matrices corresponding to the chosen enantiomers were constructed and written to MOPAC for subsequent optimisation. Heats of formation for AM1 optimised structures of 1,3-butanediol and 2,3-butanediol are given in table 4.1. The corresponding molecular pictures , as generated by CHEMX , are shown in figures 4.2 and 4.3 respectively.

| Molecule | $\Delta H_f^\circ$ (kcal) |
|---|---|
| 1,3-butanediol | -120.8 |
| 2,3-butanediol | -116.2 |

Table 4.1

It is apparent on inspection of the optimised molecular structures that , in both cases , there appears to be some sort of interaction between the hydroxyls. The intra-molecular hydrogen bond length for both molecules is 0.217nm.

It was decided to further investigate the effect of intramolecular hydrogen-bonding within these molecules on their heats of formation , the results of which are presented in the following section.

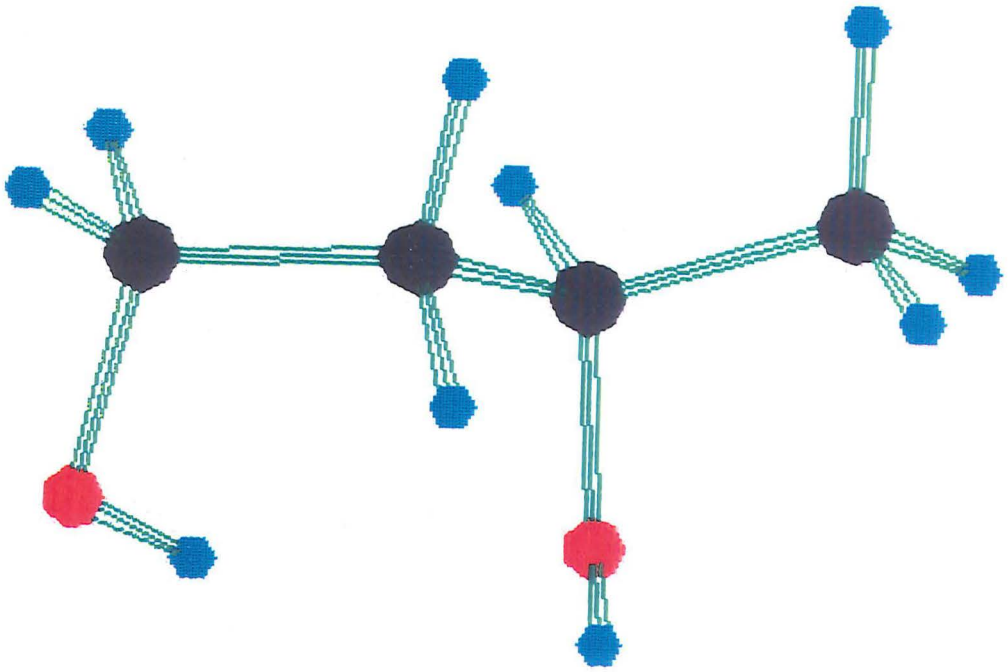

Figure 4.2

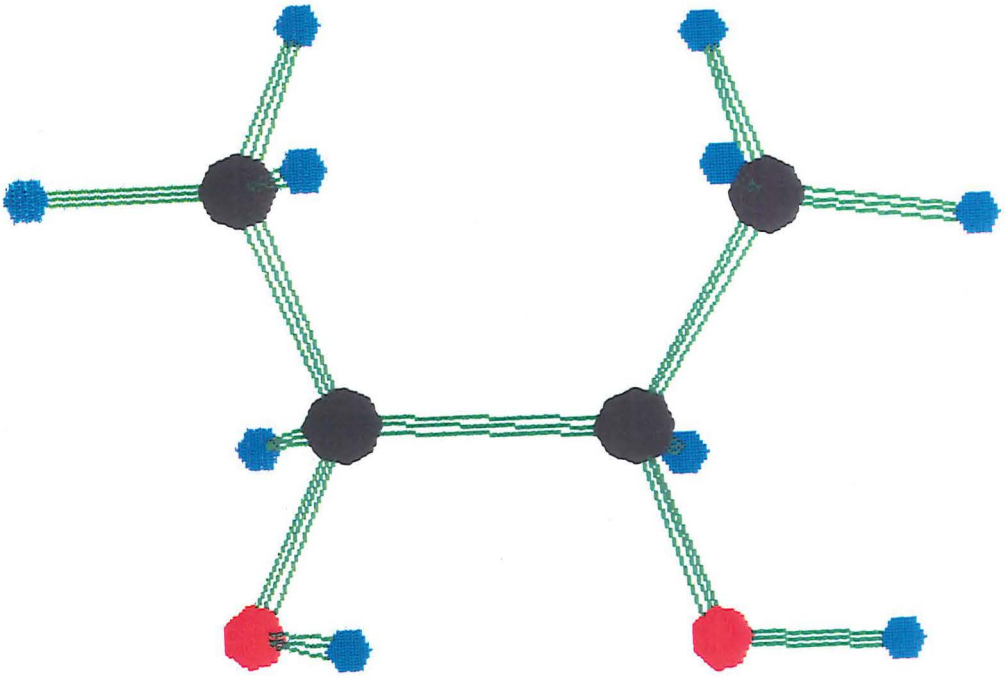

Figure 4.3

## 4.3.1 HYDROXYL ROTATION CALCULATIONS

In order to find out more about the hydrogen bonding interactios within these molecules , rotation calculations were carried out on the hydroxyl functions. This involved holding the molecule in position while rotating both hydroxyls with respect to each other and calculating the molecular heat of formation with the hydroxyls in various positions. A systematic approach was adopted. As an example , consider 2,3-butanediol and call one hydroxyl A and the other B. Hydroxyl B is held fixed while A is rotated through 360°. The heat of formation of the molecule is calculated at 20° intervals. Having completed one cycle, B is rotated through 20° , held fixed and A is again turned through 360° , calculating $\Delta H_f^\circ$ at 20° intervals. This process is repeated until B has gone through the full 360° cycle. The $\Delta H_f^\circ$ data generated can then be used to produce a contour diagram. Figures 4.4 and 4.5 show contour diagrams for rotation calculations carried out on 1,3-butanediol and 2,3-butanediol respectively.

This technique is generally used for 'fine tuning' of the optimisation of molecules (where applicable). The minima can easily be picked out from the contour diagrams and are marked with crosses. Table 4.2 summarises these points.

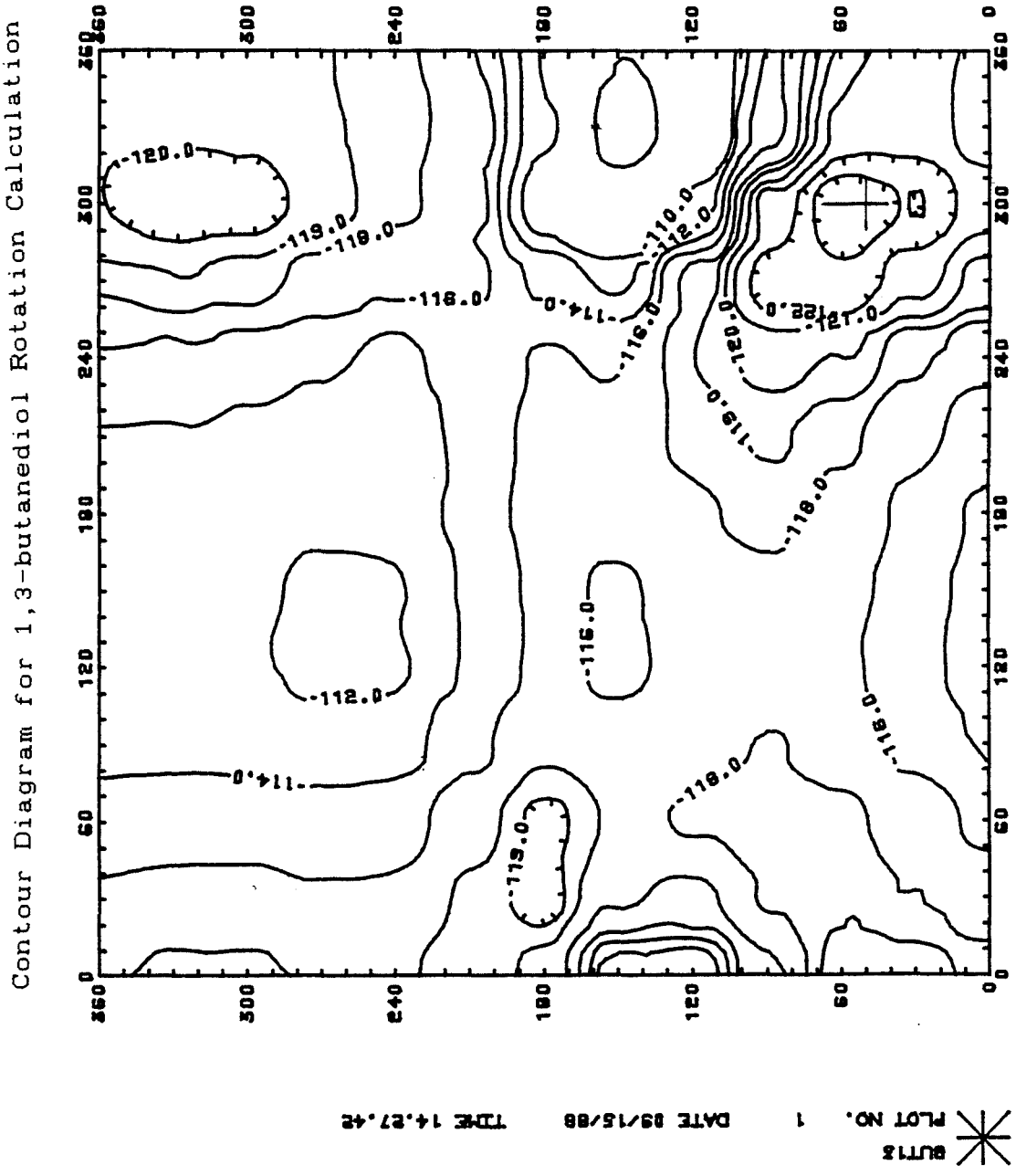
Contour Diagram for 1,3-butanediol Rotation Calculation
-120.0
-119.0
-118.0
-118.0
-114.0
-116.0
-110.0
-112.0
-122.0
-121.0
-120.0
-119.0
-118.0
-116.0
-112.0
-114.0
-119.0
-118.0
-116.0
360
300
240
180
120
60
0
BUTI3
PLOT NO. 1
DATE 89/15/88
TIME 14.27.42

Figure 4.4

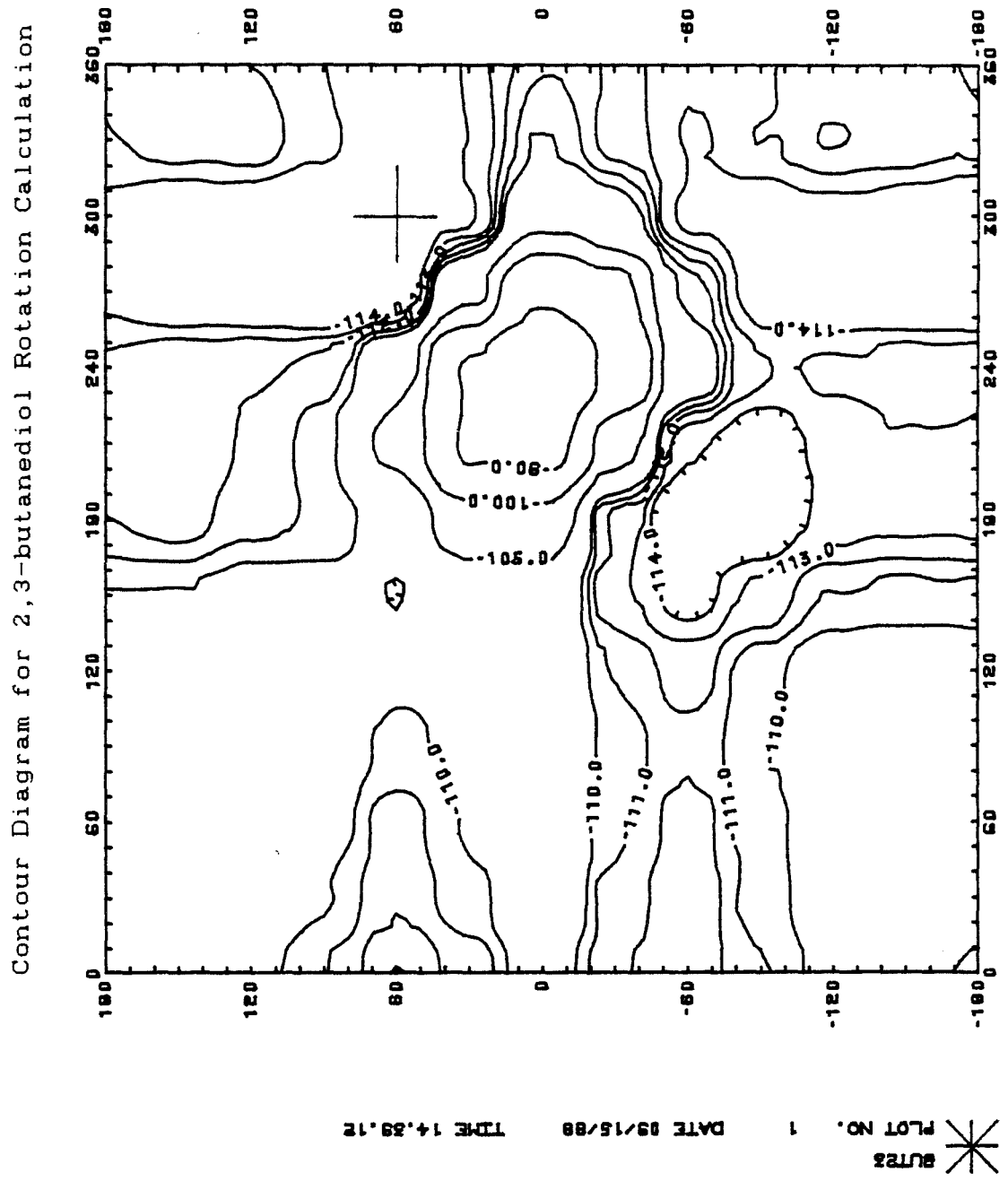
Contour Diagram for 2,3-butanediol Rotation Calculation
-114.0
-90.0
-100.0
-105.0
-114.0
-113.0
-110.0
-110.0
-111.0
-111.0
-110.0
-114.0
180
120
60
0
-60
-120
-180
360
300
240
180
120
60
0
BUTS3
PLOT NO. 1
DATE 09/15/88
TIME 14.39.12

Figure 4.5

| Molecule | $\Delta H_f^\circ$ (kcal) | Co-ords. ($OH_\alpha$,$OH_\beta$) |
|---|---|---|
| 1,3-butanediol | -124.1 | (300°,50°) |
| 2,3-butanediol | -118.8 | (300°,60°) |

Table 4.2

The values for $\Delta H_f^\circ$ are lower than those shown in table 4.1. This 'fine tuning' approach has therefore helped identify deeper minima for these molecules on the potential energy hypersurface. The rotation angles which correspond to these minima were then used to generate molecular pictures. These are shown in figures 4.6 and 4.7.

There appears to be little difference between the 'fine tuned' optimum 1,3-butanediol structure and the original. One intra-molecular hydrogen bond is formed between the proton of the primary hydroxyl and the oxygen of the secondary. The distance between the two atoms is 0.214nm and this slightly shorter H-bond lenghth possibly accounts for the decrease in energy of the molecule.

2,3-butanediol is more interesting. If figures 4.3 and 4.7 are compared (i.e. the two different optimised forms of the molecule) it is apparent that in the former , only one hydrogen bond is formed. In the latter , lower energy configuration it appears that two intra-molecular hydrogen bonds are formed ; the calculated bond lengths being 0.224nm and 0.235nm.

CHEM-X OCTOBER 1987

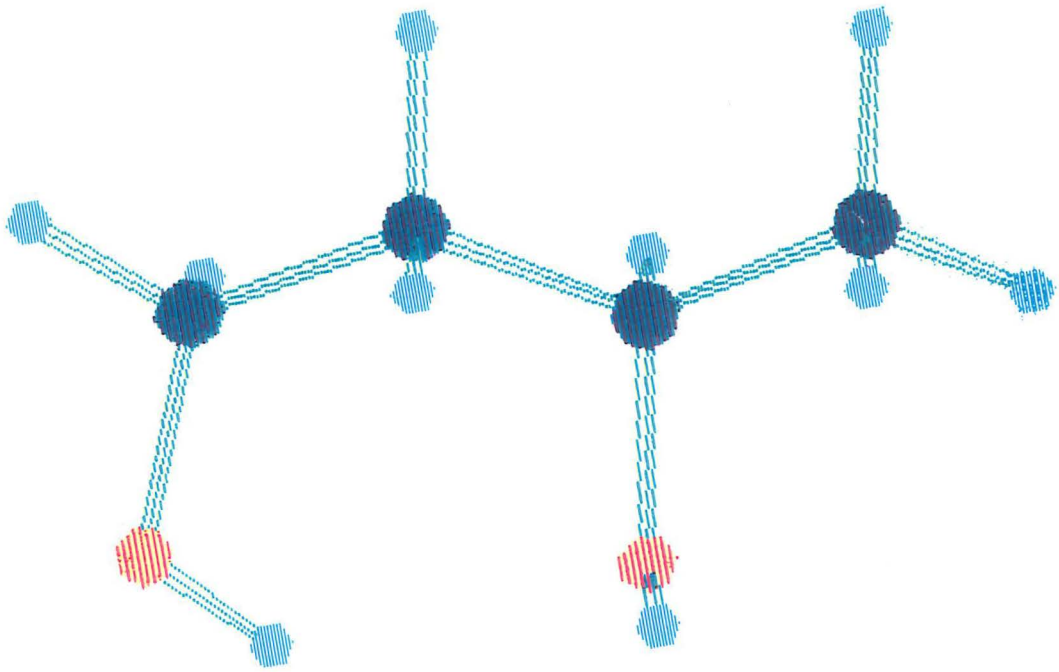

Figure 4.6

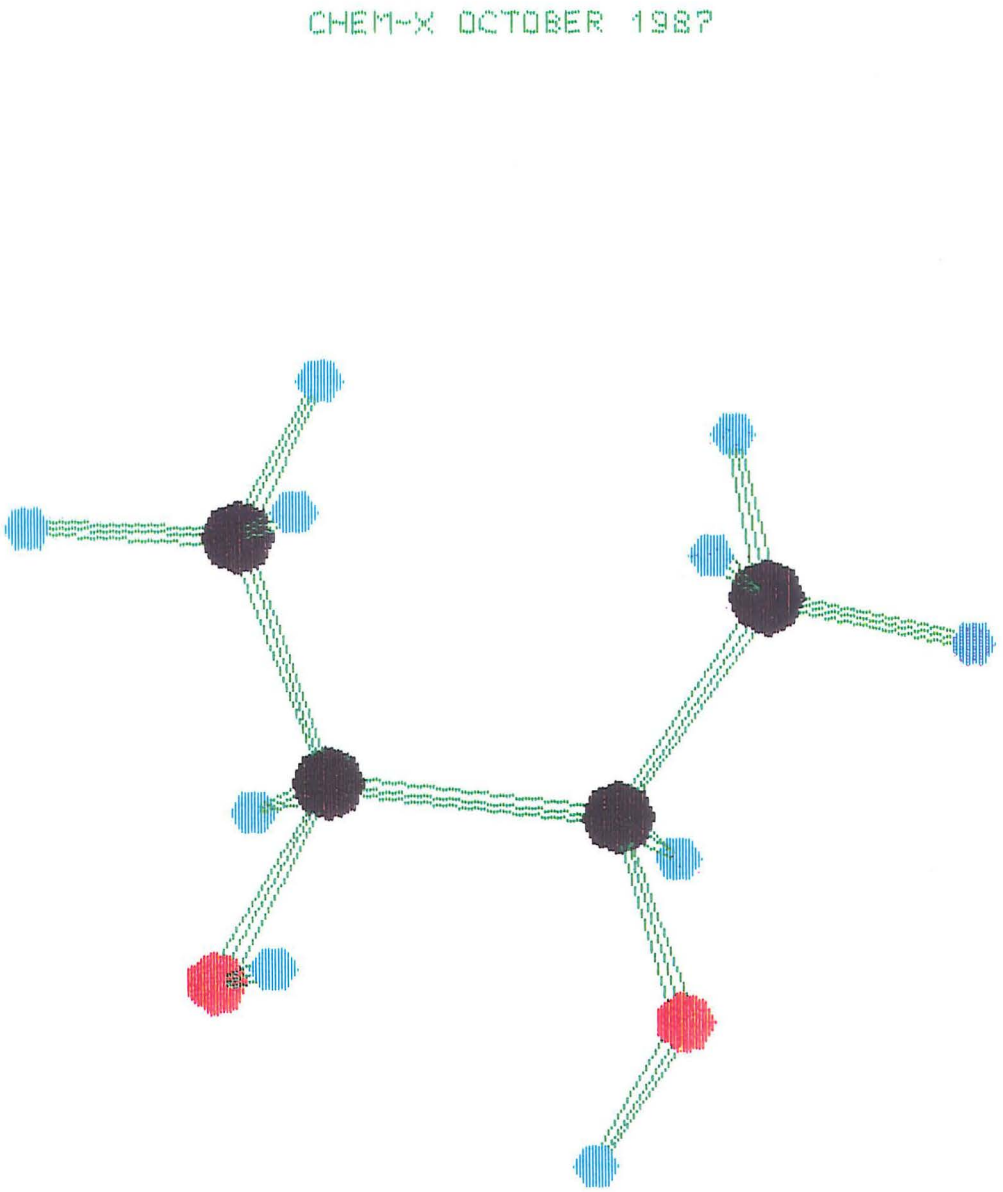


Figure 4.7

This is a particularly interesting finding. If both hydroxyls in the monomer are involved in intra-molecular hydrogen bonding then , relating this to the oxygen-uptake studies , there will be less chance of an interaction with the $TiO_2$ surface. This backs up the observation of the non-reactivity of 2,3-butanediol and may go some way to explaining its poorer absorption to silica , as noted by Rochester et.al. [53].

It is worth pointing out that this minimum energy conformation is one of (probably) several which will exist on the potential energy hypersurface for this molecule. In reality , 2,3-butanediol will flip between various minimum energy states.

## 4.4 DIMER OPTIMISATION

Having obtained minimum energy conformations for both 1,3- and 2,3-butanediol , the next step was to look at possible dimer structures. The parameter of primary interest was the minimum energy dimer conformation. The approach taken was to start with the two molecules at a sufficient distance apart so that there was no interaction between them. The total energy of the system was then the sum of the energies of the individual molecules. They were then brought together , the energy being calculated at various points during their approach. It was anticipated that a plot of energy (or heat of formation) vs. distance apart would

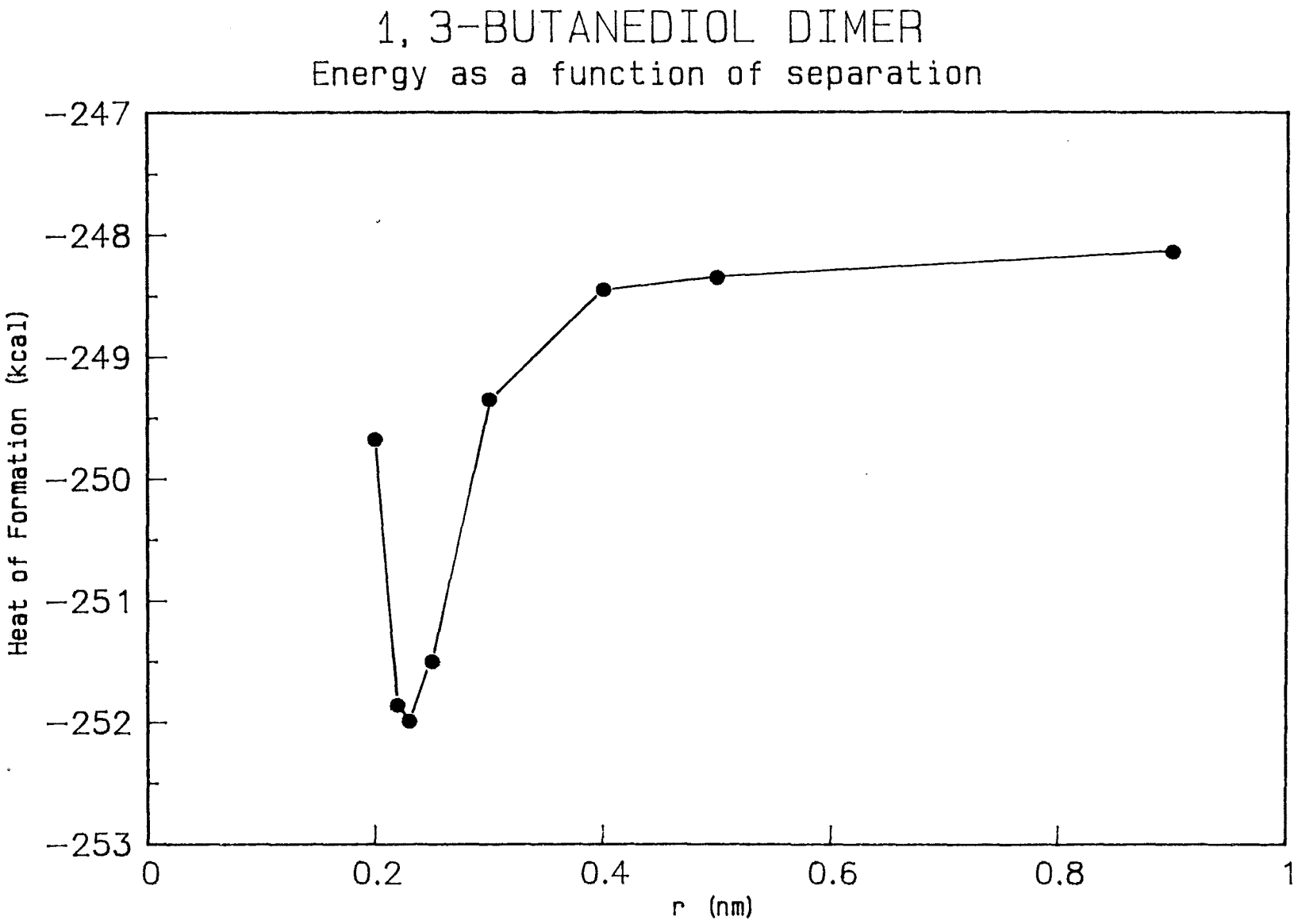
1, 3-BUTANEDIOL DIMER
Energy as a function of separation
Heat of Formation (kcal)
−247
−248
−249
−250
−251
−252
−253
0
0.2
0.4
0.6
0.8
1
r (nm)

Figure 4.8

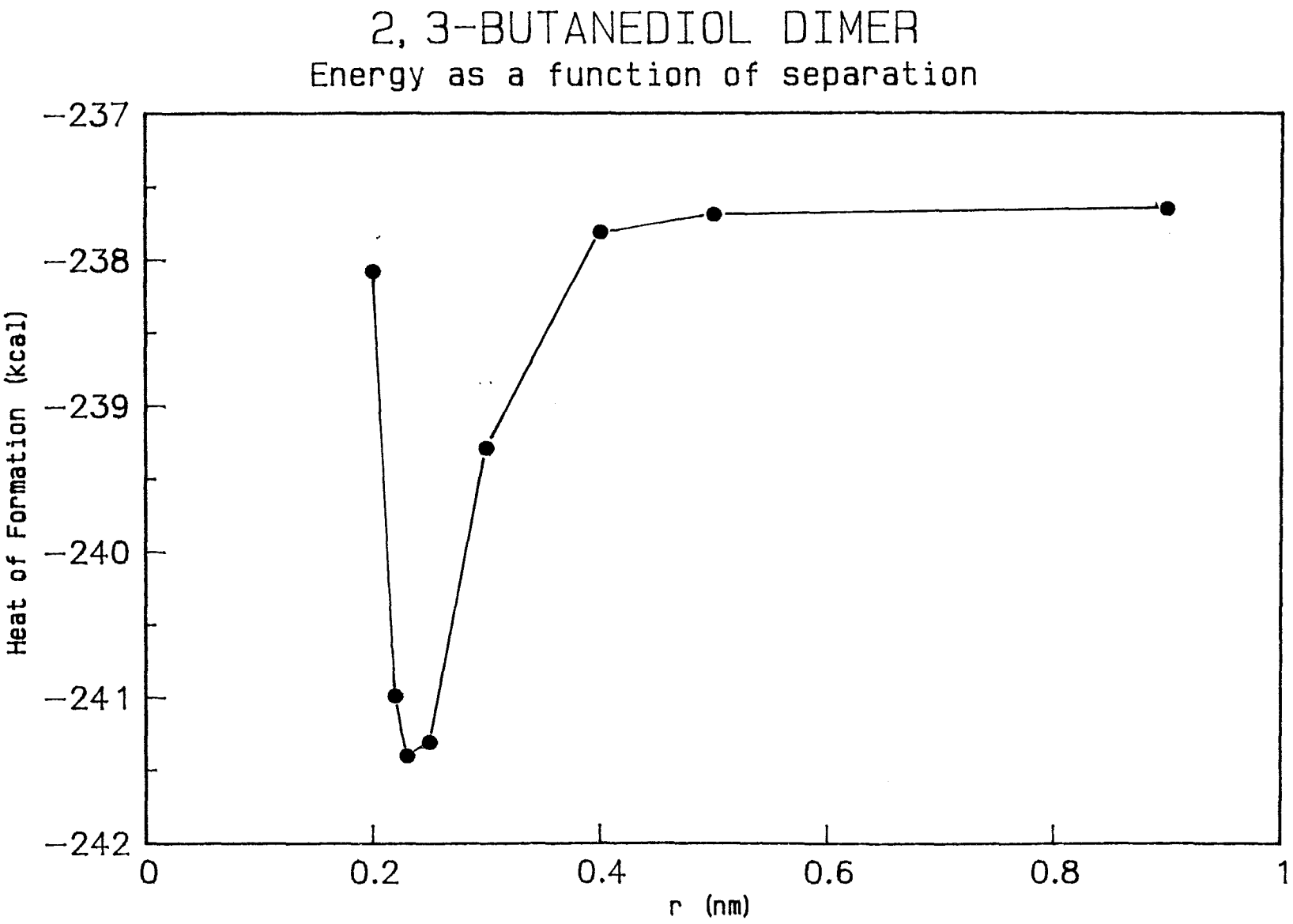
2, 3-BUTANEDIOL DIMER
Energy as a function of separation
Heat of Formation (kcal)
−237
−238
−239
−240
−241
−242
0
0.2
0.4
0.6
0.8
1
r (nm)

Figure 4.9

reveal information about the optimum dimer configuration. This was carried out for both diols and the plots are shown in figures 4.8 and 4.9.

One of the major problems with a study of this nature is that the molecules under consideration are 3-dimensional and any interaction between them occurs in 3-D space. This means that the number of directions from which molecules can approach each other is infinite , making life very complicated. In order to simplify matters , the problem was reduced to a one dimensional one. The molecules were brought together along a straight line which ran from the centre point of the bond between $C_2$ and $C_3$ of each diol. The molecules were also aligned in such a way that the hydroxyl groups were pointing towards each other , the protons of one molecule being lined up with the oxygens of the other and vice versa. In other words cyclic dimers involving all four hydroxyls were considered. While it is appreciated that these are not the only possible structures , the objective was to demonstrate that these structures were feasible , thus justifying the basic assumption made in Chapter 3 when proposing a self-association model for these diols. Figures 4.10 and 4.11 show these structures.

The plots of heat of formation against distance apart (r) are similar in shape for both diols. Both show a minimum at r = 0.23nm separation ( the

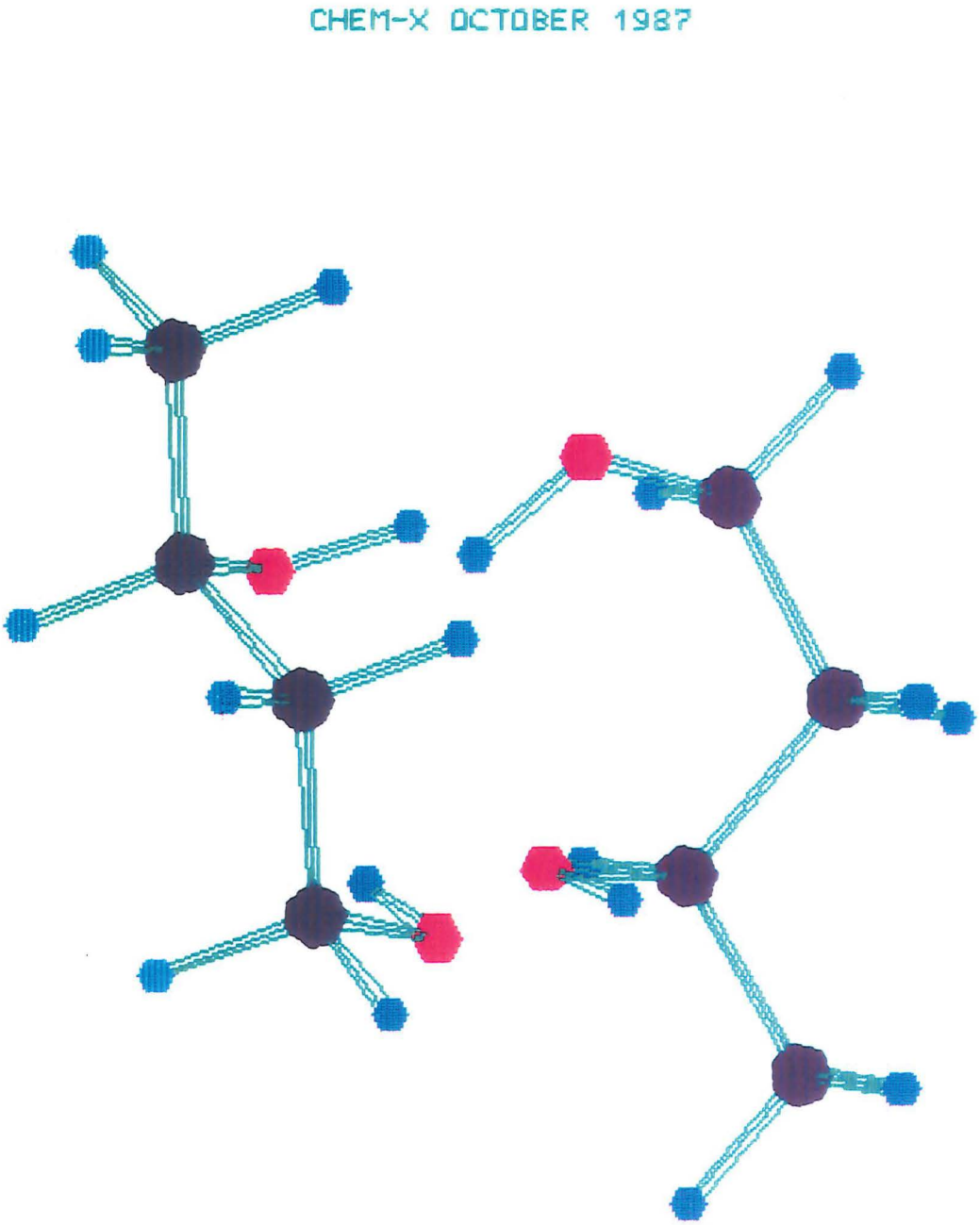


Figure 4.10

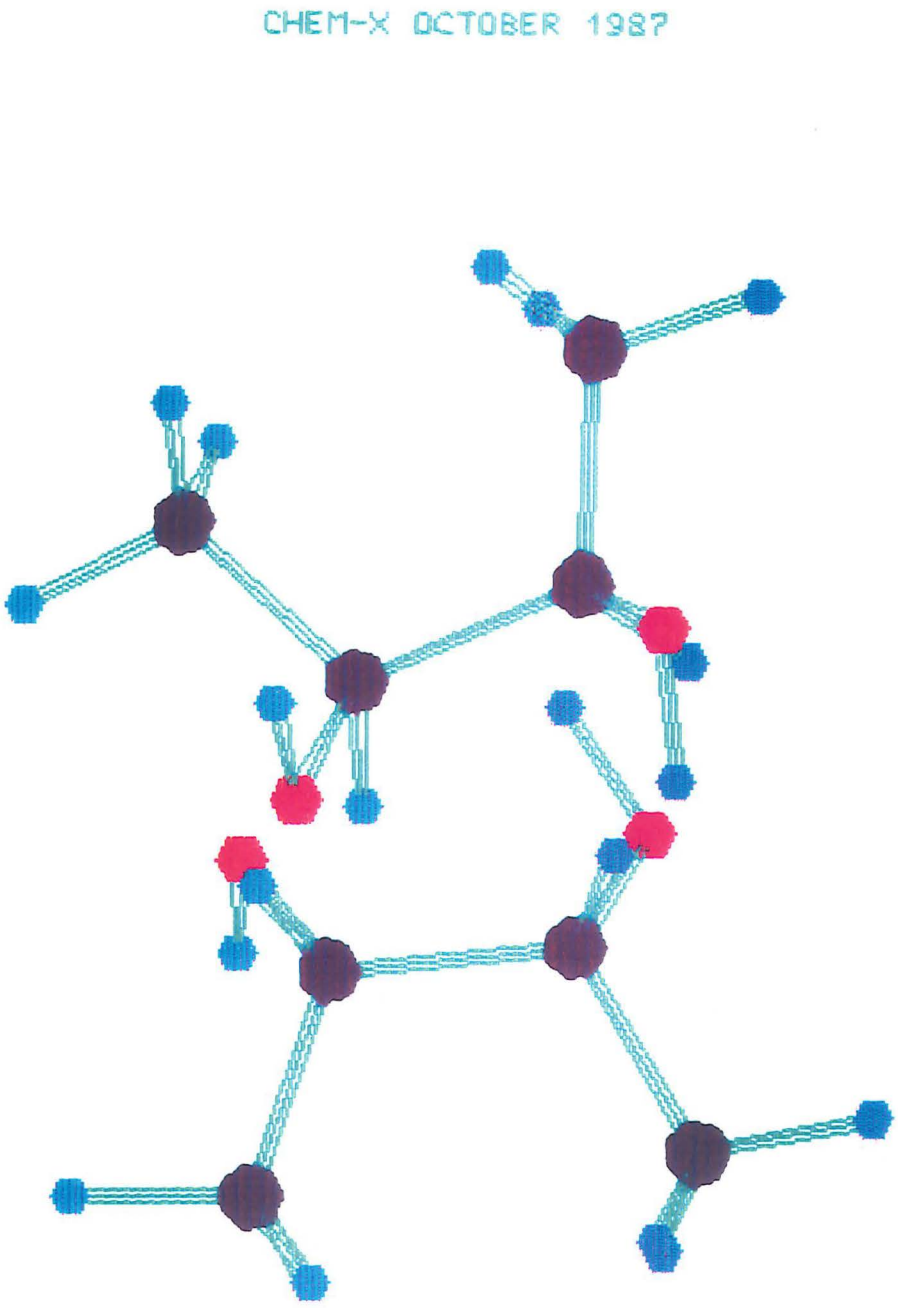


Figure 4.11

separation being the average distance apart between hydroxyls).

The energy contribution to the dimer system of hydrogen bonding can easily be calculated from the difference in energy between the associated and the non-associated states , i.e. the depth of the minimum in the energy vs separation plots. This data is summarised in table 4.3.

| Molecule | $\Delta H_f^{\ominus}$(non) (kcal) | $\Delta H_f^{\ominus}$(ass) (kcal) | $\Delta(H_f^{\ominus})$ (kcal) |
|---|---|---|---|
| 1,3-diol | -248.0 | -252.0 | -4.0 |
| 2,3-diol | -237.7 | -241.4 | -3.7 |

Table 4.3

$\Delta H_f^{\ominus}$(non) is the non-associated state of the system , $\Delta H_f^{\ominus}$(ass) is the minimum energy state and $\Delta H_f^{\ominus}$ is the difference between the two , representing the energy of association. These energies are in units of kcal. Translated to kJ these are -17.7 kJ and -16.4 kJ respectively. These can be compared to the heats of association , calculated from the $^1$H n.m.r. work described in the previous chapter which were -23.6 kJmol$^{-1}$ for 1,3-butanediol and -33.3 kJmol$^{-1}$ for 2,3-butanediol. It is apparent that the theoretical values are lower than those measured , however they are of the same order of magnitude. Also , the calculations are based on molecules in the gas phase and no account of solvent interactions , dielectric constants etc. has been taken.

In summary then , the calculated optimum structures for 1,3-butanediol and 2,3-butanediol monomers both involve intra-molecular hydrogen bonds. In the case of 2,3-butanediol , both hydroxyls appear to be invoved in intra self-association , perhaps going some way towards explaining its non-reactivity in the oxygen-uptake work.

In the $^{1}H$ n.m.r. work (Chapter 3) an assumtion was made in proposing the monomer-dimer self-association model i.e. that in the dimer , both hydroxyls were tied up in hydrogen bonding. While the work carried out in this chapter has involved using gross simplifications , it has shown that such structures , i.e. cyclic dimers, are theoretically energetically favourable.

# APPENDIX I

## LINEAR REGRESSION

At various stages throughout this work , linear regression analyses have been employed to fit data to a straight line. In this section , the methodology behind this fitting technique is outlined in brief.

Consider a series of experimental observations (responses) , $y_1$ , $y_2$ ..... $y_n$ as a function of independent variables , $x_1$ , $x_2$.....$x_n$. An example of this would be volume of $O_2$ consumed ( y-values ) as a function of time ( x-values ). If a linear fit is required then the general equation for a straight line i.e.

$$Y_i = a + bx_i \qquad (I.1)$$

can be applied where

$Y_i$ is the predicted value of the response

a is the value of the intercept

b is the value of the slope

$x_i$ is the value of the independent variable

In an ideal situation ,

$$Y_i = y_i \qquad (I.2)$$

i.e. the predicted responses and the actual responses will have the same values. In reality however , this is

seldom the case and differences will exist. These discrepancies ( $\Delta y_i$ ) may be denoted by ,

$$\Delta y_i = Y_i - y_i \qquad (I.3)$$

It is useful to quantify the difference between experimental and predicted data. The parameter which is used to do this is called "Chi-squared" ( $\chi^2$ ) and is calculated in the following way ,

$$\chi^2 = \sum ( \Delta y_i / s_i )^2 = \sum (1/s_i^2 (y_i - a - bx_i)^2) \qquad (I.4)$$

where $s_i$ is the standard deviation associated with each experimental observation.

It is clear that if the value of $\chi^2$ is minimised then the best straight line fit to the data will be obtained. This means of linear regression is known as the method of least squares. The minimisation procedure can be carried out by calculating the partial derivatives of $\chi^2$ with respect to a and b in equation (I.4). This leads to the following expressions ,

$$a = \frac{(\sum x_i^2 \sum y_i) - (\sum x_i \sum x_i y_i)}{N \sum x_i^2 - (\sum x_i)^2} \qquad (I.5)$$

$$b = \frac{N \sum x_i y_i - \sum x_i y_i}{N \sum x_i^2 - (\sum x_i)^2} \qquad (I.6)$$

N is the number of $(x_i, y_i)$ data points.

Another useful parameter which was quoted throughout this work was the correlation coefficient , r. This number gives an indication of how closely the

experimental data can be fitted to a straight line and is a measure of the linear association between two variables.

$$r = \frac{N\sum x_i y_i - \sum x_i y_i}{\{N\sum x_i^2 - (\sum x_i)^2\}^{0.5}\{N\sum y_i^2 - (\sum y_i)^2\}^{0.5}} \qquad (I.7)$$

The closer r is to unity , the better the fit.

## APPENDIX II

## LEAST SQUARES FIT TO A POLYNOMIAL

In Chapter 3 , some of the data sets were not well fitted by a straight line , in particular the $d_{obs}$ vs X points (see section 3.2). One approach which may be used to overcome this problem is to construct a more complex function which includes curvature and try varying the coefficients of this function to fit the data more closely. A useful general function for such a fit is a power series polynomial i.e.

$$y = a + bx + cx^2 + dx^3 \ldots\ldots \qquad (II.1)$$

where the dependent variable y is expressed as a sum of the independent variable x with coefficients a , b , c, d etc.

In the previous section , the method of least squares was used to optimise the values of the

coefficients a and b in fitting data to a straight line. The same method can , in principle , be applied to a polynomial. For the purposes of this work , only a second-order polynomial , or quadratic , function was considered , i.e.

$$y = a + bx + cx^2 \qquad (II.2)$$

As before , the method of least squares requires that $\chi^2$ , the square of the sum of the differences between the observed and predicted values , is minimised. In this case the expression for $\chi^2$ is as follows -

$$\chi^2 = \{1/s_i^2(y_i - a - bx_i - cx_i^2)^2\} \qquad (II.3)$$

where s is the sample standard deviation.

Setting the partial derivatives of $\chi^2$ , with respect to each of the three coefficients a , b and c , equal to zero results in 3 simultaneous equations which can be rearranged to show the interaction of the coefficients explicitly.

$$y_i = a\ 1 + b\ x_i + c\ x_i^2 \qquad (II.4)$$

$$x_i y_i = a\ x_i + b\ x_i^2 + c\ x_i^3 \qquad (II.5)$$

$$x_i^2 y_i = a\ x_i^2 + b\ x_i^3 + c\ x_i^4 \qquad (II.6)$$

These equations form the basis of the computer programme , NMR2.FOR , (see Appendix III) which was used to calculate the coefficients a , b and c. These coefficients were in turn used to calculate $d_m$ and $K_m$ values at various stages in the iterative procedure.

# APPENDIX III

```
*** Program NMR2.FOR ***
*** R.M. Calder    30/11/87

      IMPLICIT NONE
      CHARACTER*20 ANS, INFILE, OUTFILE
      INTEGER I,J,K,L,M,N,O,P,Q,R,NUM
      REAL*8 CONC(100),DOBS(100),X(100),Z(100),ROOT(100),DELM(100)
      REAL*8 SUM1,SUM2,SUM3,SUM4,SUM5,SUM6,SUM7,TOP1,TOP2,SXX,SXY
      REAL*8 GRAD,DELD,KEQ,TUM1,TUM2,TUM3,TUM4,TXX,TXY,NDELM,BOT1,BOT2
      REAL*8 BETA0,BETA1,TOP3,TOP4,TUM5,TUM6,TUM7,TTOP1,TTOP2,TTOP3,TTOP4
      REAL*8 BBOT1,BBOT2,DDELM
1     PRINT*,'Is the data in a file ?'
      READ (5,10) ANS
10    FORMAT(A)
      IF (ANS.EQ.'Y') THEN
            PRINT*
            PRINT*,'Enter filename'
            READ(5,10) INFILE
            OPEN(UNIT=16,READONLY,NAME=INFILE,STATUS='OLD')
            I=1
20          READ(16,*,END=110) CONC(I),DOBS(I)
            I=I+1
            GOTO 20
110         CLOSE(UNIT=16)
            I=I-1
      ELSE
            PRINT*,'How many points ?'
            READ*, NUM
            DO 30 I=1,NUM
            PRINT*
            PRINT*,'Enter X-coord.'
            READ*,CONC(I)
            PRINT*
            PRINT*,'Enter Y-coord.'
            READ*,DOBS(I)
            PRINT*
30          CONTINUE
      END IF
      Q=1

      PRINT*,'Enter trial monomer shift.'
      READ*,DELM(Q)
      PRINT*
40    DO 45 R=1,I
      X(R)=0
45    CONTINUE

      SUM1=0
      SUM2=0
      SUM3=0
      SUM4=0
      SUM5=0
      SUM6=0
      SUM7=0
      TUM1=0
```

```
        TUM2=0
        TUM3=0
        TUM4=0
        TUM5=0
        TUM6=0
        TUM7=0

        DO 50 J=1,I
                X(J)=SQRT(ABS(DOBS(J)-DELM(Q))/CONC(J))
50      CONTINUE

        DO 60 K=1,I
        WRITE (5,1000) X(K),DOBS(K)
1000    FORMAT (2X,F10.4,3X,F10.4)
60      CONTINUE

        PRINT*,'Do you want (X,DOBS) data put into a file ?'
        READ(5,10) ANS
        IF (ANS.EQ.'Y') THEN
                PRINT*
                PRINT*,'Please give filename'
                READ(5,10) OUTFILE
                OPEN(UNIT=16,NAME=OUTFILE,STATUS='NEW',CARRIAGECONTROL='LIST')
                DO 70 L=1,I
                WRITE(16,65) X(L),DOBS(L)
65              FORMAT(2F10.3)
70              CONTINUE
                CLOSE(UNIT=16)
        END IF


        DO 80 M=1,I
        SUM1=SUM1+X(M)
        SUM2=SUM2+(X(M)*X(M))
        SUM3=SUM3+(X(M)**3)
        SUM4=SUM4+(X(M)**4)
        SUM5=SUM5+DOBS(M)
        SUM6=SUM6+(DOBS(M)*X(M))
        SUM7=SUM7+(DOBS(M)*X(M)*X(M))
80      CONTINUE

        TOP1=(SUM3*SUM5)-(SUM2*SUM6)
        TOP2=(SUM1*SUM4)-(SUM2*SUM3)
        TOP3=(SUM1*SUM3)-(SUM2*SUM2)
        TOP4=(SUM4*SUM5)-(SUM2*SUM7)
        BOT1=(I*SUM3)-(SUM1*SUM2)
        BOT2=(I*SUM4)-(SUM2*SUM2)

        BETA0=((TOP1*TOP2)-(TOP3*TOP4))/((BOT1*TOP2)-(TOP3*BOT2))
        BETA1=(TOP1-(BETA0*BOT1))/TOP3

        KEQ=(BETA0-DELM(Q))/(2*BETA1*BETA1)
```

```
      WRITE (5,1010) BETA1
1010  FORMAT (5X,'Gradient is ',2X,F10.4)
      WRITE (5,1020) BETA0
1020  FORMAT (5X,'Intercept is',2X,F10.4)
      WRITE (5,1030) KEQ
1030  FORMAT (5X,'Keq is      ',2X,F10.4)
      PRINT*

      DO 90 N=1,I
      ROOT(N)=SQRT(ABS(1+8*KEQ*CONC(N)))
      Z(N)=(ROOT(N)-1)/(ROOT(N)+1)
90    CONTINUE

      DO 100 O=1,I
      TUM1=TUM1+Z(O)
      TUM2=TUM2+(Z(O)**2)
      TUM3=TUM3+(Z(O)**3)
      TUM4=TUM4+(Z(O)**4)
      TUM5=TUM5+DOBS(O)
      TUM6=TUM6+(DOBS(O)*Z(O))
      TUM7=TUM7+(DOBS(O)*Z(O)*Z(O))
100   CONTINUE

      TTOP1=(TUM3*TUM5)-(TUM2*TUM6)
      TTOP2=(TUM1*TUM4)-(TUM2*TUM3)
      TTOP3=(TUM1*TUM3)-(TUM2*TUM2)
      TTOP4=(TUM4*TUM5)-(TUM2*TUM7)
      BBOT1=(I*TUM3)-(TUM1*TUM2)
      BBOT2=(I*TUM4)-(TUM2*TUM2)
      Q=Q+1
      DELM(Q)=((TTOP1*TTOP2)-(TTOP3*TTOP4))/((BBOT1*TTOP2)-(TTOP3*BBOT2))

      WRITE (5,1040) DELM(Q)
1040  FORMAT (12X,'New monomer shift is',2X,F10.4)
      PRINT*

      IF (ABS(DELM(Q)-DELM(Q-1)).GE.0.0001) THEN
      GOTO 40
      ELSE
      PRINT*
      PRINT*
      WRITE (5,1050)
1050  FORMAT (20X,'Convergence has been achieved')
      PRINT*
      WRITE (5,1060) DELM(Q)
1060  FORMAT (20X,'Monomer shift is         ',F10.4)
      WRITE (5,1070) BETA0
1070  FORMAT (20X,'Dimer shift is           ',F10.4)
      WRITE (5,1080) KEQ
1080  FORMAT (20X,'Equilibrium constant is  ',F10.4)
      END IF

      PRINT*
      PRINT*,'Do you want to run the program again ?'
      READ(5,10) ANS
      IF (ANS.EQ.'Y') THEN
      GOTO 1
      END IF

      END
```

# REFERENCES

# References

1. Courtesy of Tioxide U.K.L.

2. W.A.Kampfer and F. Stieg, Color Eng. , 1967, 35 , 401

3. G.Kaempf , J. Coating Technol. , 1979 , 51 , 655

4. R.Clark ,"The Chemistry of Titanium and Vanadium" , (Elsevier , 1968)

5. J. Woning and R.A.Van Santen , Chem. Phys. Lett. , 1983 , 101(6) , 541

6. R.W.G.Wyckoff , "Crystal Structures" , (Interscience , 1963 )

7. H.S. Ritter , "Surface Properties of Titanium Dioxide Pigments" in "Pigment Handbook Vol. 3" , (Wiley - Interscience , New York , 1974)

8. H.G. Volz, G.Kaempf , H.G. Fitzky and A. Klaeren , A.C.S. Symp.. Ser. , 1981 , 151 , 163

9. T.A. Egerton and C.D. King , J.Oil Col. Chem. Assoc. 1979 , 62 , 386

10. R.D. Murley , J.Oil Col. Chem. Assoc. , 1962 , 45 , 16

11. A.L. Companion and R.E. Wyatt , J.Phys. Chem. Solids , 1963 , 24 , 1025

12. H.G. Volz , G. Kaempf and A. Klaeren , Farbe + Lack 1976 , 82 , 805

13. R.I. Bickley and F.S. Stone , J. Catalysis , 1973 , 31 , 389

14. G. Munuera , J. Catalysis , 1970, 18 , 19

15. P. Jackson and G.D. Parfitt , Trans. Farad. Soc. , 1971 , 67 , 2469

16. J.A. Hockey and P.Jones , Trans. Farad. Soc. , 1971 67 , 2679

17. A.H. Boonstra and C.A.H.A. Mutsaers , J. Phys. Chem. , 1975 , 79 , 1694

18. N.S. Allen , J.F. McKellar , G.O. Phillips and D.G.M. Wood , J. Polym. Sci., Polym. Letts. Edn. , 1974 12 , 241

19. N.S. Allen , J.F. McKellar , and D.M.G. Wood , J. Polym. Sci. , Polym. Chem. Edn. , 1975 , 13 , 2319

20. N.S. Allen , J.F. McKellar , G.O. Phillips and C.B. Chapman , J. Polym. Sci. , Polym. Letts. Edn. , 1974 , 12 , 723

21. R.B. Fox and T.R. Price , J. Appl. Polym. Sci. , 1967 , 11 , 2373

22. F.A. Bovey and I.M. Kolthoff , J. Amer. Chem. Soc., 1947 , 69 , 2373

23. B.S. Rao and M.R. Murthy , J.Polym. Sci. (B) , 1987 25 , 1897

24. B. Ranby and J. Rabek (Eds.) , "Singlet Oxygen" , (John Wiley , New York , 1978)

25. N.S. Allen , D.J. Bullen and J.F. McKellar , J. Mater. Sci. , 1979 , 14 , 759

26. L.A. Simpson , Poly. Paint Col. J. , 1986 , 408

27. N.S. Allen and J.F. McKellar (Eds.) , "Photochemistry of Dyed and Pigmented Polymers" , (Applied Science Publishers Ltd. , London , 1980)

28. J.G. Campbell , J.Oil Color Chem. Assoc. , 1955 , 38 , 550

29. P. Dunn , D. Oldfield and R.H. Stacewicz , J.Appl. Polm. Sci. , 1970 , 14 , 2107

30. B. Ranby and J.F. Rabek , "Photodegradation , Photo-oxidation and Photostabilisation of Polymers" , (Wiley-Interscience , 1975)

31. W.L. Hawkins , "Polymer Stabilisation" , (Wiley , New York , 1972)

32. J.B. Howard and H.M. Gilroy , Polym. Eng. Sci. , 1969 , 9 , 286

33. G. Irick,Jr., J. Appl. Polym. Sci. , 1972 , 16 , 2387

34. R.I. Bickley , G. Munuera and F.S. Stone , J. Catalysis , 1973 , 31 , 398

35. G. Munuera and F.S. Stone , Disc. Faraday Soc. , 1971 , 52 , 205

36. R.B. Cundall , R. Rudham and M.S. Salim , J.Chem. Soc., Farad. Trans. I , 1976 , 72 , 1642

37. P.R. Harvey , R.Rudham and S.Ward , J. Chem. Soc. , Farad. Trans. I , 1983 , 79 , 1381

38. P.R. Harvey , R.Rudham and S.Ward , J. Chem. Soc. , Farad. Trans. I , 1983 , 79 , 2975

39. F.H. Hussein and R.Rudham , J. Chem. Soc. , Farad. Trans. I , 1984 , 80 , 2817

40. I.M. Fraser and J.R. MacCallum , J. Chem. Soc. , Farad. Trans. I , 1986 , 82 , 607

41. I.M. Fraser and J.R. MacCallum , J. Chem. Soc. , Farad. Trans. I , 1986 , 82 , 2747

42. J.G. Calvert and J.N. Pitts , "Photochemistry" , (Wiley and Sons , New York , 1966)

43. M. Horvath , L. Blitzky and J. Huther , "Ozone" in "Topics in Inorganic and General Chemistry" (Elsevier , 1985)

44. G. Svehla , "Vogel's Textbook of Macro and Semimicro Qualitative Analysis" (Longman , London , 1979 )

44. G. Svehla , "Vogel's Textbook of Macro and Semimicro Qualitative Analysis" (Longman , London , 1979 )

45. D. Schwarzenbach , Inorg. Chem. , 1970 , 9(11) , 2391

46. J. Muhlebach , K. Muller and G. Schwarzenbach , Inorg. Chem , 1970 , 9(11) , 2381

47. O. Kamm , "Qualitative Organic Analysis" , 2nd. Ed. (Wiley and sons , New York , 1932)

48. I.M. Fraser , Ph. D. Thesis , University of St. Andrews , 1985

49. M.D. Lumb , "Luminescence Spectroscopy" , (Academic Press , London , 1978)

50. J.L.Latham , "Elementary Reaction Kinetics" , (Butterworths , London , 1964 )

51. E.E. Glover and G.Jones J.Chem. Soc. , 1958 , 3021

52. A. Castonguay and P. Brassard , Can J. Chem. , 1977, 55 , 1324

53. W. Neagle and C.H. Rochester , J. Chem. Soc. , Farad. Trans. I , 1983 , 79 , 263

54. G.T. Morgan , J. Chem. Soc. , 1932 , 2669

55. F. Buttner , Justus Liebigs Ann. Chem. , 1953 , 184

56. T.W.G. Solomons , "Organic Chemistry" , (John Wiley and Sons , 1984)

57. L. Streier , "Biochemistry" , 2nd. Ed. (W.H. Freeman and Co. , 1981)

58. A. Ferscht , "Enzyme Structure and Mechanism" , (W.H. Freeman , 1977)

59. G.D. Parfitt , Prog. Surf. Membr. Sci. , 1976 , 11, 181

60. R.E. Day in "Progress in Organic Coatings , Vol. 2" (Elsevier Sequoia , Lausanne , 1973/4)

61. H.P. Boehm , Disc. Farad. Soc. , 1971 , 52 , 264

62. A.N. Fletcher and C.A. Heller , J. Phys. Chem. , 1967 , 71(12) , 3742

63. C.H. Rochester , J. Graham and R. Rudham , J. Chem. Soc. , Farad. Trans. I

64. G. Wilkinson and F.S. Stone , "Advanced Inorganic Chemistry" (Wiley , 1982)

65. A.R. Gonzalez-Elipe , G. Munuera and J. Soria , J. Chem. Soc. , Farad. Trans. I , 1979 , 75 , 748

66. G.Munuera , A. Navio and V. Rives-Arnau , J.Chem.Soc. , Farad. Trans. I , 1981 , 77 , 2747

67. E.M. Ceresa , J. Mater. Sci. , 1983 , 18(1) 289

68. Y.S. Chiang , J. Craddock , D. Mickewich and J. Turkevich , J. Phys. Chem. , 1966 , 70 , 3509

69. A. Tkac , Int. J. Radat. Phys. Chem. , 1975 , 7 , 457

70. A.E. Cahill and T. Taube , J. Am. Chem. Soc. , 1952 74 , 2312

71. G.C. Pimentel and A.L. McClellan , "The Hydrogen Bond" , (W.H. Freeman and Co. , New York , 1960)

72. P. Schuster , G. Zundel and C. Zandorfy (Eds.) , "The Hydrogen Bond , Vols. 1-3" , (North Holland Publishing Co. , Amsterdam , 1976)

73. P. Huyskens , J. Mol. Struct. , 1983 , 100 , 403

74. S. Krimm , J. Chem. Phys. , 1955 , 23 , 1371

75. H. Limbach , "Studies in Physical and Theoretical Chemistry" , 1983 , 26 , 410

76. J.D. Lambert , Disc. Faraday Soc. , 15 , 226

77. N.H. Fletcher , "The Chemical Physics of Ice" , (Cambridge University Press , Cambridge , 1970)

78. R.G. Schulman , "Biological Applications of Magnetic Resonance" , (Academic Press ,New York, 1980)

79. J. C. Davis,Jr. , K.S. Pitzer and C.N.R. Rao , J. Phys. Chem. , 1960 , 64 , 1744

80. N.D. Coggeshall , J.Chem. Phys. , 1950 , 18 , 980

82. P. Bordewijk , M. Kunst and A. Rip , J.Phys. Chem., 1973 , 77 , 548

83. A.N. Fletcher , J. Phys. Chem. , 1971 , 75 , 1808

84. M. Puchalik , Acta Phys. Polon. , 1954 , 13 , 159

85. M.C.R. Symons , N.G.M. Pay and G.Eaton , J.Chem. Soc. , Farad. Trans. I , 1982 , 78 , 1841

86. M. Rappon and R.M. Johns , J. Mol. Liquids , 1989 , 40 , 155

87. M. Saunders and J.B. Hyne , J. Chem. Phys. , 1958 , 29 , 1319

88. A.B. Littlewood and F.W. Willmott , J. Chem. Soc. , Farad. Trans. I , 1966 , 62 , 3287

89. F. Strohbusch and H. Zimmerman , Ber. Bunsen. Phys. Chemie , 1969 , 71 ,679

90. H.H. Limbach , F. Strohbusch and H. Zimmermann , Ber. Bunsen. Phys. Chemie , 1970 , 74 , 3

91. J.A. Walmsley , J. Phys. Chem. , 1978 , 82 , 2031

92. H.S. Gutowsky , J. Am. Chem. Soc. , 1963 , 85 , 3065

93. J.S. Chen and R.B. Shirts , J. Phys. Chem. , 1985 , 89 , 1643

94. H.S. Gutowsky and A. Saika , J. Chem. Phys. , 1953 21 , 1688

95. N.D. Coggeshall and E.L. Saier , J. Am. Chem. Soc. 1951 , 73 , 5414

96. J.M. Purcell , H. Sus and R. Cavanagh , Can. J. Chem. , 1969 , 47 , 3655

97. J.A. Pople , W.G. Schneider and H.J. Bernstein , "Nuclear Magnetic Resonance Spectroscopy" , (McGraw-Hill , New York , 1959)

98. J. Martin , J. Chim. Physique , 1962 , 59 , 736

99. Connor and Reid , J. Mol. Spec. , 1961 , 7 , 32

100. P.A. Kollman in H. Schaefer(Ed.) , "Applications of Electronic Structure Theory",(Plenum Press , N.Y. 1977)

101. P.A. Kollman and L.C. Allen , Chem. Rev. , 1972 , 72 , 283

102. M.D. Joesten and L.J. Schaad , "Hydrogen Bonding", (Marcel Dekker , New York , 1974)

103. S. Scheiner in "Studies in Physical and Theoretical Chemistry", Volume 26

104. J.D. Hill et. al. , J. Am. Chem. Soc. , 1975 , 97, 7220

105. W.C. Topp and L.C. Allen , J. Am. Chem. Soc. , 1974 , 96 , 5291

106. M.J.S. Dewar , E.G. Zoebisch , E.F. Healy and J.J.P. Stewart , J.Am.Chem.Soc. , 1985 , 107 , 3902

107. M.J.S. Dewar and K.M. Dieter , J. Am. Chem. Soc. , 1986 , 108 , 8075

108. R.C. Bingham , M.J.S. Dewar and D.H. Lo , J.Am.Chem.Soc. , 1975 , 97 , 1285

109. M.J.S. Dewar and W.Thiel , J.Am.Chem.Soc. , 1977 , 99 , 4899 , 4907

110. J.A.Pople and N.Beveridge , "Approximate Molecular Orbital Theory" (McGraw-Hill,1970)

# APPENDICES